Statistical Effects in Anyonic Quantum Walks

By

Lauri Lehman

A thesis submitted to Macquarie University
for the degree of
Doctor of Philosophy
Department of Physics and Astronomy
June 2013

Typeset in LaTeX 2$_\varepsilon$.

Except where acknowledged in the customary manner, the material presented in this thesis is, to the best of my knowledge, original and has not been submitted in whole or part for a degree in any university.

Lauri Lehman

Acknowledgements

I would like to thank my parents Lasse and Anneli and my sister Sisko for their continuous support and understanding. They never complained about waking up at early hours for our phone calls, and were always there for me when I had a chance to visit back home during my thesis project. It has been a pleasure to host my parents during their visits to Australia, and I will always remember our adventures in the Red Centre and the Great Barrier Reef.

A special thanks goes also to my supervisor Gavin Brennen, who has been a supportive and determined coordinator for this project. When I started my thesis project back in 2009, I had no idea what kind of ride I was about to get into. Gavin's wide range of interests and his precision and creativity in research have served as an inspiration for my own research, and I consider him as a role model as a physicist. I wish him the best of luck on his career and hope that this project will not be the end of our research efforts.

Jiannis Pachos was also an inspiring supervisor during my six-month visit to Leeds in 2010. His vision and guidance were essential in delivering the results for this project. Václav Zatloukal was a good buddy, colleague and housemate in Leeds, and many of the results presented in this thesis are entirely credited to him.

I have met some great people during my stay in Australia. The student group at Macquarie: Aharon, Andrew, Chris, Gerardo, Ingo, Ivan, Johann, Mauro, Michael, Nora, Ressa, Thorn, Tommaso and Xavi have been of special importance, and our numerous coffee breaks have been vital to my well-being here. Finally, I would like to thank Andreas, Casper, Chris, Eleonora, Emma, Francesca, Georg, Helena, Hugo, Jarkko, Joe, Joppe, Jussi, Katrina, Kayla, Kyle, Kush, Magda, Matti, Michail, Mika, Mikko, Nadz, Oldoozie, Pekka, Pete, Samuli, Sara, Shira, Sia, Stephen, Thomas, Tony, Ville, Wenjie and William for being good friends!

List of Publications

- L. Lehman, V. Zatloukal, J. Pachos, G. Brennen and Z. Wang. *Quantum Walks with Non-Abelian Anyons.* Phys. Rev. Lett. 106, 230404 (2011); arXiv: 1009.0813
- L. Lehman, D. Ellinas and G. Brennen. *Quantum Walks of $SU(2)_k$ Anyons on a Ladder.* Proceedings of the International Workshop on Theoretical Aspects of the Discrete Time Quantum Walk. J. Comput. Theor. Nanosci. 10 (7), 1634 (2013); arXiv:1203.1999
- V. Zatloukal, L. Lehman, S. Singh, J. Pachos and G. Brennen. *Transport Properties of Anyons in Random Topological Environments.* Submitted. Preprint arXiv:1207.5000

Abstract

Anyonic quantum statistics is an exotic phenomenon of identical particles in quantum mechanics. When particles are confined in two spatial dimensions, exchanges of identical particles can induce phase factors in the wave function of Abelian anyons or matrix valued transformations of the wave function of non-Abelian anyons. As a result, systems of anyons may have richer properties than those of bosons and fermions in three spatial dimensions. There is strong theoretical support for the existence of anyons in some engineered two-dimensional systems such as 2D electron gases, strongly correlated spin lattices and as edge modes of nanowires. In the future, anyons could be used in topological quantum computation to perform highly efficient information processing with very small error rates.

The phases of matter described by dynamically interacting anyons have recently been studied in chains where anyons interact via Heisenberg-type exchange interactions. In this thesis, new kind of anyonic interactions are studied, induced purely by braiding during free evolution. Such interactions are of topological origin, and the information about the interactions is stored non-locally. A quantum walk model is used to study the effects of these braiding interactions on the dynamical behaviour of anyons.

The anyonic quantum walk is a quasi-one-dimensional generalization of the discrete-time quantum walk which allows the simulation of anyonic dynamics analytically. The moving anyon and a chain of stationary anyons interact via braiding statistics, and the behaviour of the anyon is studied in three cases. Striking differences are found between particles with conventional boson or fermion statistics and non-Abelian anyonic statistics.

The random walk is a dynamical model that describes the motion of a particle on a lattice. In physics, it is used to describe Brownian motion of fluids and gases. In such systems, energy transport is diffusive, and the order of the system approaches a highly mixed state without any information content. The quantum version of the random walk, the quantum walk, has nonintuitive properties. Generally, the information content in a unitarily evolving system is fixed, which leads to unexpected transport phenomena. An initially localized particle does not propagate diffusively, but escapes the starting point with ballistic speed.

Most of our results for non-Abelian anyons use the Ising model anyon which is most likely to be measured in experiments. First, when each anyonic site is occupied by one Ising anyon, the propagation of the anyon becomes diffusive. More precisely, the variance of the spatial probability distribution of the particle depends linearly on the number of time steps. This is in stark contrast to bosons, fermions and Abelian anyons which propagate ballistically, and the variance depends linearly on the square of the

number of time steps. The essential reason for this slowdown is that the non-Abelian anyons possess an extra degree of freedom called the fusion Hilbert space. This space can be viewed as an environment for the normal degrees of freedom of the particle, inducing decoherence in the quantum walk. This thesis opens the line for studies of this novel kind of decoherence mechanism in quantum walks.

In the second case the study is extended to more general anyon models by losing some of the information about the history of the evolution. In this case the system is subject to decoherence, and the total system evolution is not unitary. The behaviour of the particle in this model is found to be diffusive for all the non-Abelian anyon models studied, while Abelian anyons behave ballistically also in this model.

One peculiarity of quantum systems is their behaviour under disorder. Quantum mechanical particles moving in random local potentials are known to freeze and not move at all. Such a phenomenon is known as Anderson localization. Studies have shown that Anderson localization happens also in quantum walks with random spatial fluctuations in the coin parameters. In the third case, the transport properties of anyons are studied under topological randomness, allowing the occupations of anyons change between experiments. Bosons and fermions would propagate ballistically under such randomness, and Abelian anyons are shown to localize. The results show that non-Abelian anyons behave diffusively at short time scales, and it is argued that they do so in the long time limit as well.

In all cases, non-Abelian anyons are shown to have very different dynamical properties than bosons, fermions and Abelian anyons. A possible simulation of the anyonic quantum walk in Fractional Quantum Hall systems is also discussed.

Statement of Contribution

The author carried out the numerical calculations the results of which are presented in Sections 2.4, 2.5, 3.2, 4.3, 5.2 and 5.3.3. The author also analysed the results of the numerical calculations in Section 5.3.2. The author calculated the analytical bounds for variance presented in Sec. 3.3 and contributed to the proof for analytical bounds found in Sec. 3.4, and calculated the CP map elements in Sec. 4.2.

Gavin Brennen, Jiannis Pachos and Zhenghan Wang derived the analytical formula for the probability distribution in Section 3.1.

Václav Zatloukal performed independent numerical calculations presented in Section 3.2, and proved the analytical results in Sections 3.4, 5.2.1 and 5.3.1.

Gavin Brennen initiated the idea of simulating the anyonic quantum walk in Fractional Quantum Hall systems. He also found the asymptotic formula for probability distribution in Section 4.5, and did independent numerical calculations for the model discussed in Sec. 5.2.

Demosthenes Ellinas found the approximation of Kraus generators in Section 4.4.

Václav Zatloukal and Jiannis Pachos performed the numerical calculations for the discrete model in Sec. 5.3.2 and Sukhwinder Singh performed the numerical calculations for the continuous-time model in the same section.

Contents

1 Introduction

Since the inception of quantum mechanics, systems of identical particles have been of special interest. Identical particles are defined as objects which have exactly the same physical properties, and no experiment can distinguish between them even in principle. The same results in experiments would be obtained regardless of which copy of the particle was chosen. Physically, the particles have some defining properties such as rest mass, electric charge and intrinsic spin, which must all be identical if the particles are to be considered as identical.

In classical mechanics particles are always point-like and they follow well-defined trajectories. Therefore identical particles are distinguishable in principle. In quantum mechanics, however, the situation is different. The wave functions of particles extend over the whole space, and the identity of a particle is related to the knowledge of the observer about the particle. Before the measurement has happened the observer should have no information about the identities of particles and they must be regarded as indistinguishable. If one puts no additional constraints on the mathematical description of a set of particles, they must however be considered as distinguishable. To demand indistinguishability is then to pose some constraints on the representation of the physical state of the system. Perhaps surprisingly, this has far-reaching consequences on the physics of the system. Particle indistinguishability demands that the physical properties must not change if the mere positions of the particles are exchanged. These exchanges are called permutations, and the requirement that the state is invariant under permutations is called permutation symmetry. Strictly speaking all local observables and the representation of the state (up to an overall phase) must be invariant under the permutation symmetry.

In three spatial and one time dimensions, the requirement of permutation symmetry allows two kinds of mathematical descriptions for the system. This leads to a clear-cut division between particles: the ones described by the first kind are called bosons and the ones described by the second kind are called fermions. All *elementary* particles

are thus bosons or fermions. The boson/fermion nature of particles is called quantum statistics.

Although the division to bosons and fermions is clear in fundamental physics, there are situations where this classification is not adequate. Sometimes, collections of elementary particles such as electrons form collective states which are stable in time. These collective states can be viewed as particles themselves, if they interact with their environment as a single entity. Such states are called quasiparticles to emphasize that they are not elementary particles. Quasiparticles can have different physical properties than their constituent particles, and the effective description of a quasiparticle is usually simpler than the full characterization of its constituents. Familiar examples of quasiparticles are phonons, mobile disturbances of the lattice structure in condensed matter, and holes, states which can occupy electrons but are missing them.

In general, the quantum statistics of quasiparticles should not be altered: two identical quasiparticles should still be either bosons or fermions. This is however not the case if particle exchanges are interpreted in the physical sense such that the particles draw trajectories in space-time, and if the particles are effectively confined on a plane. If the quasiparticles are two-dimensional, and the particles are not allowed to collide (interact in close range), then there are many ways to choose the trajectories when particles are exchanged, but none of these is preferred unless additional constraints are imposed. Thus, fermionic and bosonic quantum statistics are not enough to describe the constraints imposed by permutation symmetry in two spatial dimensions. The correct formalism to account for quantum statistics is then called anyonic braiding statistics, and the quasiparticles that obey such statistics are called anyons.

Quantum statistics has very profound consequences in physical systems. The spin-statistics theorem states that statistics is intimately connected to the intrinsic spin that particles carry. The exclusion principle states that no two fermions can exist in the same physical state. Since the mathematical description of anyons is much richer than that of bosons and fermions (bosons and fermions can be viewed as special kinds of anyons), it is expected that the physics of anyons is rich and complex. The study of anyonic properties is currently an active and developing area of research, partly because of intrinsic theoretical interest and partly because of possible applications in quantum computing. The question posed in this thesis is: what are the effects of anyonic braiding statistics on the dynamics of a system of particles? In other words, how does the pure quantum statistics affect the time evolution of wave packets that describe the particles? In the models that are studied here, it turns out that there are qualitative differences between the dynamics of particles that obey Abelian and non-Abelian anyonic statistics.

There has recently been some related work on quantum walks in topological phases [1–4]. These walks possess a chiral symmetry, such that the quasi-momentum vector $\mathbf{n}(k)$ winds non-trivially around the Bloch sphere as k goes from $-\pi$ to π. There are bound edge states of energy 0 or π, which are robust against perturbations of the Hamiltonian if these perturbations do not break the chiral symmetry. These quantum walks have a variety of topological phases characterized by the winding number. The existence of anyons in such topological phases has not been studied so far. Other related work has been done with interacting anyons in one-dimensional chains [5].

This Heisenberg-type interaction model favours energetically the fusion of neighbouring anyons into certain fusion channels. It was shown that a chain of Fibonacci anyons preferring fusion to vacuum is critical and is described by two-dimensional conformal field theory.

The first part of this Chapter introduces the concept of anyonic braiding statistics, highlighting the differences between conventional quantum statistics and anyonic statistics, and introducing the mathematical tools needed to understand anyons. The second part discusses the quantum walk, setting the ground for the formalism that will be used to study the anyonic quantum walk model.

1.1 Anyonic quantum statistics

Anyonic statistics extends the idea of conventional quantum exchange statistics. Exchange statistics in quantum mechanics is a procedure to fix the problem of exchange degeneracy [6], which means that a particular physical state can be described by several different wave functions in a many-body system. The relative phases of these states carry information about the identities of the particles, so they must be considered as fundamentally distinguishable. To describe systems of indistinguishable particles, it is necessary to pose further constraints on the states to remove the exchange degeneracy.

Exchange degeneracy is removed by requiring that the physical properties of the state do not change under permutations of identical particles. The overall phase of the wave function might change but it is still constrained to certain values. If P_{ij} is the permutation operator that exchanges particles labelled i and j, this operator must commute with the total Hamiltonian if the physical properties are to be invariant under permutations. The allowed physical states for identical particles must therefore be eigenstates of P_{ij}. Another constraint on the wave functions is that exchanging particles twice must give the original state, $P_{ij}^2\big|\Psi\big\rangle = \big|\Psi\big\rangle$. This property implies that permutation operators have only two distinct eigenvalues, $+1$ and -1. The eigenstates corresponding to these eigenvalues are called symmetric, $P_{ij}\big|\Psi_{\mathrm{S}}\big\rangle = \big|\Psi_{\mathrm{S}}\big\rangle$, and antisymmetric, $P_{ij}\big|\Psi_{\mathrm{A}}\big\rangle = -\big|\Psi_{\mathrm{A}}\big\rangle$. They can be formally written as

$$\big|\Psi_{\mathrm{S}}\big\rangle = \frac{1}{\sqrt{N!}}\sum_{\alpha} P_\alpha\big|\Psi\big\rangle \tag{1.1}$$

$$\big|\Psi_{\mathrm{A}}\big\rangle = \frac{1}{\sqrt{N!}}\sum_{\alpha} \epsilon_\alpha P_\alpha\big|\Psi\big\rangle \tag{1.2}$$

where α labels the $N!$ permutations of N objects (including identity permutation) and ϵ_α is $+1$ (-1) for all even (odd) permutations. The class of particles which are described by completely symmetric and antisymmetric states are called bosons and fermions respectively. The requirement that systems of identical particles must be described by either a symmetric or antisymmetric wave function is called the symmetrization postulate. The boson/fermion characteristic is fundamental to elementary particles, protected by a superselection rule so that one can not turn to the other.

Quantum exchange statistics is quite an abstract concept, a mathematical constraint derived from physical principles. In that context, the exchange of particles is

not to be understood as a physical process where the positions of two particles are exchanged. It is rather a reshuffling of the particle indices in the mathematical representation of the state. It is therefore of interest to consider particle exchange in a more concrete way, such that the exchange is interpreted to occur in physical phase space, perhaps as a result of interactions, and particles draw trajectories in space-time as they change positions. Such a treatment was given by Leinaas and Myrheim [7], who considered the exchange of single-particle wave functions via parallel transport. They pointed out that the configuration space of N particles is not a Cartesian product of the single particle spaces X^N, but the real configuration space is X^N/S_N, the product of single particle spaces modulo the permutation group for N particles. In X^N/S_N the singular points where the particle positions coincide are related to the topology of the configuration space. When a vector is parallel transported around a singular point, its direction might change so that it is not equal to the original vector. Trajectory loops are therefore divided into different classes that record information about the singular points. A translation in the spatial coordinates causes a gauge transformation in the wave function, $\big|\psi(x)\big\rangle \to \big|\psi'(x)\big\rangle = e^{i\chi}\big|\psi(x)\big\rangle$, where the total phase $\chi = \chi_{\text{dyn}} + \chi_{\text{geom}} + \varphi$ can in general be the sum of dynamical, geometric and exchange phases, respectively. The exchange phase φ is a characteristic number of the many-body system of identical particles. Values $\varphi = \{0, \pi\}$ correspond to bosonic and fermionic systems respectively. In three spatial dimensions, the configuration space is doubly connected, so that encircling a singular point twice takes the state back to its original configuration. Thus, the constraint $P_{ij}^2 = e^{i2\varphi} = 1$ allows only bosonic and fermionic behaviour, and the symmetrization postulate is already built into the theory. This is more intuitive than requiring symmetrized states which assume entanglement between particles that possibly have never interacted. In two spatial dimensions, the configuration space can be infinitely connected, and there are no restrictions on the gauge condition. The wave function can acquire any phase when the particle indices are interchanged, and a new form of statistics emerges: anyonic quantum statistics.

The notion of anyonic statistics was independently discovered by Frank Wilczek, who was investigating particles with fractional angular momentum [8, 9]. A two-dimensional composite particle with charge q orbiting a magnetic monopole (flux tube in three dimensions) with flux Φ is quantized in units $l = \text{integer} - q\Phi/2\pi$, and the interchange of two composite particles yields a phase factor $e^{iq\Phi}$ on observables. This is a consequence of the fact that the gauge transformation which removes the azimuthal vector potential is not 2π-periodic. If the two-anyon wave function $\big|\Psi\big\rangle$ is characterized by the relative polar coordinates r and ϕ of the particles, the wave function is subject to constraint $\big|\Psi(r, \phi + \pi)\big\rangle = e^{i2\pi\Delta}\big|\Psi(r, \phi)\big\rangle$. Now the parameter Δ interpolates between bosonic and fermionic character. The spin of the anyon is $s_a = \text{integer} + s + \Delta$, where s is the intrinsic spin of the charged particle. The total phase acquired when the anyons are interchanged is $e^{i2\pi s_a}$, so the connection between spin and statistics holds also in the more general case.

The above examples show that quantum statistics can be altered in two spatial dimensions, such that the wave function can acquire an arbitrary phase $e^{i\phi}$ when identical particles are exchanged. The phase is determined by the physical laws governing the system. Some examples of the physical situations where anyonic phases might appear

are reviewed below. In the course of the past decades, it has been realized that there exists another possibility for quantum statistics in two dimensions, where the particle exchanges can not be represented by simple phase factors. Rather, a permutation of particles results in a non-trivial rotation of the wave function:

$$\big|\Psi_{2,1}\big\rangle = B\big|\Psi_{1,2}\big\rangle. \tag{1.3}$$

Thus, there exists a Hilbert space $\mathcal{H}_A$ with $\dim(\mathcal{H}_A) > 1$ that describes different particle configurations. The particles must be indistinguishable, so the states in this Hilbert space can not be distinguished by any local observable, and the states belong to the same superselection sector of the total Hamiltonian of the system. This kind of exotic quantum statistics is called non-Abelian braiding statistics, while the simpler case where $B = e^{i\varphi}$ is a phase factor is called Abelian statistics.

Non-Abelian quantum statistics is a hypothetical form of effective interactions in two spatial dimensions, where information is stored non-locally in the collective many-body state of identical particles. The information can be manipulated by exchanging (braiding) the particles. The idea of non-Abelian statistics arises from theoretical ideas in $(2+1)$-dimensional electromagnetism and (lattice) gauge theory.

One theoretical platform with non-Abelian statistics is the relativistic $(2+1)$-dimensional quantum electrodynamics with a non-Abelian symmetry group. It is described by the Chern-Simons action

$$I_{\mathrm{CS}} = \frac{k}{8\pi}\int_M \epsilon^{ijk}\mathrm{Tr}\big(A_i(\partial_j A_k - \partial_k A_j) + \frac{2}{3}A_i[A_j, A_k]\big) \tag{1.4}$$

where the coupling constant k is called *the level* of the theory, $\overline{A}$ is $SU(2)$-valued gauge field, and gauge invariance requires that k is quantized in integer values. The Chern-Simons term does not include a metric, which means that it is a generally covariant quantum field theory: all observables of the theory are topological invariants which remain unchanged under the action of any local operator. To find the quantum numbers of the theory, one can define the most general gauge-invariant observable, the Wilson loop. It is the trace in the representation R of the holonomy of connection A_i around an oriented closed curve C in the manifold M:

$$W_R(C) = \mathrm{Tr}_R P \exp\big(\int_C A_i dx^i\big). \tag{1.5}$$

The observable is then defined as the Feynman path integral

$$\int D\mathcal{A}\, e^{iI_{\mathrm{CS}}} \prod_{i=1}^{r} W_{R_i}(C_i) \tag{1.6}$$

where C_i are r oriented and non-intersecting *knots* on the three-manifold M. The union of these knots constitute *a link*, and the integral above can be viewed as the expectation value of the link or a partition function of M. Witten has shown that this expectation value is related to the Jones polynomial [10], which is a polynomial invariant used to classify classical knots and links. Moreover, the sources of the theory have anyonic statistics.

Non-Abelian anyons emerge also in the Drinfel'd quantum double construction [11]. There one considers a system which is invariant under some continuous non-Abelian symmetry group G. As the system enters the ground state, this symmetry is spontaneously broken to some discrete residual symmetry $H \subset G$ via the Higgs mechanism [12]. The force carriers acquire a mass and the fields are expelled from the bulk due to a sort of Meissner effect. There are thus no long-range interactions between the particles. The system has also topological excitations which are quantum numbers that are protected by a global symmetry. This quantum number is called a charge. In general, there are two kinds of irreducible representations (particles) in the theory: fluxes and charges. Together they can form dyonic combinations which have non-Abelian anyonic statistics.

Another platform where non-Abelian anyons are found is the conformal field theory describing the critical Ising model [13]. The excitations of this model have anyonic statistics, and they are generally called *Ising anyons*. The anyons studied in this thesis are Ising anyons, although in Chapter 4 more general $SU(2)_k$ anyons are also considered.

To this date there has been no conclusive evidence for the existence of non-Abelian anyons in experiments. Non-Abelian Ising anyons have been however long thought to exist at certain plateaus of the Fractional Quantum Hall Effect. Also quasiparticles called Majorana fermions have non-Abelian anyonic statistics [14]. Recently, strong evidence for the existence of Majorana fermions has been found in semiconductor nanowires coupled to s-wave superconductors [15].

1.1.1 Braiding and isotopy invariance

The permutation statistics of identical particles acquires new meaning when the particle exchanges are interpreted in a physical sense, such that each trajectory between points a and b in phase space is assigned an amplitude $K^\alpha(a,b)$. The Feynman path integral [16, 17] integrates the kernel K over all paths between a and b in the homotopy class $f_{ab}(\alpha)$. The overall probability amplitude is a weighted sum over the homotopy classes:

$$K(a,b) = \sum_\alpha \chi(\alpha) K^\alpha(a,b) \tag{1.7}$$

where the weight factors $\chi(\alpha)$ are given by (scalar) unitary representations of the fundamental group Π_1 [18]. The fundamental group $\Pi_1(M)$ records information about holes in a manifold M. Specifically, given a point on the manifold, the elements of the group correspond to equivalence classes of paths starting from the point, such that all paths in an equivalence class can be continuously deformed into each other without taking the path over holes. The group multiplication is given by adjoining paths from their final and initial points. If the particles are not allowed to coincide, the fundamental group of a three (spatial) dimensional manifold with N holes is isomorphic to the permutation group of N objects:

$$\Pi_1(M_3^N) \simeq S_N. \tag{1.8}$$

The configuration space of indistinguishable particles is the quotient space Y_N/S_N, where Y_N is the coordinate space of N distinguishable particles. In three dimensions, there are two unitary scalar representations of S_N: the trivial and the alternating representation, which is $+1$ for even permutations and -1 for odd permutations. The trivial representation corresponds to bosonic statistics and the alternating representation corresponds to fermionic statistics. Similar conclusions were drawn by Leinaas and Myrheim by considering parallel transport instead of path integrals [7]. Note that there exist also higher dimensional irreducible representations of S_N, and this other form of exotic quantum statistics is called parastatistics.

In two spatial dimensions, the picture changes. The 2-dimensional spatial manifold with holes is multiply connected, since trajectories can not be continuously deformed into each other without taking them over the holes. The fundamental group is now isomorphic to the Artin braid group:

$$\Pi_1(M_2^N) \simeq B_N. \tag{1.9}$$

The weight factors $\chi(\alpha)$ corresponding to different homotopy classes α are now given by representations of the braid group [19]. The elements B_i of the braid group correspond to different ways of tangling N strands with each other, the inverse elements B_i^{-1} correspond to the braids where each crossing in B_i is reversed, and the group multiplication is given by joining the outgoing ends of a braid B_i with the incoming ends of a braid B_j. The braid group is completely described by $N-1$ generators b_k which are just single crossings between adjacent strands k and $k+1$. Any element of the braid group can be given as a product of the generators: $B = b_i b_j \dots b_x$. The generators are constrained by the relations [20]

$$b_j\, b_k = b_k\, b_j, \qquad |j-k| \geq 2 \tag{1.10}$$

$$b_k\, b_{k+1}\, b_k = b_{k+1}\, b_k\, b_{k+1}. \tag{1.11}$$

That is, distant braids of two adjacent strands commute, while braiding of close by strands obeys a specific rule.

A convenient feature of the braid group is that it allows diagrammatic representations of the elements. The generators braid two adjacent strands:

$b_k \;\widehat{=}$ 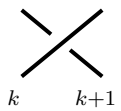

$b_k^{-1} \;\widehat{=}$ 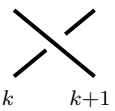

and multiplication of braids corresponds to stacking the diagrams on top of each other such that the ends of the strands coincide. The convention followed here is that time flows from the bottom of the page to the top, such that a braid $b_j b_k$ is represented by putting b_j on top of b_k in the diagram. These diagrams are very similar to those encountered in the study of links in the next section, and in fact there exists a mathematical relationship between the braid group and link invariants. Equations (1.10) and (1.11) can now be written using the diagrammatic representation as

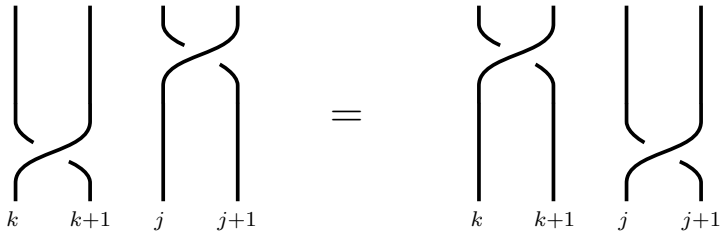

(1.12)

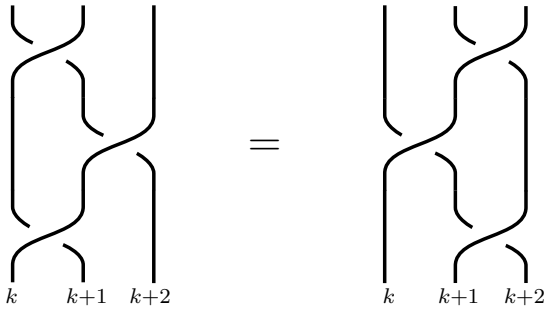

(1.13)

The first relation is just saying that if the strands touched by the generators b_k and b_j are distinct, the order of the braids is irrelevant. The second relation expresses the braiding rule when one of the strands is mutual. The diagrammatic representation of this rule shows that the second relation expresses the fact that strands can slide over crossings, as long as the initial braid can be deformed into the final braid without cutting any strands.

The invariance under continuous deformations of strands is called isotopy. In mathematics, the isotopy invariance can be studied using knot or link theory, where originally 3-dimensional links are projected on a plane, and the analysis concentrates on the planar diagrams of links. In knot theory, the goal is to construct isotopy invariants which take the same value for isotopic knots, regardless of the representation.

1.1.2 Link invariants

The study of knots and links has a long history in mathematics, and is still developing. In general, a knot can be defined as a particular embedding of a closed, nonintersecting curve in $\mathbb{R}^3$, and links are defined as nonintersecting unions of knots. If two knots can be deformed into each other via continuous moves such that the curve never intersects with itself, they are considered as equivalent, and called *ambient isotopic* to each other. Knots are usually studied using planar diagrams, two-dimensional projections of knots. Obviously, knots can have several different presentations as planar diagrams. The aim of knot and link theory is to define invariant quantities which are equivalent for all presentations of ambient isotopic knots and links. Ideally, these quantities should also be distinct for structures which are not ambient isotopic.

Remarkably, ambient isotopy is captured by four simple local moves on planar diagrams shown in Fig. 1.1. Reidemeister showed that two links are ambient isotopic to each other if and only if they can be deformed into each other using these moves [21], now known as Reidemeister moves. Each strand in these figures is taken to be

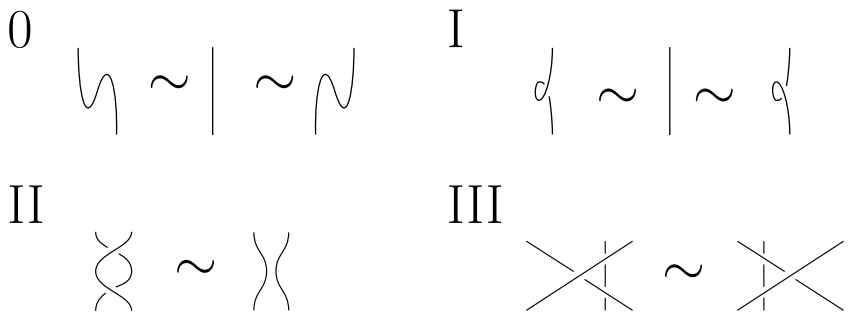

Figure 1.1: Reidemeister moves. For move I, there are also additional moves with the loop on the right side. For move II, there is also an additional move with both crossings reversed, and for move III one where the central crossing is reversed.

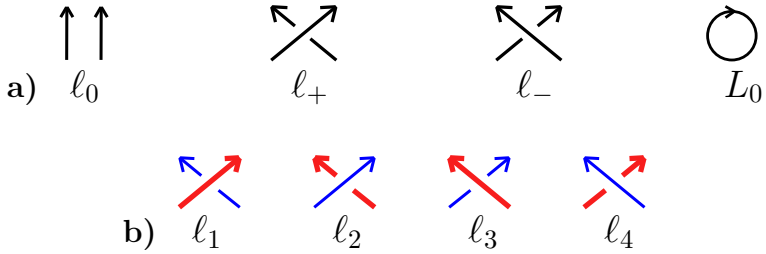

Figure 1.2: a) Elementary types of crossings ℓ_0, ℓ_+ and ℓ_-, and the trivial link L_0. Note that the two strands in the crossings may or may not belong to the same component. b) Elementary types of crossings between two distinct strands.

part of a larger diagram, so the endpoints and the angles at the endpoints must be assumed to be fixed during these moves. If two link diagrams are related via moves 0, II and III (but not I) they are called *regular isotopic* [22].

Each individual knot in a link is called a component. An oriented link is one where each curve has a preferred direction to it, indicated with an arrow. Two simple link invariants of oriented links are *the writhe* and *the linking number*. The writhe w of a link L is the difference between the number of positive and negative crossings:

$$w(L) = \#(\ell_+) - \#(\ell_-) \tag{1.14}$$

where the crossings ℓ_+ and ℓ_- are defined in Fig. 1.2a). Note that the writhe is not invariant under the Reidemeister move I, and thus it is an invariant of regular isotopy. The linking number counts how many times different components are wound with each other. It is defined as the sum over positive and negative crossings when the strands are distinct, divided by two. Using the crossings defined in Fig. 1.2b), it can be written

$$lk(L) = \frac{\#\ell_1 + \#\ell_2 - \#\ell_3 - \#\ell_4}{2}. \tag{1.15}$$

The linking number is an invariant of ambient isotopy.

Link invariants can also be defined via local surgery moves, which assign coefficients for different smoothings of a crossing in a link diagram. These moves are

generally known as skein relations. For example, the writhe and the linking number are determined by the respective skein relations as follows [23]

$$\ell_+ - \ell_- = 2 \tag{1.16}$$

$$\ell_+ - \ell_- = \begin{cases} 1, & \text{strands different} \\ 0, & \text{same strand} \end{cases} \tag{1.17}$$

The link invariants can be computed by forming the diagram for the link, and using the skein relations for each crossing. The result is a sum over links. By applying the skein relations and Reidemeister moves, each diagram can be deformed into the trivial link L_0. By defining $L_0 = 1$, one finally gets the number that is the value of the invariant for the link.

In the previous section it was mentioned that the generators of the Artin braid group allow a diagrammatic representation as crossings, just like the elementary crossings in link diagrams. In fact, a theorem by Alexander states that links may be represented by an element of the braid group [24]. A link is obtained from a braid by simply connecting the ends of the strands to each other. Such a process is called *the closure* of a braid B, and the link thus obtained is denoted $L(B) = (B)^{\mathrm{C}}$, where C is some scheme for connecting the ends of the strands. The most common scheme is the Markov closure where the first incoming strand is connected to the first outgoing strand, second to second, and so on.

The connection between links and braids was used by Jones to define a polynomial invariant of links, called the Jones polynomial [25]. It is given by the trace closure over the von Neumann algebra representation r_q of the braid B:

$$V_L(q) = (-(q+1)/\sqrt{q})^{n-1}\mathrm{Tr}(r_q(B)). \tag{1.18}$$

where the parameter $q \in \mathbb{C}$ and n is the number of strands. It is a Laurent polynomial in the variable $\sqrt{q}$:

$$V_L(q) = \sum_{i=-\infty}^{\infty} a_i \sqrt{q}^{\,i} \tag{1.19}$$

with integer coefficients and it is an ambient isotopy invariant of oriented links. It is the first link invariant to distinguish mirror images of links. The skein relations for the Jones polynomial are written

$$q^{-1}\ell_- - q\ell_+ = (\sqrt{q} - \sqrt{q}^{-1})\ell_0 \tag{1.20}$$

and the Jones polynomial of the trivial link is

$$V_{L_0} = 1. \tag{1.21}$$

Another invariant of regular isotopy is the Kauffman bracket [26]. It is defined by the relations

$$\ell_+ = A\ell_0 + A^{-1}\ell_0' \tag{1.22}$$

$$\big\langle L_0 \cup L \big\rangle = d\big\langle L \big\rangle; \quad L \neq \emptyset \tag{1.23}$$

$$\big\langle L_0 \cup \emptyset \big\rangle = 1 \tag{1.24}$$

where $d = -A^2 - A^{-2}$ and ℓ_0' is the (unoriented) crossing obtained from ℓ_0 by rotating it 90 degrees. These relations are applied repeatedly to smooth a link to a disjoint collection of loops and the result is a polynomial in A and A^{-1}. In Sec. 4.2 they are used to calculate the values of the Kauffman bracket explicitly. For a generic link diagram without the types of the crossings specified, a state S represents a particular choice for the directions of the crossings. The bracket polynomial can then be expressed as

$$\langle L \rangle = \sum_S \langle L|S \rangle d^{|S|-1} \tag{1.25}$$

where $\langle L|S \rangle$ is a polynomial in the parameter A, obtained from the link diagram corresponding to choice S by using the skein relations, and $|S|$ is the number of components in the diagram of choice S. The bracket polynomial is an invariant of unoriented links. Although it is not an invariant of ambient isotopy, it can be normalized via the writhe to yield the Jones polynomial. By introducing an orientation to a link L, the Kauffman bracket and the Jones polynomial are related via

$$\langle L \rangle(A)|_{A \to q^{-1/4}} = (-q^{1/4})^{-3w(L)}\, V_L(q) \tag{1.26}$$

$$V_L(q)|_{q \to A^{-4}} = (-A)^{-3w(L)}\, \langle L \rangle(A). \tag{1.27}$$

and the correspondence between the parameters of the Jones polynomial and the Kauffman bracket is $A = q^{-1/4}$.

1.1.3 Representation theory of non-Abelian anyons

The existence of non-Abelian anyons arises from some residual global symmetry in the ground state of the parent system. The quantum numbers induced by such a symmetry are topological, which means that they are preserved under the action of any local operator. The information contained in these quantum numbers can be manipulated by operating on the topological states of the system. Concretely this is done by braiding anyons around each other.

The addition of the topological quantum numbers does not follow the usual paradigm of quantum number algebra. The global symmetry imposes constraints on the possible values of the composite of two quantum numbers. The addition of topological quantum numbers is called fusion algebra, and it is described formally by fusion tensors N. The fusion tensors include information about the symmetry, and they label the possible fusion outcomes of the composite charge c when the charges a and b are fused: [27]

$$a \times b = \sum_c N_{ab}^c c. \tag{1.28}$$

Equations like this are called the fusion rules of the theory. Fusion of Abelian anyons is always trivial in the sense that the fusion channels are unambiguous and N is non-zero for only one value of c. The fusion rules arise from the underlying symmetry of the system, and they define *anyon models*. The braiding statistics of non-Abelian anyon models is completely determined by these fusion rules. The fusion outcomes give rise

to a collective Hilbert space for the two charges. The states of this space can be labeled as $|c, \mu\rangle$, where c is the composite charge, and μ labels the number of ways to combine a and b to get total charge c. For the most common anyon models $N_{ab}^c = 1$ and the degeneracy index is redundant. The collective many-body Hilbert space is called *the fusion space* and is denoted $\mathcal{H}_{\mathrm{F}}$.

The total Hilbert space size for N_A anyons can be calculated from the fusion rules:

$$\dim(\mathcal{H}_{\mathrm{F}}) = N_{a_1 a_2}^{c_1} N_{c_1 a_3}^{c_2} N_{c_2 a_4}^{c_3} \cdots N_{c_{N_A-2} a_{N_A}}^{c_{N_A-1}} \tag{1.29}$$

where Einstein summation convention is assumed. The non-local fusion Hilbert space does not admit a tensor product decomposition in terms of Hilbert spaces of individual charge labels. Instead, it grows as $\dim(\mathcal{H}_{\mathrm{F}}) \propto d^{N_A}$, where d is called *the quantum dimension*. The quantum dimension is not necessarily an integer, and it is a characteristic quantity of particular anyon models. For example, the quantum dimension of Ising model anyons is $d = \sqrt{2}$.

As mentioned above, the particle exchange operators for N_A anyons must be representations of the braid group B_{N_A}. In addition, the exchange operators must respect the global symmetry of the system. In summary, one is looking for unitary solutions to the quantum Yang-Baxter equation: [22]

$$R_{12} R_{13} R_{23} = R_{23} R_{13} R_{12}. \tag{1.30}$$

where R_{ij} denotes the exchange of labels i and j. The solutions of the quantum Yang-Baxter equation also satisfy the Artin braid group relation (1.11). The solutions are obtained via quasi-triangular Hopf algebras, also known as quantum groups, as introduced by Drinfel'd [11].

The representations of the braiding matrices are most easily understood via diagrams. A fusion state $|a \times b \to c\rangle$ can be represented by a vertex with two incoming indices and one outgoing index, and the matrix R_{ab}^c implements a braid:

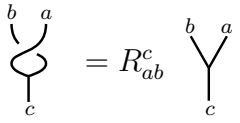

(1.31)

(strictly speaking, the lines should have orientations, but when the charges are self-conjugate the orientations can be omitted). The state of N_A particles is represented by fusing two particles to get the fusion outcome c_1, fusing the third particle with c_1 to get c_2, fusing the fourth with c_2, and so on. The intermediate charges $\{c_j\}$ are the quantum numbers which span the fusion Hilbert space: $\mathcal{H}_{\mathrm{F}} = \mathrm{span}\{c_j\}_{j=1}^{N_A-1}$, and the order in which the anyons are fused can be regarded as a choice of basis. A change of basis can be done via so called F-moves:

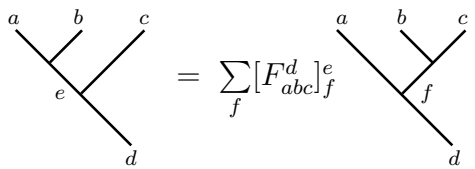

(1.32)

where degeneracy labels μ have been omitted for clarity. (the F-tensor should not be confused with the coin flip matrix F used throughout this thesis). The basis choice on the left-hand side of Eq. (1.32) is known as the standard basis. The F-moves could be viewed as deformations of the $6-j$ symbols for ordinary $SU(2)$ angular momentum. The R and F tensors are completely determined by the fusion rules of the theory. They can be derived using consistency conditions known as pentagon and hexagon equations [27, 28]. The representation for the exchange of any particle labels c_i and c_j can then be constructed by using the F-moves to bring these labels together, using the R-matrix to exchange them, and reverting the F-moves.

Most results in this thesis are derived for *Ising anyons*. The charges of this anyon model are 1, σ and ψ. The fusion rules are

$$1 \times \{1, \sigma, \psi\} = \{1, \sigma, \psi\}, \quad \sigma \times \sigma = 1 + \psi, \quad \psi \times \psi = 1. \tag{1.33}$$

and the non-trivial F and R matrices are [29]

$$F^{\sigma}_{\sigma\sigma\sigma} = \frac{1}{\sqrt{2}} \begin{pmatrix} 1 & 1 \\ 1 & -1 \end{pmatrix} \tag{1.34}$$

where the first column/row corresponds to 1 and the second to ψ, and

$$[F^{\psi}_{\sigma\psi\sigma}]^{\sigma}_{\sigma} = [F^{\sigma}_{\psi\sigma\psi}]^{\sigma}_{\sigma} = -1 \tag{1.35}$$

$$R^{1}_{\sigma\sigma} = e^{-i\frac{\pi}{8}}, \quad R^{\psi}_{\sigma\sigma} = e^{i\frac{3\pi}{8}}, \quad R^{1}_{\psi\psi} = -1 \tag{1.36}$$

$$R^{\sigma}_{\sigma\psi} = R^{\sigma}_{\psi\sigma} = -i. \tag{1.37}$$

The quantum dimensions are $d_1 = d_\psi = 1$, $d_\sigma = \sqrt{2}$.

In Chapter 4 the anyons are spin-1/2 irreducible representations (irreps) of the quantum groups $SU(2)_k$, parametrized by the integer k called the level. These are the anyons which arise in the Witten-Chern-Simons theory [10]. The charges of the theory are $\{0, \frac{1}{2}, 1, \ldots, \frac{k}{2}\}$, and the fusion rules satisfy the triangle inequality and integer sum condition as in $SU(2)$:

$$j_1 \times j_2 = \sum_{j=|j_1-j_2|}^{j_1+j_2} j$$

but with two restrictions on the total spin charge j:

$$j \leq k/2; \quad j_1 + j_2 + j \leq k.$$

The non-trivial R and F tensors for $SU(2)_k$ anyons are [29]

$$F^{\frac{1}{2}}_{\frac{1}{2}\frac{1}{2}\frac{1}{2}} = \frac{1}{[2]_q} \begin{pmatrix} 1 & \sqrt{[3]_q} \\ \sqrt{[3]_q} & -1 \end{pmatrix} \tag{1.38}$$

$$R^{0}_{\frac{1}{2}\frac{1}{2}} = -e^{-i\frac{3\pi}{2(k+2)}}, \qquad R^{1}_{\frac{1}{2}\frac{1}{2}} = e^{i\frac{2\pi}{4(k+2)}} \tag{1.39}$$

where the so called quantum integers are given by

$$[n]_q = \frac{q^{n/2} - q^{-n/2}}{\sqrt{q} - 1/\sqrt{q}}, \qquad q = e^{i\frac{2\pi}{k+2}}. \tag{1.40}$$

For the special case k=2, the R and F tensors become

$$F^{\frac{1}{2}}_{\frac{1}{2}\frac{1}{2}\frac{1}{2}} = \frac{1}{\sqrt{2}} \begin{pmatrix} 1 & 1 \\ 1 & -1 \end{pmatrix} \tag{1.41}$$

$$R^0_{\frac{1}{2}\frac{1}{2}} = -e^{-i\frac{3\pi}{8}}, \qquad R^1_{\frac{1}{2}\frac{1}{2}} = e^{i\frac{\pi}{8}}. \tag{1.42}$$

Note that the case k=2 is closely related to the Ising model, since $F^{\frac{1}{2}}_{\frac{1}{2}\frac{1}{2}\frac{1}{2}} = F^{\sigma}_{\sigma\sigma\sigma}$ and $R^*_{\frac{1}{2}\frac{1}{2}} = -iR_{\sigma\sigma}$ where the star denotes complex conjugation. Thus up to phase factors and complex conjugation, the Ising and $SU(2)_2$ models act similarly under braiding of spin-1/2 irreps with charge correspondence $\{1, \sigma, \psi\} \mathrel{\widehat{=}} \{0, \frac{1}{2}, 1\}$.

1.1.4 AJL algorithm

Apart from being a delicate theoretical construction, non-Abelian quantum statistics might have applications in quantum computing. The braiding of anyons induces matrix valued transformations in the wave function, which could be seen as quantum gates in the circuit model of quantum computing. The fusion Hilbert space of non-Abelian anyons could thus be used to encode quantum information, and the information could be manipulated by braiding anyons around each other. The fusion space is a very favourable place to store information: the size of the Hilbert space grows exponentially as a function of the number of particles, so that large quantities of information can be represented by a moderate number of particles. Moreover, the states are protected by a global symmetry, such that local perturbations can not change the state of the system. This property makes topological systems robust against interactions with the environment, which are the biggest challenge in realizing quantum computing in more conventional systems.

An explicit quantum algorithm for anyonic systems has recently been constructed by Aharonov, Jones and Landau (AJL) [30–32]. It approximates the Jones polynomial of links at any primitive root of unity, $q = e^{i2\pi/k}$. This approximative algorithm scales polynomially in the number of strands, crossings and k, while the best exact classical algorithm scales exponentially [33]. The algorithm was also extended to approximate the Tutte polynomial, with the Jones polynomial as a special case [34]. The connection between topological systems and link invariants was first made by Witten [10], who showed that the skein relations of the Jones polynomial arise from the expectation value of the product of Wilson loops, with the value $q = e^{i\frac{2\pi}{k+2}}$ of the parameter in the Jones polynomial for deformations of the Lie group $SU(2)$. The computability of topological quantum field theories was further discussed in a series of papers by Freedman *et al* [35–38]. Their results implied that there exists an efficient quantum

algorithm to evaluate the Jones polynomial at $q = e^{i\frac{2\pi}{5}}$, but such an algorithm was not constructed explicitly.

The virtue of the AJL algorithm is that it allows the calculation of braid closures directly, without relying on formalism of field theories. Unitary representations of the braid group can be mapped to the so called Temperley-Lieb algebra, which can be used to define a trace. The trace maps elements of the Temperley-Lieb algebra to complex numbers, which are the values of the Jones polynomial. Since the trace over the Temperley-Lieb algebra satisfies the Markov property, it is unique and the trace is thus well defined. The trace of a unitary matrix can be approximated efficiently by the Hadamard test, which yields the algorithm to approximate the Jones polynomial at roots of unity.

The AJL algorithm provides a way to calculate the expectation values of unitary representations of the braid group using link polynomials. If the state $\big|\chi_0\big\rangle$ represents a configuration where N_A particles are created from the vacuum and $\mathcal{B}$ is a braid word which braids the particles, then the expectation value of $\mathcal{B}$ is related to the Jones polynomial as

$$\big\langle\chi_0\big|\mathcal{B}\big|\chi_0\big\rangle = \frac{(-q^{3/4})^{w(\mathcal{B}^{\mathrm{tr}})}}{d^{N_A-1}} V_{\mathcal{B}^{\mathrm{tr}}}(q) \tag{1.43}$$

where $\mathcal{B}^{\mathrm{tr}}$ is the link obtained from the braid word $\mathcal{B}$ via closure defined by the state $\big|\chi_0\big\rangle$, and w is the writhe. The importance of this relation must be emphasized, as most results in this thesis rely on it. The connection to the probability distribution of the anyonic quantum walk is discussed in Sec. 2.3.

1.2 Quantum Walks

With the rise of quantum information science, quantum walks have emerged as a simple model that provides a platform for investigating dynamical quantum effects. The simplicity of the model allows to keep complete account of degrees of freedom during time evolution and the models can be often solved analytically to get the asymptotic behaviour of several quantities. It can also be used to construct quantum algorithms. One of the best features of the quantum walk model is that there is a corresponding classical model, the random walk, which provides a reference point for comparing differences between classical and quantum systems in motion. Most notably, the performance of quantum systems in algorithmic applications almost always supersedes that of classical systems.

The random walk is a simple model in probability theory and computer science which can be used for studying algorithms and queueing theory, for example. Random walk is a kind of cellular automaton where the system is described by a set of nodes, one or more of the nodes occupied by a moving object called the walker, and the system evolves in discrete time steps according to some transition rule. The nodes are connected by edges which define the neighbour sites where the walker is allowed to move. Each edge is assigned a transition probability which determines the probability for moving between connected sites during a single time step. By its definition, the random walk is a Markov process: the next state of the system depends only on the

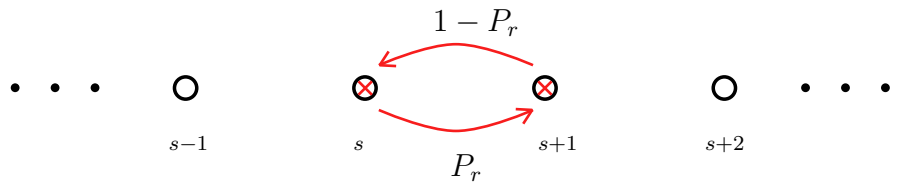

FIGURE 1.3: The classical random walk on a line. Circles represent the nodes that the walker can occupy. P_r is the probability that the walker (red cross) at site s at time instant t moves to $s+1$ at time $t+1$. Conservation of total probability requires that the probability to move left is $1-P_r$.

present state and the transition rule, not past states of the system. A schematic picture of random walk dynamics is given in Fig. 1.3. When the state space (nodes) is discrete, random walks are also called Markov chains, sequences of random variables ordered in time, the random variable being the position of the walker at each time step. In physics, random walks are widely used to describe Brownian motion in fluids and gases.

The coin flips in random walks are sequences of Bernoulli trials, where the probability of each outcome is constant for each trial. The position s of the walker is a random variable, which is distributed according to the binomial distribution. When the probabilities for each outcome are equal, the walk is said to be symmetric or unbiased, and the probability to be at site s at time t can be written [39]

$$p_{\mathrm{RW}}(s,t) = \frac{1}{2^t}\binom{t}{H_s} \tag{1.44}$$

where H_s is the number of right-moves needed to reach the site s in t time steps, starting from the initial site s_0. Random walks can be characterized by various quantities, such as the probability to return to the origin and the probability of last visit to the node. In this thesis, the probability distributions are characterized by how spread out they become in course of time. This property can be quantified by *the variance* of the distribution as defined below.

The idea of a quantum version of random walks was initiated by Aharonov, Davidovich and Zagury [40]. They imagined the quantum walk as a discrete process where a particle is moving in space, with an additional degree of freedom called *the quantum coin*. The quantum coin could be any physical degree of freedom belonging to a particle if it can be used to construct a basis, such as the z component of the particle spin. The coin basis elements represent different outcomes of a coin flip, for example heads and tails can correspond to eigenstates of spin up and spin down. The quantum coin is measured at discrete time intervals, and the motion of the particle is coupled to the coin such that measurement outcome up (down) indicates that the particle has moved right (left). If the wave packet describing the particle is initially centered at x_0, its state can be written $|\Psi\rangle = |\psi(x_0)\rangle\big(c_0|0\rangle + c_1|1\rangle\big)$ where 0 and 1 label the coin outcomes. The state evolves according to the time evolution operator $U = \exp(-iS_zPl/\hbar)$ to $|\Psi'\rangle = c_0|\psi(x_0-l)\rangle|0\rangle + c_1|\psi(x_0+l)\rangle|1\rangle$, where S_z is the spin operator (generator of rotations) and P is the momentum operator (generator of translations). After the

measurement, the coin state is reset to the initial state, and the process is repeated t times. If the initial wave packet is Gaussian, the dynamics sees the wave packet shift and change its shape in time. Perhaps the most interesting feature of the quantum walk of Aharonov *et al* is that for some values of the parameters the wave packet shifts by an amount which is larger than the maximum classically allowed value.

Quantum walks can also be formulated as decision trees [41, 42]. In this model, the wave packet is initially localized at a certain node. This node branches into two separate nodes such that the walker has a certain probability of ending up on either node. Similarly, as time passes each node branches into two new ones at constant time intervals. The system evolves continuously in time, governed by a Hamiltonian that gives the transition amplitudes between the nodes. This model does not include a coin degree of freedom at all. For some tree structures the classical algorithm takes a time exponential in the number of elementary time steps to reach a certain node, but the quantum algorithm can reach the same node in polynomial time. Another model that is closely related to quantum walks is the quantum cellular automaton as defined by Meyer [43]. There space consists of discrete cells, and a transition rule defines the evolution of a field ϕ defined on the cells. This model can be formulated as a lattice gas where a particle jumps between lattice sites. Meyer proves that in one dimension there exists no nontrivial, homogeneous, local, scalar quantum cellular automaton. To define a unitary QCA, Meyer relaxes the homogeneity condition, whereas in coined quantum walks the scalar condition is relaxed.

In a certain sense, the Feynman path integral method [16, 17] is also a type of quantum walk. The path sum method gives the transition amplitude between two space-time points as a sum over all possible paths, each path weighted by their classical action. At each discrete time interval ϵ, the particle can move left or right, and between the time intervals the particle propagates at the speed of light. The path sum becomes the path integral by passing to the continuous limit of space and time. In fact, as shown in the next section, the transition amplitudes for the discrete-time coined quantum walk can also be expressed as a sum over paths of constant length. In that case, each path is weighted by a product of coin terms.

The most studied quantum walk presently is perhaps the discrete-time quantum walk on graphs [44, 45], described in the next section. The anyonic quantum walk presented in the next chapter is also a variant of this walk. For reviews on the theory of quantum walks the reader is directed to Refs. [46–48].

1.2.1 Discrete-time quantum walk in one dimension

The one-dimensional anyonic quantum walk is defined as a discrete-time and discrete-space quantum walk on a line. The non-anyonic version of this walk was analyzed by Ambainis *et al* [44], who introduced the coin operator F which acts on the coin degree of freedom at each time step, after the state of the coin is measured. The time evolution of the combined space-coin system is then unitary. Ambainis *et al* [44] solved the wavepacket dynamics in the absence of boundaries and for absorbing boundaries,

using the Hadamard operator as the coin flip operator:

$$F = \frac{1}{\sqrt{2}} \begin{pmatrix} 1 & 1 \\ 1 & -1 \end{pmatrix}. \tag{1.45}$$

This walk is known as the Hadamard walk. The walker starts initially localized at some site s_0 at time instant $t = 0$. In the case of infinite lattice, the expected distance from the initial site is linearly proportional to t the number of time steps, in contrast to classical random walks where the expected distance is proportional to $\sqrt{t}$.

Aharonov *et al* [45] analyzed a similar discrete-time model on finite graphs with arbitrary vertex degrees (number of edges going out from a vertex), and arbitrary coin flip operators. Their model is defined as a quantum Markov chain, when the position of the particle at a given time step is interpreted as a random variable. The time evolution of the probability distribution on the nodes of the graph does not tend to any limiting distribution. They show however that the time average of the probability distribution always tends to a limiting distribution. The limiting distribution depends in general on the initial state and the eigenvectors of the time evolution operator, but if all the eigenvalues of the time evolution operator are distinct, then the limiting distribution is uniform on the nodes.

The quantum walk on the line is defined by the unitary time evolution operator U and initial state $\big|\Psi(0)\big\rangle$. The time evolution operator propagates the wave function forward in time by one time step: $\big|\Psi(t+\Delta t)\big\rangle = U\big|\Psi(t)\big\rangle$, and for simplicity the unit of time is set as $\Delta t = 1$. The total Hilbert space, $\big|\Psi\big\rangle \in \mathcal{H}_{\mathrm{QW}}$, is the composite space of spatial and coin spaces: $\mathcal{H}_{\mathrm{QW}} = \mathcal{H}_{\mathrm{S}} \otimes \mathcal{H}_{\mathrm{C}}$. On an N-site lattice, the spatial space is spanned by N position basis vectors: $\mathcal{H}_{\mathrm{S}} = \mathrm{span}\{\big|s\big\rangle\}_{s=1}^{N}$, and the coin space is spanned by two basis vectors: $\mathcal{H}_{\mathrm{C}} = \mathrm{span}\{\big|0\big\rangle, \big|1\big\rangle\}$. The position states can be thought as the eigenstates of an abstract position operator, $S\big|s\big\rangle = e_s\big|s\big\rangle$, and the coin states can be thought as the eigenstates of some physical two-dimensional degree of freedom of the particle, such as spin, $C\big|c\big\rangle = e_c\big|c\big\rangle$, although these operators are not usually defined.

The transformation rule for a single time step is depicted in Fig. 1.4. First, the $\big|s\big\rangle\big|c\big\rangle$-component of the wave function, $\psi(s,c,t) = \big(\big\langle s\big|\big\langle c\big|\big)\big|\Psi(t)\big\rangle$, moves into a superposition: $\psi(s,c,t) \to u_{0c}\,\psi(s,0,t) + u_{1c}\,\psi(s,1,t)$. This action can be represented by a coin flip matrix

$$F = \begin{pmatrix} u_{00} & u_{01} \\ u_{10} & u_{11} \end{pmatrix} \tag{1.46}$$

such that the action of the coin flip operator on the wave function is

$$\big|\Psi(t)\big\rangle \to \big(\mathbb{I}_{\mathrm{S}} \otimes F\big)\big|\Psi(t)\big\rangle \equiv \mathcal{F}\big|\Psi(t)\big\rangle. \tag{1.47}$$

Next, the position becomes correlated with the coin, such that outcome 0 shifts the walker to the left and 1 shifts the walker to the right:

$$\big|\Psi(t+1)\big\rangle = \big(T^{-}P_0 + T^{+}P_1\big)\big|\Psi(t)\big\rangle \equiv \mathcal{S}\big|\Psi(t)\big\rangle \tag{1.48}$$

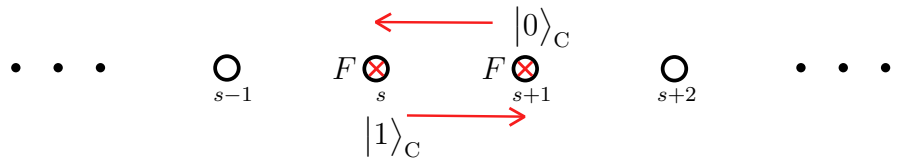

Figure 1.4: The discrete-time and discrete-space quantum walk model in one dimension. The coin flip operator F acts first on the coin degrees of freedom. Then the 0-component of the wave function at each site shifts left and the 1-component shifts right.

where the translation operators $T^{\pm}$ and the projectors to coin states are

$$T^{+} = \sum_{s=1}^{N-1} |s+1\rangle\langle s| \otimes \mathbb{I}_C \tag{1.49}$$

$$T^{-} = \sum_{s=1}^{N-1} |s\rangle\langle s+1| \otimes \mathbb{I}_C \tag{1.50}$$

$$P_c = \mathbb{I}_S \otimes |c\rangle\langle c|. \tag{1.51}$$

A single time step of the walk is then given by $|\Psi(t+1)\rangle = U|\Psi(t)\rangle = \mathcal{S}\mathcal{F}|\Psi(t)\rangle$ and the wave function at time step t is obtained by repeated applications of U:

$$|\Psi(t)\rangle = U^t|\Psi(0)\rangle. \tag{1.52}$$

Note that the shift operator $\mathcal{S}$ is not unitary at the boundaries. This can be fixed by redefining the shift operator as $\mathcal{S} + T_{\mathrm{BC}}$, where T_{BC} is a boundary condition term. By choosing the boundary conditions in a suitable way, the total evolution becomes unitary. Details of boundary conditions are discussed in Sec. 2.4.1.

The full solution of the dynamics of the walk requires diagonalization of U. If the coin operators are identical on every site, the walk is translationally invariant and diagonalization can be done by moving to the momentum basis by taking the Fourier transform. Anyonic walks are not in general translationally invariant which complicates solution. The full solution is not obtained here, but instead the analysis concentrates on the time evolution of the spatial probability distribution of the walker. The information about the spatial degrees of freedom is carried by the reduced density matrix of the position space ρ_S, which is obtained from the total pure state density matrix $|\Psi\rangle\langle\Psi|$ by tracing out all other than spatial degrees of freedom. The density matrix of the position space after t time steps is

$$\rho_S(t) = \mathrm{Tr}_C\left(U^t\rho(0)(U^\dagger)^t\right) \tag{1.53}$$

where the initial state is $\rho(0) = |\Psi(0)\rangle\langle\Psi(0)|$, and the wave packet is localized at some initial position s_0: $|\Psi(0)\rangle = |s_0\rangle\big(\psi(s_0,0,0)|0\rangle + \psi(s_0,1,0)|1\rangle\big) \equiv |s_0\rangle|c_0\rangle$.

In the one-dimensional case, the time evolution operator U has transition elements only between adjacent sites. This means that for a bounded wave packet, there is a

maximal distance that the edges of the packet can propagate in a given time interval T, such that there exists a causal light cone. Also, the probability to be at site s at time t is given by interference of all probability amplitudes starting at some site s' at time instant $t-T$, and of all paths which lead from site s' to s in time interval T. This becomes concrete when the elements of the spatial density matrix are calculated explicitly:

$$\big(\rho_{\mathrm{S}}(t)\big)_{s,s'} = \big\langle s\big|\, \rho_{\mathrm{S}}(t)\, \big|s'\big\rangle \tag{1.54}$$

$$= \sum_{c} \big\langle s\big|\big\langle c\big|\, U^t\, \big|s_0\big\rangle\big|c_0\big\rangle\, \big\langle s_0\big|\big\langle c_0\big|\, (U^\dagger)^t\, \big|s'\big\rangle\big|c\big\rangle. \tag{1.55}$$

From the above formula, the spatial and coin states can now be treated separately. The coin amplitudes consist of repeated applications of the coin matrix F and projectors P_c:

$$\begin{aligned}\big\langle c\big|\, U^t\, \big|c_0\big\rangle &= \sum_{c_1=\{0,1\}} \dots \sum_{c_t=\{0,1\}} \big\langle c\big|\, P_{c_t} F P_{c_{t-1}} F \dots P_{c_2} F P_{c_1} F\, \big|c_0\big\rangle \\ &= \sum_{c_1=\{0,1\}} \dots \sum_{c_t=\{0,1\}} \big\langle c\big|c_t\big\rangle\big\langle c_t\big|F\big|c_{t-1}\big\rangle \dots \big\langle c_2\big|F\big|c_1\big\rangle\big\langle c_1\big|F\, \big|c_0\big\rangle,\end{aligned}$$

where the sums are taken over all coin outcomes at each time step. Each term is just a product of elements of the coin matrix F. The conditional shift operator $\mathcal{S}$ associates a shift T^- (T^+) to each coin outcome 0 (1), such that for each choice of coin outcomes $\{c_{t'}\}_{t'=1}^{t}$ there is a corresponding string of shift operators $T^{a_t}T^{a_{t-1}}\dots T^{a_2}T^{a_1}$, $a_{t'} \in \{-,+\}$. Changing the notation such that $a_{t'} \in \{0,1\}$ and $T^{a_{t'}} = \sum_s \big|s+2a_{t'}-1\big\rangle\big\langle s\big|$ allows to write

$$\begin{aligned}\big\langle s\big|\, U^t\, \big|s_0\big\rangle =& \big\langle s\big|\, T^{a_t}T^{a_{t-1}}\dots T^{a_2}T^{a_1}\, \big|s_0\big\rangle \\ =& \sum_{s_1}\dots\sum_{s_t} \big\langle s\big|s_t+2a_t-1\big\rangle\, \big\langle s_t\big|s_{t-1}+2a_{t-1}-1\big\rangle\, \big\langle s_{t-1}\big|s_{t-2}+2a_{t-2}-1\big\rangle \\ & \dots \big\langle s_3\big|s_2+2a_2-1\big\rangle\big\langle s_2\big|s_1+2a_1-1\big\rangle\big\langle s_1\big|s_0\big\rangle \\ =& \delta\big(s, s_0+2\sum_{t'=1}^{t} a_{t'} - t\big)\end{aligned}$$

where $\delta(\cdot,\cdot)$ is the Kronecker delta function. Observing the second line above, it is seen that the time evolution operator connects only sites $s_{t'}$ and $s_{t'}\pm 1$ between time steps $t'-1$ and t'. The last line shows that only the coin histories $\{a_{t'}\}_{t'=1}^{t} \equiv \overline{a}^t$ which satisfy $s = s_0 + 2\sum_{t'=1}^{t} a_{t'} - t$ are allowed in the transition matrix which connects positions s and s_0. Such coin histories correspond to paths which start at site s_0 at time $t'=0$ and end up at s_0 at time $t'=t$. From now on, the vector $\overline{a}$ is used as a synonym for the path of the walker (the t-index is dropped to simplify the notation). Each element of $\overline{a}$ indicates the direction of the walker at each time step, for example $\overline{a} = (00101)^T$ means that the walker goes left twice, then right, left and right.

Substituting the spatial and coin amplitudes to Eq. (1.54) gives the following compact formula for the elements of the spatial density matrix:

$$\begin{aligned}\big(\rho_{\mathrm{S}}(t)\big)_{s,s'} &= \sum_{\overline{a},\overline{a}'} \delta\Big(s, s_0 + 2\sum_{t'=1}^{t} a_{t'} - t\Big)\, \delta\Big(s', s_0 + 2\sum_{t'=1}^{t} a'_{t'} - t\Big) \\ &\quad \times \delta\big(a_t, a'_t\big)\, \mathcal{C}(\overline{a}, c_0)\, \mathcal{C}(\overline{a}', c_0)^* \\ &= \sum_{\substack{\overline{a}\rightsquigarrow s \\ \overline{a}'\rightsquigarrow s'}} \mathcal{C}(\overline{a}, c_0)\, \mathcal{C}(\overline{a}', c_0)^* \end{aligned} \tag{1.56}$$

where the abbreviation $\sum_{a_1=\{0,1\}} \sum_{a_2=\{0,1\}} \cdots \sum_{a_{t-1}=\{0,1\}} \sum_{a_t=\{0,1\}} \equiv \sum_{\overline{a}}$ has been used, and $\overline{a} \rightsquigarrow s$ means that the summation is done only over paths for which $s = s_0 + 2\sum_{t'=1}^{t} a_{t'} - t$ and $a'_t = a_t$ hold. Path $\overline{a}$ corresponds to ket evolution and path $\overline{a}'$ to bra evolution before the partial tracing is carried out. The coin terms are given by

$$\mathcal{C}(\overline{a}, c_0) = \big\langle a_t \big| F \big| a_{t-1} \big\rangle \ldots \big\langle a_2 \big| F \big| a_1 \big\rangle \big\langle a_1 \big| F \, \big| c_0 \big\rangle. \tag{1.57}$$

The condition $a'_t = a_t$ comes from tracing over coin degrees of freedom: $\sum_c \big\langle c \big| a_t \big\rangle \big\langle a'_t \big| c \big\rangle = \delta(a_t, a'_t)$. Eq. (1.56) expresses the elements of the spatial density matrix as sums over forward and backward paths $\overline{a}$ and $\overline{a}'$ (with some constraints on the paths), in other words it can be regarded as a path sum representation. An analogous expression will later be derived (see Sec. 3.1) for anyonic quantum walks, and in fact the treatment of coin degrees of freedom in anyonic quantum walks is identical to usual quantum walks.

The probability distribution across the sites is given by the diagonal elements of the spatial density matrix.

$$p(s,t) = \big(\rho_{\mathrm{S}}(t)\big)_{s,s} = \sum_{\overline{a},\overline{a}'\rightsquigarrow s} \mathcal{C}(\overline{a}, c_0)\, \mathcal{C}(\overline{a}', c_0)^* \tag{1.58}$$

where the abbreviation $\overline{a}, \overline{a}' \rightsquigarrow s$ means that the summation is done over all paths that satisfy $a_t = a'_t$ and $\sum_{t'=1}^{t} a_{t'} = \sum_{t'=1}^{t} a'_{t'} = (s - s_0 + t)/2$. This notation will be used throughout the thesis.

A particularly neat formula for the probability distribution at time t can be obtained by choosing the initial coin state $\big|c_0\big\rangle = \big|0\big\rangle$ and using the Hadamard coin given in Eq. 1.45. The coin elements are $\big\langle a_t \big| F \big| a_{t-1} \big\rangle = -\frac{1}{\sqrt{2}}$ if $a_t = a_{t-1} = 1$, and $\big\langle a_t \big| F \big| a_{t-1} \big\rangle = \frac{1}{\sqrt{2}}$ otherwise. The coin term in Eq. (1.57) takes the form

$$\mathcal{C}(\overline{a}, 0) = \frac{(-1)^{z(\overline{a})}}{2^{t/2}} \tag{1.59}$$

where $z(\overline{a}) = \sum_{t'=1}^{t-1} a_t a_{t+1}$ is the number of occurrences of two subsequent 1's in $\overline{a}$. Substituting in Eq. (1.58), the probability distribution for the Hadamard walk is

$$p(s,t) = \frac{1}{2^t} \sum_{\overline{a},\overline{a}'\rightsquigarrow s} (-1)^{z(\overline{a})+z(\overline{a}')}. \tag{1.60}$$

Because of this compact form, the Hadamard coin will be used in the anyonic quantum walk formalism. Note that the Hadamard walk is only symmetric for the initial states

$|c_0\rangle = (|0\rangle \pm i|1\rangle)\sqrt{2}$ (Hadamard coin is a real-valued matrix so real and complex parts of the wave function do not interfere), therefore choosing $|c_0\rangle = |0\rangle$ implies that the position distribution does not evolve symmetrically. The loss of generality by specifying initial state and the coin is not dramatic. Although the details of the position distribution depend on the initial state and the coin, relevant quantities such as the variance of the probability distribution are not sensitive to them.

The analysis of anyonic quantum walks concentrates mainly on the variance, which is the square of the expected distance from the initial site. The variance (or dispersion) is a measure of likelihood to find the walker far from the initial location. The random variable in quantum walks is the position s, and its variance is written

$$\sigma^2 = \langle (s - s_0)^2 \rangle = \langle s^2 \rangle - 2s_0 \langle s \rangle^2 + s_0^2 \tag{1.61}$$

where $\langle \cdot \rangle$ denotes the expectation value. When the variance is small, the probability of getting a value near the initial site s_0 is large. If the variance is large, the probability distribution $p(s)$ associated to the random variable s is spread out, and the probability of getting a value near s_0 is small. If s is distributed according to the discrete probability distribution $p(s,t)$ at time t, and the probability to get a value s_i is $p(s_i,t)$, the expectation value is the first moment of s: $\langle s \rangle = \sum_i p(s_i)s_i$. Similarly, by writing out the second moment of s the variance can be written

$$\sigma^2(t) = \sum_i p(s_i,t)s_i^2 - 2s_0 \sum_i p(s_i,t)s_i + s_0^2 \tag{1.62}$$

where s_i runs through N sites.

One of the qualitative differences between random walks and quantum walks is the time dependence of variance. The probability distribution of the symmetric random walk on the line is binomial, and the variance depends linearly on the number of time steps. The probability distribution of the discrete-time quantum walk is roughly uniform around the initial site with peaks close to the edges of the causal light cone, and the variance depends linearly on the square of the number of time steps [44]. To summarize,

$$\sigma^2_{\mathrm{RW}}(t) = t \tag{1.63}$$
$$\sigma^2_{\mathrm{QW}}(t) = C_2 t^2 + C_1 t + C_0. \tag{1.64}$$

with $C_2 > 0$. When the variance is quadratic in time, the walk is said to be *ballistic*, since any initially localized particle propagates away with a velocity that is close to the maximum allowed velocity. Linear dispersion is called *diffusive*, as the probability to find the particle close to its initial location is still highest, and the probability mass diffuses slowly out of the initial region. A third distinct behaviour is *localization*: the whole probability mass is frozen around the initial point and does not evolve in time. This implies that the variance stays constant in time, ie. there exists a constant C such that

$$\sigma^2(t) < C, \quad \forall t. \tag{1.65}$$

In general, there are different definitions for localization. In Chapter 5, dynamical localization is defined such that the probability falls off exponentially as a function

of the distance from the initial site. Another definition might be partial localization, which means that there is a finite probability to be at the initial site at the asymptotic limit $t \to \infty$, but this definition is not used here.

1.2.2 Decoherence in quantum walks

One of the hallmarks of the quantum walk from a theoretical viewpoint is that it provides a simple yet untrivial platform for investigating differences between classical (statistical) dynamics and quantum dynamics. Unitary quantum dynamics is memory preserving, and the system dynamics is dependent on the initial state. One might then ask what are the conditions under which quantum dynamics becomes classical dynamics, where systems evolve stochastically and information about past states of the system disappears eventually.

Decoherence in quantum walks refers generally to any non-unitary dynamics of the composite space and coin system [49]. The state of the system goes from a pure to a mixed state, described by a density matrix ρ_{QW}. The time evolution of the initial density matrix $\rho_{\mathrm{QW}}(0)$ to $\rho_{\mathrm{QW}}(t)$ is given by a completely positive map, the superoperator $\mathcal{E}$, expressed in terms of the Kraus generators E_j:

$$\rho_{\mathrm{QW}}(t) = \mathcal{E}\big(\rho_{\mathrm{QW}}(0)\big) = \sum_j E_j \rho_{\mathrm{QW}}(0) E_j^\dagger. \tag{1.66}$$

If the system interacts with an environment and the total evolution of the system and environment is unitary, the index j runs over the environment degrees of freedom.

Decoherence processes can be modeled in numerous ways. Usually one is interested in the average distribution, sampling over a range of random parameters. Mackay *et al* [50] investigated the average distribution in one and two dimensions numerically, when the coin operator is a random unitary deformation of the Hadamard coin. They observed classical diffusive behaviour, with the average distribution approaching the binomial distribution. Brun et al [51, 52] studied decoherent quantum coins from a more general point of view, constructing the superoperator when the coin is subject to measurement with probability p at each time step. If the coin is measured at each time step, the variance of the distribution is equal to the classical random walk variance. For smaller p, the variance is initially quadratically dependent on number of time steps, but tends to linear behaviour, with the coefficient inversely proportional to p.

The time evolution of the walk does not always have to be non-unitary for the dynamics to become classical-like. If the coin flip operator is changed at every time step, the distribution resembles the random walk distribution and the variance depends linearly on the number of time steps [53]. In general, the effect of decoherence is that it mixes the phase relations between quantum states in such a way that quantum interference effects are erased. Decoherence can be seen as the theoretical mechanism for transition from quantum to classical behaviour. The physical origin of decoherence are interactions between the system and the environment: when the system is coupled to the environment, the interactions cause entanglement between the system and the environment and the system can no longer be described as a pure state. As shown

in Sec. 2.4.2, the anyonic fusion degrees of freedom can be seen as an environment for the space and coin system, and the anyonic quantum walk can be interpreted as a decoherent quantum walk.

Perhaps surprisingly, decoherence can also serve to speed up processes in quantum dynamics. Kendon and Tregenna [54] found that a small amount of decoherence speeds up the mixing time on a cyclic graph and the hitting time on hypercube. A review of decoherence effects in quantum walks can be found in Ref. [49]. Recently, the effects of disorder in quantum systems have also been investigated in the literature. These results are discussed in Chapter 5.

2
Anyonic Quantum Walk

The anyonic quantum walk [55] is a modification of the one-dimensional discrete-time quantum walk of Ambainis *et al* [44]. The motivation for this model is to understand the effect of pure braiding interactions of anyons in motion. The braiding interactions induce non-local correlations between anyons, protected by a global symmetry of the wave function. The single-particle anyonic quantum walk describes the time evolution of a single anyon wave packet when the motion of the anyon is coupled to an ancillary degree of freedom called the quantum coin. As time evolves, the walker anyon exhausts all the possible paths between the initial and starting point, ending up at site s at time instant t with probability $p(s,t)$. As a consequence of non-trivial quantum statistics in two dimensions, this probability depends on the mutual statistics of the mobile anyon and other anyons in the system, if the mobile anyon is allowed to circumvent them. The other anyons in the system are taken to be localized with frozen dynamics, in other words they have a definite location in space and do not move during the time evolution of the walk. This motivates to think of them as background anyons.

It should be emphasized that the anyonic quantum walk model captures only the non-local braiding interactions of anyons. Additional interactions such as Aharonov-Bohm phases or close-range interactions between the particles are not considered, so it is a toy model which might describe the essential physics in some situations. One possible application of the theory presented here could be in the multipoint contact version of the Fabry-Perot type Fractional Quantum Hall interferometer. This possibility is discussed in Sec. 2.5.

From the perspective of quantum walks, the anyonic quantum walks provide a tool to investigate novel types of decoherence mechanisms. The anyonic fusion Hilbert space can be seen as an environment of the quantum walk Hilbert space that consists of space and coin. This environment is non-local and its dynamics is strongly correlated with the quantum walk system. As the total evolution of the state is unitary, the environment can have an infinitely long memory, and the system and the environment

remain entangled for the whole evolution of dynamics.

The purpose of this chapter is to introduce the discrete-time anyonic quantum walk and highlight some of its features. The definition of the model is given in Sec. 2.1. The construction of representations of the braid generators is discussed in Sec. 2.2, and calculation of the probability distribution using link invariants is discussed in Sec. 2.3. Section 2.4 presents some results on finite graphs and discusses the role of decoherence in anyonic quantum walks. A possible implementation of the anyonic quantum walk in Fractional Quantum Hall systems is given in Sec. 2.5.

2.1 Quantum walk model

The anyonic quantum walk describes the discrete time evolution of a particle moving on a lattice of spatial sites. Between each spatial site, there is an additional anyon such that the moving anyon braids with these anyons as it hops between the lattice sites. The positions of the additional anyons can be thought to form a dual lattice, the sites on the dual lattice are called *islands*, and the anyons placed on the islands are called *stationary anyons*. Importantly, the walker anyon can never go inside an island and interact with the stationary anyons in close range. A close range interaction would lift the degeneracy of the state and destroy the non-local information about the particle configuration. The results presented here are therefore valid in cases where the distances between the particles are significantly larger than their localization lengths, and the interactions between the particles are purely statistical braiding interactions. Although only one-dimensional lattices will be considered in what follows, it is necessary to think about the anyons as existing in two dimensions, such that the walker can encircle an island without crossing it.

The special case where all anyons are of the same type, and there is only stationary anyon on each island is called a *uniform* configuration of charges. The models studied in chapters 3 and 4 are uniform. The general case where anyon types or occupation numbers of the islands are different are called *disordered* charge configurations, studied in Chapter 5.

The setup for the anyonic quantum walk scheme is depicted in Fig. 2.1. It is very similar to the usual one-dimensional discrete-time quantum walk setup described in Sec. 1.2.1, except one has to define which way the walker passes the island. In Fig. 2.1, the walker always passes the island from above if it is going left and from below if right. Therefore, there is a preferred direction for the motion of the particle, and the model is called chiral. This choice of direction facilitates calculations, but a more realistic model would take both directions into account. However, the chiral model should capture the essential dynamics of the system, and all the results obtained for it are expected to hold also for non-chiral models. This assumption is supported by results in Sec. 5.3.2, where a continuous-time Hamiltonian model for anyonic walks is discussed. This model is non-chiral, and the variance of this walk is linear in the number of time steps just like in the chiral model.

As explained in Sec. 1.1.3, a braid generator b_k represents a counterclockwise braid of anyons labelled k and $k+1$. In principle, the positions of the anyons are exchanged

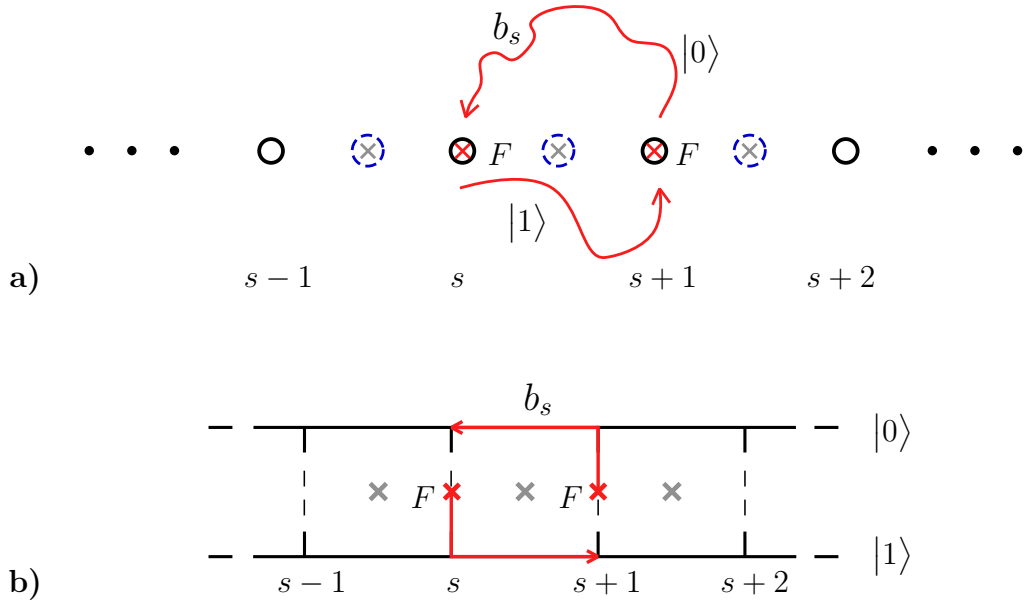

Figure 2.1: Anyonic discrete-time quantum walk model. The red and grey crosses represent the walker and stationary anyons, respectively. States $|0\rangle$ and $|1\rangle$ are the coin states and b_s is the generator that braids anyons s and $s+1$. a) Schematic drawing of the dynamics during a single step of the anyonic quantum walk. After the coin flip F, the coin state is in superposition and the component 0 travels left, passing the stationary anyon from above, and the component 1 travels right, passing the stationary anyon from below. The sites which the walker can occupy are drawn as solid circles and the islands on the dual lattice which the stationary anyons occupy are drawn as dashed circles. Since the system is assumed to be topological, only the direction in which the walker passes the island is relevant, not the details of the path. b) A setup equivalent to a), but now the coin state is represented as another spatial degree of freedom. The coin flip matrix F can be viewed as a tunneling matrix describing the hopping amplitudes between the upper and lower edges at discrete locations. Each edge is associated with a unique direction of motion, such that ending up in coin state $|0\rangle$ ($|1\rangle$) implies that the walker travels left (right). This scheme can be naturally extended to an experimental setup in Fractional Quantum Hall Systems as discussed in Sec. 2.5.

such that after the braid anyon k has moved to position of anyon $k+1$ before the braid and vice versa. In Fig. 2.1, however, the braid generator b_s is associated with the walker moving between sites s and $s+1$ and the stationary anyon staying in its original place, so strictly speaking their positions are not exchanged during each braid. Since the system is topological, this is not relevant, because after the walker has hopped from site s to $s+1$ for example, the configuration is topologically equivalent to the configuration where the final positions are shifted to the left by one lattice site, such that the final positions are identical to the initial positions. Topological nature of the spatial manifold also ensures that the exact path of the walker is not important, and only the direction (above or below) in which the walker passes the island matters.

To make the labelling of anyons explicit, the fusion tree for the initial state of the quantum walk is shown in Fig. 2.2. The walker anyon starts in the middle of the fusion

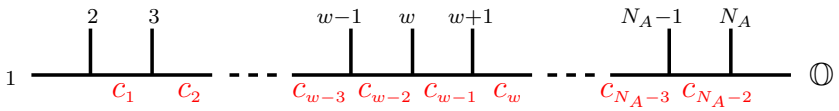

FIGURE 2.2: Initial fusion state of the anyonic quantum walk with N_A anyons in the standard basis. The walker anyon is labelled w and it is initially located in the middle of the fusion tree. The fusion degrees of freedom are labelled by the intermediate fusion charges $\{c_j\}$. The total charge of all anyons is the vacuum $\mathbb{O}$.

tree, such that it has the same amount of stationary anyons to the left and right. The anyons are thought to be created from vacuum, such that their total charge is trivial (depending on the fusion rules, it is sometimes necessary to add an ancillary stationary anyon to make the total charge vacuum). If the label of the walker charge is made equal to the initial site of the walker $k = s_0$, it is guaranteed that the braid generators are always assigned with correct spatial translations of the walker.

The transformation rule $\big|\Psi(t+1)\big\rangle = U\big|\Psi(t)\big\rangle$ for the anyonic quantum walk is only a slight modification of the corresponding rule for usual discrete-time quantum walks. There, coin outcomes 0 and 1 were associated with uniform translation operators T^- and T^+ respectively. In the anyonic version, each site-specific translation $T^-_{s+1} = \big|s\big\rangle_{\mathrm{S}}\big\langle s+1\big|$ and $T^+_s = \big|s+1\big\rangle_{\mathrm{S}}\big\langle s\big|$ is associated with a braid generator b_s. As the braid generators act on different fusion charges at different locations, they break the translational invariance which holds in the usual quantum walk with a uniform coin. The braid generators act in the fusion Hilbert space $\mathcal{H}_{\mathrm{F}}$ only, and to accommodate the Hilbert space for the fusion degrees of freedom, the total Hilbert space is extended to the tensor product of spatial, fusion and coin degrees of freedom: $\mathcal{H} = \mathcal{H}_{\mathrm{S}} \otimes \mathcal{H}_{\mathrm{F}} \otimes \mathcal{H}_{\mathrm{C}}$. The discrete N-site space is spanned by N basis vectors $\big\{\big|s\big\rangle\big\}_{s=1}^{N}$, the fusion space for N_A anyons is spanned by $\{\otimes_{j=1}^{N_A-2}\big|c_j\big\rangle\}$, where c_j are the intermediate charges and the dimension is $\dim(\mathcal{H}_{\mathrm{F}}) \propto d^{N_A}$ with quantum dimension d, and the coin is spanned by $\{\big|0\big\rangle, \big|1\big\rangle\}$.

The time evolution operator can be decomposed into coin-flip and conditional shift operators: $U = \mathcal{S}\mathcal{F}$, with the coin-flip defined similarly as for usual quantum walks:

$$\mathcal{F} = \mathbb{I}_{\mathrm{S}} \otimes \mathbb{I}_{\mathrm{F}} \otimes F. \tag{2.1}$$

The conditional shift operator $\mathcal{S}$ associates a braid b_s with translations T^-_{s+1} and T^+_s, and is given by

$$\mathcal{S} = \sum_{s=1}^{N-1} (T^-_{s+1} b_s P_0 + T^+_s b_s P_1) + T_{\mathrm{BC}} \tag{2.2}$$

Where T_{BC} stands for boundary condition terms (see Sec. 2.4.1).

Note that by defining $T^- = \sum_s T^-_{s+1} b_s$ and $T^+ = \sum_s T^+_s b_s$ as generalized translation operators, the transformation rule can be written exactly the same way as for usual quantum walks: $\mathcal{S} = T^- P_0 + T^+ P_1$. The position space and fusion space can then be seen as a generalized position space, and the translation operators act only in this space, while the projectors and the coin flip operator act only in the coin space. The

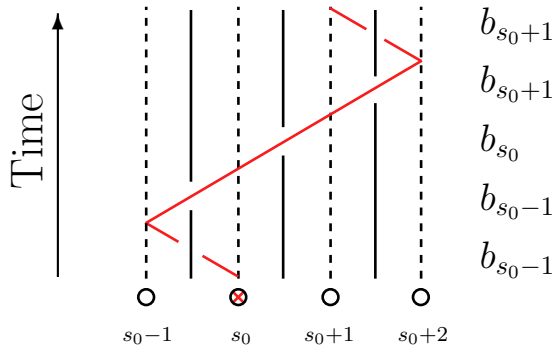

Figure 2.3: The path $\overline{a} = (01110)$, and the corresponding braid word $\mathcal{B} = b_{s_0+1}b_{s_0+1}b_{s_0}b_{s_0-1}b_{s_0-1}$. The solid lines represent stationary strands and the dashed lines mark the spatial sites which the walker can occupy. The red walker component starts from site s_0.

coin degrees of freedom can therefore be handled separately from the spatial degrees of freedom, in the same way that was done for usual quantum walks in Sec. 1.2.1.

In Sec. 1.2.1 the coin histories were recorded in vector $\overline{a}$, and each vector corresponds to a distinct path. If the fusion state is initially $\big|\chi_0\big\rangle$, each application of the time evolution operator U multiplies the fusion state by a braid generator: $\big|\chi_0\big\rangle \to b_{s_t}b_{s_{t-1}}\dots b_{s_2}b_{s_1}\big|\chi_0\big\rangle$, where s_t is the braid index at time step t. It is useful derive an expression for the indices of the braid generators in terms of the coin history $\overline{a}$. If the walker is at site $s = s_0 + 2\sum_{t'=1}^{t-1} a_{t'} - (t-1)$ at time step $t-1$, then the braid index is $s_t = s + a_t - 1$, ie. $s_t = s-1$ if the walker went left and $s_t = s$ if right. Thus the index is $s_t = s_0 + 2\sum_{t'=1}^{t} a_{t'} - a_t - t$. As an example, consider the coin history for five time steps $\overline{a} = (01110)$ (time going left to right). It can be checked that starting from the initial site s_0, the string of braid generators $\mathcal{B} = b_{s_0+1}b_{s_0+1}b_{s_0}b_{s_0-1}b_{s_0-1}$ (time going right to left) is applied to the fusion state. Such strings of generators are called *braid words* from now on. The braid representation corresponding to the above coin history is shown in Fig. 2.3. It is also possible to write the braid word $\mathcal{B}^t_{\overline{a}}$ corresponding to a path $\overline{a}$ of t time steps in a very compact form:

$$\mathcal{B}^t_{\overline{a}} = \prod_{r=0}^{t-1} b_{s_r} \tag{2.3}$$

$$s_r = s_0 + 2\sum_{t'=1}^{t-r} a_{t'} - a_{t-r} - (t-r). \tag{2.4}$$

Here the index s_r is chosen such that the order of generators is correct (time goes right to left). This formula will be very useful when taking the trace over the fusion space.

In the quantum walk evolution, one is mainly interested in the probability distribution over sites as a function of time steps. The information about the spatial degrees of freedom is carried by the reduced density matrix of the position space $\rho_S(t)$. Since the time evolution operator U entangles spatial states with coin and fusion states, the

spatial states are mixed most of the time, but unitarity of U ensures that the total density matrix $\rho(t) = \big|\Psi(t)\big\rangle\big\langle\Psi(t)\big|$ is always pure. The spatial density matrix is obtained from the total density matrix by tracing out the coin and fusion degrees of freedom:

$$\rho_{\mathrm{S}}(t) = \mathrm{Tr}_{\mathrm{C}}\mathrm{Tr}_{\mathrm{F}}\Big(U^t\big|\Psi_0\big\rangle\big\langle\Psi_0\big|(U^\dagger)^t\Big) \tag{2.5}$$

The braid generators b_s act only on the fusion Hilbert space, so the fusion trace can be carried out separately from the coin degrees of freedom. The sequence of braid generators applied on the state depends on the path of the walker, whether it went left or right at each time step. The elements of the spatial density matrix are now given by

$$\big(\rho_{\mathrm{S}}(t)\big)_{s,s'} = \sum_{\substack{\overline{a},\overline{a}' \\ \text{st. } a'_t=a_t \\ \overline{a}\rightsquigarrow s,\overline{a}'\rightsquigarrow s'}} \mathcal{C}(\overline{a},c_0)\,\mathcal{C}(\overline{a}',c_0)^*\,\mathrm{Tr}\,\Big(\mathcal{B}^t_{\overline{a}}\big|\chi_0\big\rangle\big\langle\chi_0\big|(\mathcal{B}^t_{\overline{a}'})^\dagger\Big) \tag{2.6}$$

where the coin terms are expressed by recalling Eq. (1.57):

$$\mathcal{C}(\overline{a},c_0) = \big\langle a_t\big|F\big|a_{t-1}\big\rangle\ldots\big\langle a_2\big|F\big|a_1\big\rangle\big\langle a_1\big|F\,\big|c_0\big\rangle.$$

Eq. (2.6) is very similar to the corresponding expression for usual quantum walks, Eq. (1.56), except for the extra factor $\mathrm{Tr}\,\Big(\mathcal{B}^t_{\overline{a}}\big|\chi_0\big\rangle\big\langle\chi_0\big|(\mathcal{B}^t_{\overline{a}'})^\dagger\Big)$ which can be seen as the anyonic term. The anyonic coefficient multiplies each path component by a complex number, thus distorting the ordinary quantum walk dynamics. The spatial probability distribution is given by diagonal values of the density matrix:

$$p(s,t) = \big(\rho_{\mathrm{S}}(t)\big)_{s,s} = \sum_{\overline{a},\overline{a}'\rightsquigarrow s} \mathcal{C}(\overline{a},c_0)\,\mathcal{C}(\overline{a}',c_0)^*\,\mathrm{Tr}\,\Big(\mathcal{B}^t_{\overline{a}}\big|\chi_0\big\rangle\big\langle\chi_0\big|(\mathcal{B}^t_{\overline{a}'})^\dagger\Big). \tag{2.7}$$

Recall from Sec. 1.2.1 that the notation $\overline{a},\overline{a}' \rightsquigarrow s$ means that the sum is taken over paths with $a_t = a'_t$ and $s = s_0 + 2\sum_{t'=1}^{t} a_{t'} - t$. In what follows, the main concern is the evaluation of the anyonic trace term. One approach is to construct representations for the braid generators in the fusion basis, and take the matrix trace over the representations of the braidwords, as explained in Sec. 2.2. Another approach in Sec. 2.3 uses relations between braid closures and link invariant polynomials. The latter approach proves to be more efficient in some cases, and provides a visual way of thinking about anyon trajectories as links. It is also used to derive the main results.

Eq. (2.7) gives a neat formula for calculating the probability distribution of the walker at time step t: for a fixed site, the probability is a sum of fixed-length paths starting from the initial site and leading to s (the length of the path is the real distance traveled by the walker, not the distance between s and s_0). Of course, this method allows only the calculation of the spatial density matrix, and the full information about the wave function is lost. It is good to keep in mind that this formula holds specifically for an initially localized particle. To extend the analysis for an initially delocalized particle, the initial state would be a superposition of position states, and one would have to sum over all initial locations, and consider all fixed-length paths from each initial site to site s.

For the sake of numerical calculations, it is interesting to consider the computational complexity of evaluating the probability distribution as the number of time steps increases. For each pair of paths $(\overline{a}, \overline{a}')$, one has to evaluate the product $\mathcal{C}(\overline{a}, c_0)\mathcal{C}(\overline{a}', c_0)^*$ $\times \mathrm{Tr}\left(\mathcal{B}^t_{\overline{a}}|\chi_0\rangle\langle\chi_0|(\mathcal{B}^t_{\overline{a}'})^\dagger\right)$. The evaluation of each of these quantities as a function of path pair $(\overline{a}, \overline{a}')$ is a task of its own, but some insight is obtained by considering the number of terms in the path sum, since the number of elementary operations is bounded from below by this number. The number of terms in the path sum is just the number of pairs of paths leading to site s (remember the pairs of paths correspond to bra and ket evolution of the walker), with the constraint that the last coin outcomes must be the same: $a_t = a'_t$. From analysis of standard random walks, it is known that the probability to reach a site after t time steps is $\binom{t}{H}$, where H is the number of right-moves taken by the walker (note that the number of left-moves is given by $L = t - H$). In terms of the path vector, the number of right-moves is given simply by the sum of its elements: $H = \sum_t a_t$. In computer science, the sum of elements of a binary string is called the Hamming weight. To fix the site where the walker ends up, one can write $H_{s,t} = \{\sum_{t'} a_{t'} \mid s = s_0 + 2\sum_{t'} a_{t'} - t\}$, or written in a more compact form,

$$H_{s,t} = \frac{s - s_0 + t}{2}. \tag{2.8}$$

Since the last coin outcomes must be the same, the number of pairs of paths leading to s is just the number of pairs of paths leading to $s-1$ ($a_t = a'_t = 1$) plus the number of paths leading to $s+1$ ($a_t = a'_t = 0$) at time step $t-1$. The number of single paths leading to $s-1$ is $\binom{t-1}{H_{s-1,t-1}}$, so squaring this number gives the number of pairs of paths. Using similar reasoning for $s+1$, and identities $H_{s-1,t-1} = H_{s,t} - 1$ and $H_{s+1,t-1} = H_{s,t}$, the number of pairs of paths is given by

$$\#(\overline{a}, \overline{a}')_{\text{st. } \overline{a},\overline{a}' \rightsquigarrow s} = \binom{t-1}{H_{s,t}-1}^2 + \binom{t-1}{H_{s,t}}^2. \tag{2.9}$$

The expression above implies that the number of elementary additions needed to evaluate $p(s,t)$ grows exponentially as a function of t. On top of addition, the coin and anyonic terms need to be evaluated and multiplied for each path, which increases the number of elementary operations significantly. As will be shown later, the coin and anyonic terms can be identical for different paths, and recognizing these symmetries reduces the amount of additions needed. However, even in the presence of these symmetries the probability distribution will still be exponentially hard in time to evaluate.

2.2 Construction of braid generators in the standard basis

As discussed in Sec. 1.1.3, the matrix representations of the braid generators can be constructed using R- and F-tensors, which give the coefficients for two-particle braiding and three-particle basis changes for the anyon model in question. These matrix representations are constructed in the standard basis as shown in Fig. 2.2. The

trace over the fusion space can then be computed by constructing the initial state in the standard basis, applying the braid generators and taking the matrix trace.

In the fusion basis labeled by intermediate charges $\{c_j\}$, the elements of the braid generators for N_A identical σ anyons are given explicitly as [55]

$$\left\langle \Psi(\{c'_j\}) \middle| b_k \middle| \Psi(\{c_j\}) \right\rangle = \begin{cases} \prod_{m=k}^{N_A-2} \delta_{c_m,c'_m} R^{c_1}_{\sigma\sigma}, & k=1 \\ \prod_{m=k}^{N_A-2} \delta_{c_m,c'_m} & \\ \quad \times \sum_x ([F^{c_k}_{\sigma\sigma\sigma}]^{-1})^{c'_{k-1}}_x R^x_{\sigma\sigma} (F^{c_k}_{\sigma\sigma\sigma})^x_{c_{k-1}}, & k=2 \\ \prod_{l=1}^{k-2} \delta_{c_l,c'_l} \prod_{m=k}^{N_A-2} \delta_{c_m,c'_m} & \\ \quad \times \sum_x ([F^{c_k}_{c_{k-2}\sigma\sigma}]^{-1})^{c'_{k-1}}_x R^x_{\sigma\sigma} (F^{c_k}_{c_{k-2}\sigma\sigma})^x_{c_{k-1}}, & 2<k<N_A-1 \\ \prod_{m=k}^{N_A-2} \delta_{c_m,c'_m} R^{c_{N_A-2}}_{\sigma\sigma}, & k=N_A-1 \end{cases} \tag{2.10}$$

This expression gives the matrix elements of the braid generators in terms of the R and F tensors and is applicable for any anyon model with degeneracy-free fusion.

The fusion space of spin-1/2 irreps of $SU(2)_2$ anyons and the σ charges of the Ising anyon model has a very convenient tensor product structure in terms of qubits. For example, two spin-1/2's can fuse to either vacuum 0 or spin 1: $\frac{1}{2} \times \frac{1}{2} = 0 + 1$. Thus the fusion charge can take values $c_1 = \{0, 1\}$. But when c_1 is fused with another spin-1/2, the fusion outcome is necessarily 1/2: $c_2 = c_1 \times \frac{1}{2} = \frac{1}{2}$, according to the fusion rules of $SU(2)_2$. The degeneracy of the fusion outcome is 2, as it can be obtained in two different ways. One can continue with similar logic and find that every even intermediate charge is $c_{2j} = \frac{1}{2}$, and every odd charge forms a qubit: $c_{2j+1} = \{0, 1\}$. The total degeneracy is equal to the dimension of the Hilbert space. Requiring that the total charge is zero, the fusion space then consists of $m = N_A/2 - 1$ qubits: $\mathcal{H}_\mathrm{F} \simeq (\mathbb{C}^2)^{\otimes m}$. The braid generators of $SU(2)_2$ and Ising anyons thus admit a simple structure where the non-trivial matrices acting on the fusion space are at most 4-by-4:

$$\begin{aligned} &b_1 = R \otimes_{j=2}^m \mathbb{I}_2, \quad b_2 = B \otimes_{j=2}^m \mathbb{I}_2, \quad b_3 = A \otimes_{j=3}^m, \\ &b_{2k} = \otimes_{j=1}^{k-1} \mathbb{I}_2 \otimes B \otimes_{j=k+1}^m \mathbb{I}_2, \quad b_{2k+1} = \otimes_{j=1}^{k-1} \mathbb{I}_2 \otimes A \otimes_{j=k+2}^m \mathbb{I}_2; \quad 1<k<m, \\ &b_{n-3} = \otimes_{j=1}^{m-2} \mathbb{I}_2 \otimes A, \quad b_{n-2} = \otimes_{j=1}^{m-1} \mathbb{I}_2 \otimes B, \quad b_{n-1} = \otimes_{j=1}^{m-1} \mathbb{I}_2 \otimes R. \end{aligned} \tag{2.11}$$

For Ising anyons, the non-trivial matrices are

$$R = e^{-i\frac{\pi}{8}} \begin{pmatrix} 1 & 0 \\ 0 & i \end{pmatrix}, \quad B = \frac{e^{-i\frac{\pi}{8}}}{\sqrt{2}} \begin{pmatrix} e^{i\frac{\pi}{4}} & e^{-i\frac{\pi}{4}} \\ e^{-i\frac{\pi}{4}} & e^{i\frac{\pi}{4}} \end{pmatrix},$$

$$A = e^{-i\frac{\pi}{8}} \begin{pmatrix} 1 & 0 & 0 & 0 \\ 0 & i & 0 & 0 \\ 0 & 0 & i & 0 \\ 0 & 0 & 0 & 1 \end{pmatrix}$$

and for the $SU(2)_2$ anyons $R \to iR^*$, $B \to iB^*$ and $A \to iA^*$.

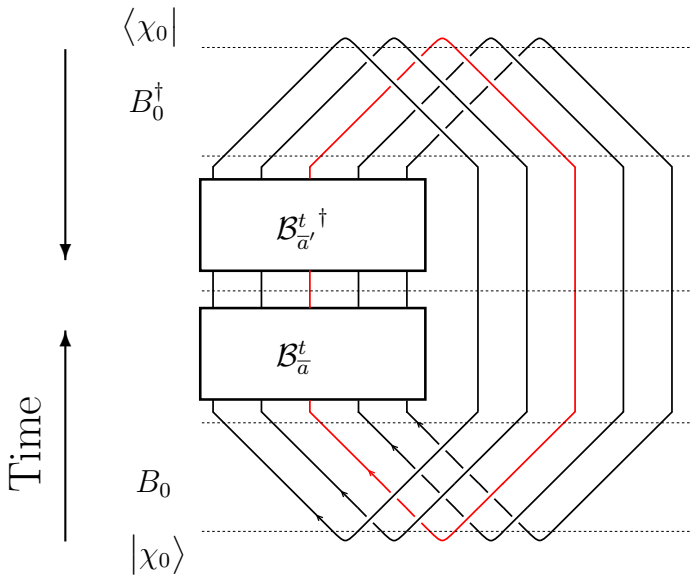

FIGURE 2.4: The structure of the links encountered in the anyonic quantum walk. The initial fusion state is $|\Phi_0\rangle = B_0|\chi_0\rangle$, such that the trace closure corresponds to Markov closure. The total braid word $(\mathcal{B}_{\bar{a}'}^t)^\dagger\mathcal{B}_{\bar{a}}^t$ is a product of the bra- and ket-evolution.

2.3 Relation to link invariants

An alternative route to evaluating the trace over the fusion degrees of freedom comes from link invariant polynomials. As discussed in Sec. 1.1.4, the expectation values of braid words are related to the Jones polynomial via Eq. (1.43). Using the completeness of the fusion basis, the trace over the fusion degrees of freedom can be expressed as an expectation value over the initial state: $\mathrm{Tr}\big(\mathcal{B}_{\bar{a}}^t|\chi_0\rangle\langle\chi_0|(\mathcal{B}_{\bar{a}'}^t)^\dagger\big) = \langle\chi_0|(\mathcal{B}_{\bar{a}'}^t)^\dagger\mathcal{B}_{\bar{a}}^t|\chi_0\rangle$. If $|\chi_0\rangle$ is an initial state where $2N_A$ particles are created from the vacuum, and B_0 is a braid word that drags the left member of each pair to the left, then the expectation value over the state $|\Phi_0\rangle = B_0|\chi_0\rangle$ corresponds to Markov closure of the braid word $(\mathcal{B}_{\bar{a}'}^t)^\dagger\mathcal{B}_{\bar{a}}^t$, forming a link L:

$$\langle\Phi_0|(\mathcal{B}_{\bar{a}'}^t)^\dagger\mathcal{B}_{\bar{a}}|\Phi_0\rangle \mathrel{\widehat{=}} \big((\mathcal{B}_{\bar{a}'}^t)^\dagger\mathcal{B}_{\bar{a}}^t\big)^{\text{Markov}} \mathrel{\widehat{=}} L(\bar{a},\bar{a}')$$

This is illustrated in Fig. 2.4. The Markov closure means that the outgoing ends of each strand are joined together with their respective incoming ends.

By invoking the relationship with the expectation values and the Jones polynomial, the fusion trace can now be expressed as

$$\mathrm{Tr}\left(\mathcal{B}_{\bar{a}}^t|\Phi_0\rangle\langle\Phi_0|(\mathcal{B}_{\bar{a}'}^t)^\dagger\right) = \frac{(-q^{3/4})^{w(L(\bar{a},\bar{a}'))}}{d^{N_A-1}}V_{L(\bar{a},\bar{a}')}(q). \tag{2.12}$$

Here the parameter of the Jones polynomial is $q = e^{i\frac{2\pi}{k+2}}$, and $d = -A^2 - A^{-2} = -q^{-1/2} - q^{1/2} = 2\cos\frac{\pi}{k+2}$ for spin-1/2 irreps of $SU(2)_2$.

A similar expression can be given in terms of the Kauffman bracket. The bracket is related to the Jones polynomial via $V_L(q)|_{q\to A^{-4}} = (-A)^{-3w(L)}\,\langle L\rangle(A)$ with the correspondence $q = A^{-4}$. The fusion trace is now given by

$$\mathrm{Tr}\left(\mathcal{B}^t_{\overline{a}}\big|\Phi_0\big\rangle\big\langle\Phi_0\big|(\mathcal{B}^t_{\overline{a}'})^\dagger\right) = \big\langle L(\overline{a},\overline{a}')\big\rangle/d^{N_A-1}, \tag{2.13}$$

where $A = ie^{\frac{i\pi}{2(k+2)}}$. Note that the writhe and the Jones polynomial, but not the Kauffman bracket, require a choice of orientation for the link components, and the orientation is picked such that all the strands which take part in the walk (the left half in Fig. 2.4) have the same orientation.

Although these formulas strictly hold for the spin-1/2 irreps of $SU(2)_k$, they can also be used anyonic walks with Ising anyons. For more detailed description of this correspondence see Secs. 3.1 and 5.3.1.

2.4 Finite chains

This section discusses anyonic quantum walks in chains of finite length. To ensure unitarity of the walk, the boundary conditions must be defined correctly. One motivation to study finite chains is that the size of the fusion Hilbert space remains constant, and long time scale simulations of the walk become possible. Results on entropy and mixing of the probability distribution are given.

2.4.1 Boundary conditions

The boundary conditions describe how the components of the wave packet transform when the walker reaches the edges of the system. If the total evolution of the system is assumed to be unitary, then the boundary condition terms must also be unitary. In fact, the boundary conditions are needed so that the total evolution of the system is unitary. Although the middle terms given in Eqs. (2.1) and (2.2) are unitary in general, the components $\big|1\big\rangle_{\mathrm{S}}\big|0\big\rangle_{\mathrm{C}}$ and $\big|1\big\rangle_{\mathrm{S}}\big|1\big\rangle_{\mathrm{C}}$ are connected only in one way, ie. there is no amplitude connecting the first component forward in time or the second component backward in time, therefore the total probability is not conserved. It is thus necessary to define how these components transform at the boundary. The boundaries can also be thought as an interface between the quantum walk system and its environment, such that the walker interacts with the environment when it reaches the boundary. In this case the interaction might cause decoherence of the quantum walk evolution, and the evolution is not necessarily unitary.

The most common way to define unitary boundary conditions are periodic boundary conditions. The ends of the lattice are joined together to form a ring graph, such that a left moving walker at site 1 moves to site N and a right moving walker at site N moves to site 1. The coin state does not change during the shift between lattice sites 1 and N, but the fusion labeling of non-Abelian anyons does. For example, if the walker is initially at site 1, its corresponding anyonic charge is labelled as 1, and if the walker

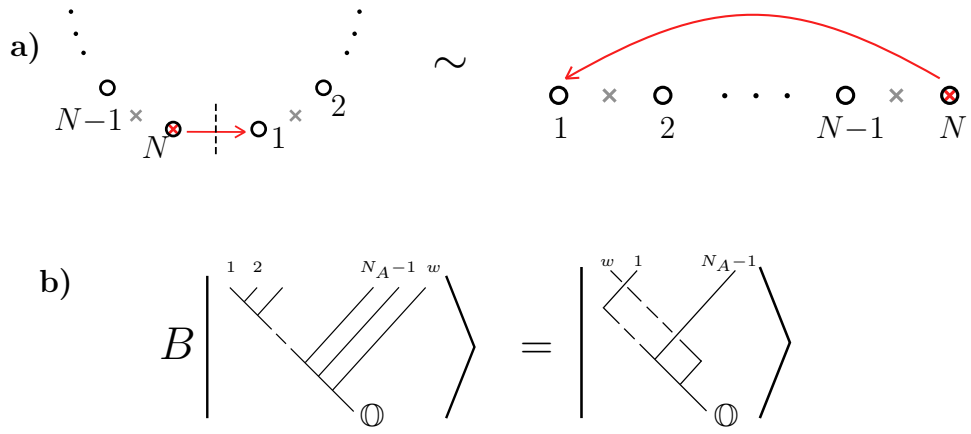

FIGURE 2.5: Periodic boundary conditions for anyons in the discrete-time quantum walk. a) The transition $N \to 1$ on the circle (left), and a path isotopic to it when the circle is stretched to a line (right). b) The periodic boundary condition moves the anyon with the last label (walker) to the first label. This move is represented by the braid matrix B.

is the last site N, its charge is labelled as N_A. The periodic boundary conditions must therefore be defined in such a way that also the fusion state transforms correctly.

The transition from site N to site 1 is shown in Fig. 2.5a). The walker does not braid directly with stationary anyons as it crosses the boundary, but the path corresponding to the lattice shift $N \to 1$ is isotopic to the path that goes *over* all the stationary anyons, when the ring is stretched out as a line in such a way that none of the anyon worldlines cross. In this case, all the braids are counterclockwise. The shift $1 \to N$ is isotopic to the path where the walker goes from 1 to N *under* the stationary anyons, and all the braids are clockwise. If the labelling of the sites around the ring was chosen in clockwise direction, then the shift $N \to 1$ would correspond to the path where the walker is taken under the stationary anyons and conversely for $1 \to N$.

The periodic boundary conditions for anyons are represented by a braid word B which implements a braid that moves the walker between the first and last anyon. This braid can be represented in the fusion basis as shown in Fig. 2.5b). It moves the anyon with the last label to the first and moves all the other anyons to the right by one step. The braid word can be decomposed to generators as

$$B = \prod_{k=1}^{N_A-1} b_k. \tag{2.14}$$

If the sites on the ring are labelled counterclockwise, then the shift $N \to 1$ is associated with B and $1 \to N$ is associated with $B^\dagger$. The boundary condition terms in Eq. (2.2) can thus be written

$$T_{\text{pbc}} = |1\rangle\langle N| \otimes B \otimes P_1 F + |N\rangle\langle 1| \otimes B^\dagger \otimes P_0 F. \tag{2.15}$$

The setup for reflective boundary conditions is slightly different. To connect the unconnected components of the wave function, one could define boundary conditions

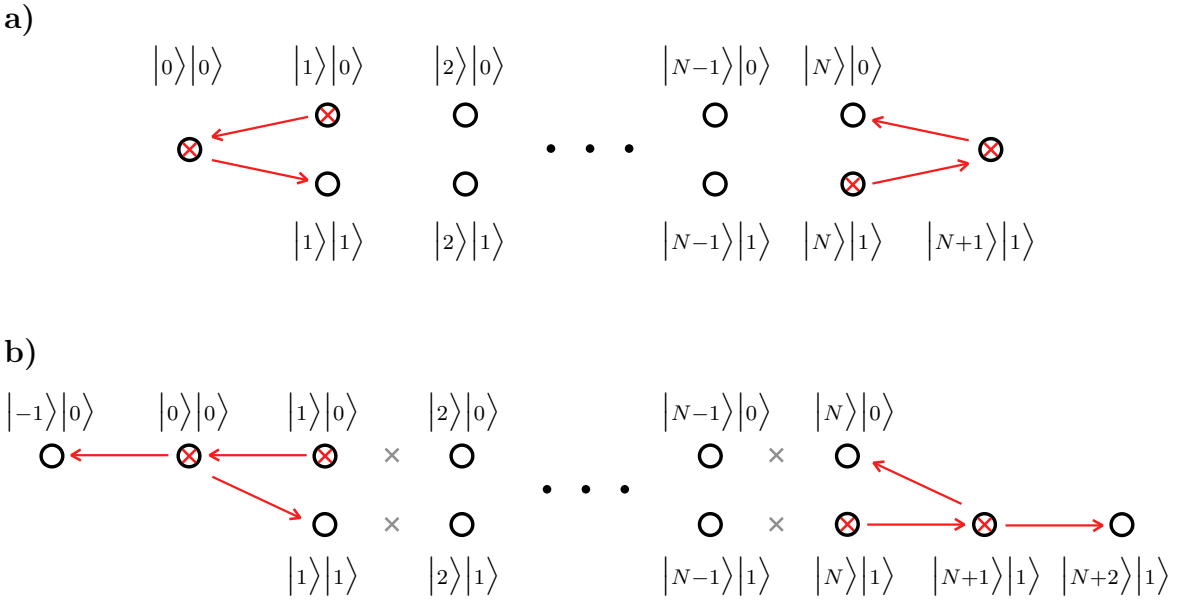

FIGURE 2.6: Dynamics at the boundaries. a) Reflective boundary conditions. Two ancillary states $|0\rangle_s|0\rangle_c$, $|N+1\rangle_s|0\rangle_c$ are attached to the left and right ends of the chain. The walker returns from the endsites with unit amplitude and its coin state is flipped. b) Absorbing boundary conditions. A walker arriving at the boundary sites can either tunnel through the boundary or be reflected with its coin state flipped. The tunneling amplitudes at the boundaries are given by some tunneling matrix F_B. Once the walker has passed the boundary, it can not return to the system.

where the coin component 0 at site 1 stays at the same site, and its coin state is changed to 1 after the coin flip. Such a setup would however break the convention that the walker moves either left ot right on every time step, and never stays in place after one time step. To construct well defined boundary conditions, it is therefore necessary to add ancillary states $|0\rangle_S|0\rangle_C$ and $|N+1\rangle_S|1\rangle_C$ to the left and right boundaries, as shown in Fig. 2.6a). Then a walker at site 1 moves to $|0\rangle_S|0\rangle_C$ if its coin state is 0 after the coin flip, and a walker at site N moves to $|N+1\rangle_S|1\rangle_C$ if its coin state is 1 after the coin flip. There are no coins at the ancillary sites, such that the walker moves from $|0\rangle_S|0\rangle_C$ to $|1\rangle_S|1\rangle_C$ with unit amplitude, and similarly at the last site. The coin state is flipped as the walker moves back from the ancillary sites. There are no stationary anyons between the middle sites and the ancillary sites, so braiding is trivial during these shifts.

In the case of reflective boundary conditions, the boundary can be thought as separating the quantum walk system from its environment. When the walker is reflected back from the boundary, its direction of motion and the coin state have changed, as a consequence of the interaction between the walker and the environment. In this case however, the interaction does not cause decoherence, and time evolution is unitary.

The boundary terms for reflective boundary conditions can be written

$$\begin{aligned} T_{\text{ref}} &= \big|0\big\rangle\big|0\big\rangle\big\langle 1\big|\big\langle 0\big|F \;+\; \big|1\big\rangle\big|1\big\rangle\big\langle 0\big|\big\langle 0\big| \\ &\quad +\; \big|N+1\big\rangle\big|1\big\rangle\big\langle N\big|\big\langle 1\big|F \;+\; \big|N\big\rangle\big|0\big\rangle\big\langle N+1\big|\big\langle 1\big|, \end{aligned} \tag{2.16}$$

where the first state in the tensor product $\big|s\big\rangle\big|c\big\rangle$ is to be understood to lie in the position space and the second state in the coin space.

Absorbing boundary conditions can be defined similarly as reflective boundary conditions, except there are now two ancillary states on the left and right, see Fig. 2.6b). Sites $\big|0\big\rangle_{\text{S}}\big|0\big\rangle_{\text{C}}$ and $\big|N+1\big\rangle_{\text{S}}\big|1\big\rangle_{\text{C}}$ act as partially transparent boundaries such that a walker arriving from the middle sites to the boundary has some probability of passing through the boundary and some probability to be reflected back to the system. Once the walker has passed through the boundary it has been absorbed by the environment and it can not return to the system, so there is no probability to return from the ancillary states $\big|-1\big\rangle_{\text{S}}\big|0\big\rangle_{\text{C}}$ and $\big|N+2\big\rangle_{\text{S}}\big|1\big\rangle_{\text{C}}$. This property makes the dynamics irreversible, and the total time evolution is not unitary. The tunneling amplitudes are given by a tunneling matrix F_C, which is just a specific coin flip operator attached to the boundary sites. The boundary terms can then be written as:

$$\begin{aligned} T_{\text{abs}} = \big|0\big\rangle\big|0\big\rangle\big\langle 1\big|\big\langle 0\big|\,F \;+\; \big|1\big\rangle\big|1\big\rangle\big\langle 0\big|\big\langle 0\big|\,(\big|0\big\rangle\big\langle 1\big|F_C) \;+\; \big|-1\big\rangle\big|0\big\rangle\big\langle 0\big|\big\langle 0\big|\,F_C \\ +\; \big|N+1\big\rangle\big|1\big\rangle\big\langle N\big|\big\langle 1\big|\,F \;+\; \big|N\big\rangle\big|0\big\rangle\big\langle N+1\big|\big\langle 1\big|\,(\big|1\big\rangle\big\langle 0\big|F_C) \\ +\; \big|N+2\big\rangle\big|1\big\rangle\big\langle N+1\big|\big\langle 1\big|\,F_C. \end{aligned} \tag{2.17}$$

In this case, the probabilities $p(s=-1,t) = \big|\big\langle -1\big|\Psi(t)\big\rangle\big|^2$ and $p(s=N+2,t) = \big|\big\langle N+2\big|\Psi(t)\big\rangle\big|^2$ are the instantaneous probabilities for the walker to occupy the ancillary states $\big|-1\big\rangle_{\text{S}}\big|0\big\rangle_{\text{C}}$ and $\big|N+2\big\rangle_{\text{S}}\big|1\big\rangle_{\text{C}}$. If the N-site lattice is seen as a finite cavity, these are the probabilities for the walker to exit the cavity from left or right at time t. Thus $p(s=0,t)$ for example gives the probability distribution in time for the walker to exit the cavity from left. Note that although the dynamics is not unitary, the total probability is conserved in the sense that the time integrated exit probabilities plus the site probabilities at time t is conserved: $\sum_{t'=1}^{t-1}(p(s=-1,t')+p(s=N+2,t')) + \sum_{s=-1}^{N+2} p(s,t) = 1$.

2.4.2 Decoherence

As discussed in Sec. 1.2.2, interaction with an environment mixes the phase relations of quantum states, and depending on the type of interaction the effective behaviour of the system may look classical (stochastic). This phenomenon is generally known as decoherence. Note that the total Hilbert space in non-Abelian anyonic quantum walks is $\mathcal{H} = \mathcal{H}_{\text{S}} \otimes \mathcal{H}_{\text{F}} \otimes \mathcal{H}_{\text{C}} = \mathcal{H}_{\text{QW}} \otimes \mathcal{H}_{\text{F}}$, ie. the fusion space $\mathcal{H}_{\text{F}}$ can be seen as the environment for the walker. Equivalently, the joint system of the coin and fusion degrees of freedom can be seen as an extended coin space: $\mathcal{H} = \mathcal{H}_{\text{S}} \otimes \mathcal{H}_{\text{F}} \otimes \mathcal{H}_{\text{C}} = \mathcal{H}_{\text{S}} \otimes \mathcal{H}_{\text{C}'}$. The total state evolves unitarily in time, but the spatial and coin degrees of freedom are not in a pure state, but instead in a mixed state described by the density matrix ρ_{QW}.

The dynamics of the spatial and coin degrees of freedom in the anyonic quantum walk can be described by defining a superoperator $\mathcal{E}$ acting on the initial (pure) density matrix $\rho_{\mathrm{QW}}(0)$. The initial density matrix of the total system is $\rho(0) = \rho_{\mathrm{QW}}(0) \otimes \big|\chi_0\big\rangle\big\langle\chi_0\big|$. The density matrix at time step t is obtained by applying the time evolution operator t times: $\rho(t) = U^t\rho(0)(U^\dagger)^t$. The Kraus generators of $\mathcal{E}$ are obtained by tracing over the fusion (environment) degrees of freedom:

$$\rho_{\mathrm{QW}}(t) = \mathrm{Tr}_{\mathrm{A}}\big[U^t\rho(0)(U^\dagger)^t\big] \tag{2.18}$$

$$= \sum_f E_f \rho_{\mathrm{QW}}(t) E_f^\dagger \tag{2.19}$$

$$\equiv \mathcal{E}\big(\rho_{\mathrm{QW}}(0)\big) \tag{2.20}$$

where the generators are given by

$$E_f = \big(I \otimes \big\langle f\big|\big)U^t\big(I \otimes \big|\Phi_0\big\rangle\big) \tag{2.21}$$

and f runs through the basis elements of the fusion space. The superoperator $\mathcal{E}$ defines a completely positive (CP) trace-preserving map on the density matrix of the space and coin system. The states of the environment drive the quantum walk dynamics to decoherence channels labeled by f, and the system chooses the channel randomly. When the number of anyons in the system is high, the dimension of the fusion Hilbert space is high and it is expected that the degree of decoherence is high as well.

It is interesting to see how the decoherence from the fusion space affects the quantum walk dynamics. The degree of disorder in a quantum state ρ can be measured by its von Neumann entropy:

$$S(\rho) = -\mathrm{Tr}\big(\rho \ln \rho\big) \tag{2.22}$$

$$= -\sum_j \lambda_j \ln \lambda_j \tag{2.23}$$

where λ_j are the eigenvalues of ρ. The von Neumann entropy is zero if and only if the state is pure, and equal to the maximum value $\ln d$ if and only if the state is completely mixed (d is the dimension of ρ) [56]. In a certain sense, the von Neumann entropy measures the departure of the state from a pure state. Since the total state is pure, the von Neumann entropy is also a measure of entanglement between the system described by ρ and its environment. The von Neumann entropy of the spatial and coin degrees of freedom in the non-Abelian anyonic quantum walk with Ising anyons is plotted in Fig. 2.7. Note that the entropy for an Abelian anyonic quantum walks is always zero as the fusion space of Abelian anyons is one-dimensional. The plots show that when the number of sites is small, the entropy fluctuates randomly around some mean value. When the number of sites is large, the entropy seems to converge to some value very close to the maximum entropy, and the entropy increases on every time step.

Since the speedup of quantum walks with respect to random walks seems to originate from the quantum correlations between the spatial and coin states, it is therefore of interest to compare how these correlations are affected when the walker interacts

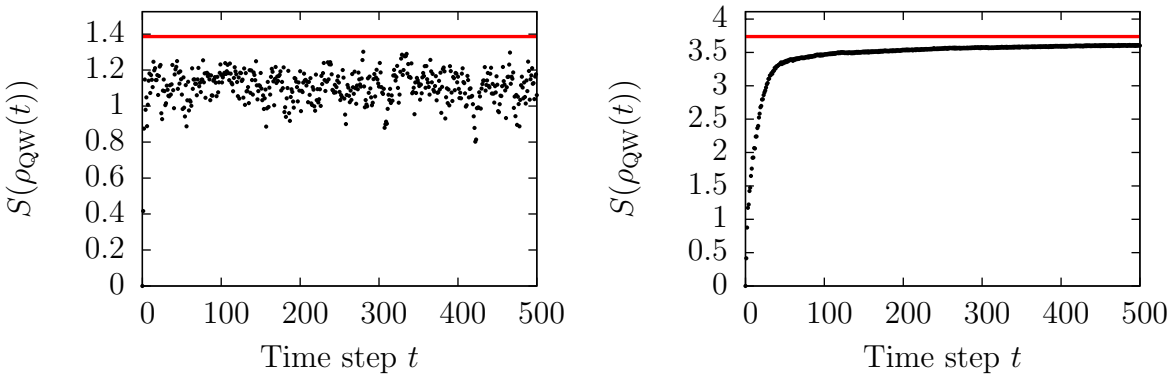

Figure 2.7: Von Neumann entropy of the composite space and coin system in the non-Abelian anyonic walk with Ising anyons and periodic boundary conditions. The maximum entropy is marked with a red line. a) $N_{\mathrm{sites}} = 5$. b) $N_{\mathrm{sites}} = 21$.

with an environment. The spatial entropy of ρ_{S} in the Hadamard walk with periodic boundary conditions is plotted in Fig. 2.8 a) and b). In the non-anyonic walk the spatial entropy is equal to coin entropy, and the maximum entropy is always $\ln 2 \approx 0.693$. The entropy fluctuates randomly, but the values become restricted to some interval as the number of sites grows. A similar effect is seen for anyonic walks in Fig. 2.8 c), where the entropy is also restricted to a bounded interval even when the lattice has only 5 sites. For 21 sites, the entropy tends to the maximum entropy and increases on every time step, similarly as the entropy for the combined space and coin system. Note that the calculation of the maximum entropy in anyonic walks is a bit more cumbersome than in quantum walks. For example, if there are five sites in the system, the Hilbert space dimension of the position space is $\dim(\mathcal{H}_{\mathrm{S}}) = 5$. There are 6 anyons in the system (4 stationary, walker, plus ancillary anyon so that the total charge is vacuum), and their fusion space dimension is $\dim(\mathcal{H}_{\mathrm{F}}) = 2^{6/2-1} = 4$. The dimension of the coin+fusion space is thus $\dim(\mathcal{H}_{\mathrm{F}} \otimes \mathcal{H}_{\mathrm{C}}) = 4 \times 2 = 8$. The maximum entropy is calculated with respect to the smaller system so that $S(\rho_{\mathrm{S}})^{N=5}_{\mathrm{max}} = \ln 5 \approx 1.609$.

These examples show that the coupling of the space and coin with fusion degrees of freedom changes the dynamics of the quantum walk significantly. The system goes from a pure state to a mixed state, and the correlations between the spatial and coin degrees of freedom become degraded as the system is subject to decoherence. As shown in the next chapter, this decoherence has profound effects on the dispersion of a particle on an infinite line. The effective dynamics becomes classical-like, as the size of the environment grows exponentially in time.

2.4.3 Mixing time

It is known that on finite graphs, the quantum walk does not converge into any asymptotic distribution (unless it starts from an eigenstate of the time evolution operator, in

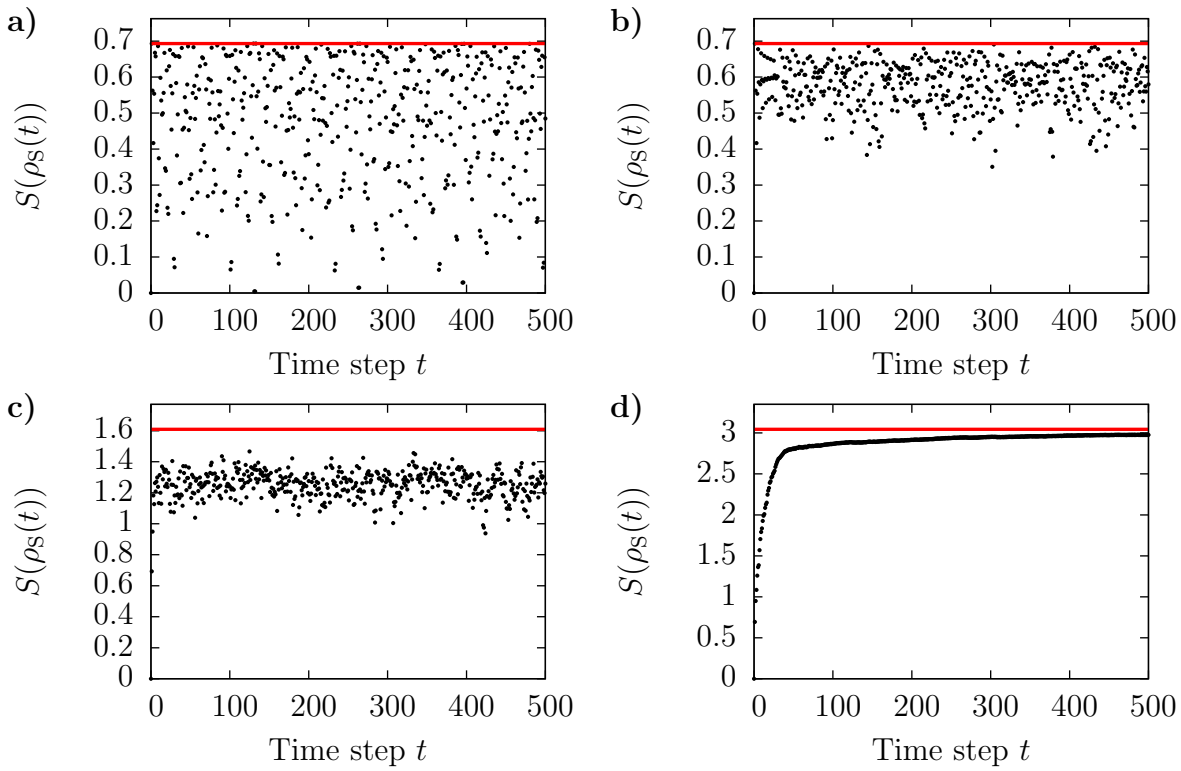

FIGURE 2.8: Entropy of spatial states. Upper row: normal quantum walk with a) 5 and b) 21 sites. Lower row: Ising anyons with c) 5 and d) 21 sites. The maximum entropy is marked with a red line. Periodic boundary conditions were used.

which case the walk is trivial). However, the time-averaged probability distribution,

$$\overline{p}(s,t) = \frac{1}{t+1}\sum_{t'=0}^{t} p(s,t) \tag{2.24}$$

has been shown to converge [45]. Moreover, by suitably tuning the decoherence parameters the converge rate can increase [54]. It is therefore interesting to compare how the anyonic decoherence affects the mixing properties of the Hadamard walk. The ϵ-mixing time is defined as [45]

$$M_\epsilon = \min\{T | \forall t \geq T,\ ||D_t - \pi|| \leq \epsilon\} \tag{2.25}$$

where D_t is the probability distribution at time step t, the asymptotic distribution is $\pi = \lim_{t\to\infty} D_t$, and the distance measure between two probability distributions is the total variation distance defined as $||D_1 - D_2|| = \sqrt{\sum_i (D_1(i) - D_2(i))^2}$.

As the asymptotic distribution is not known, an operational measure of convergence is defined as the total variation distance to the final time-averaged distribution at time step T:

$$D(t,T) = ||\overline{p}(s,t) - \overline{p}(s,T)|| \tag{2.26}$$

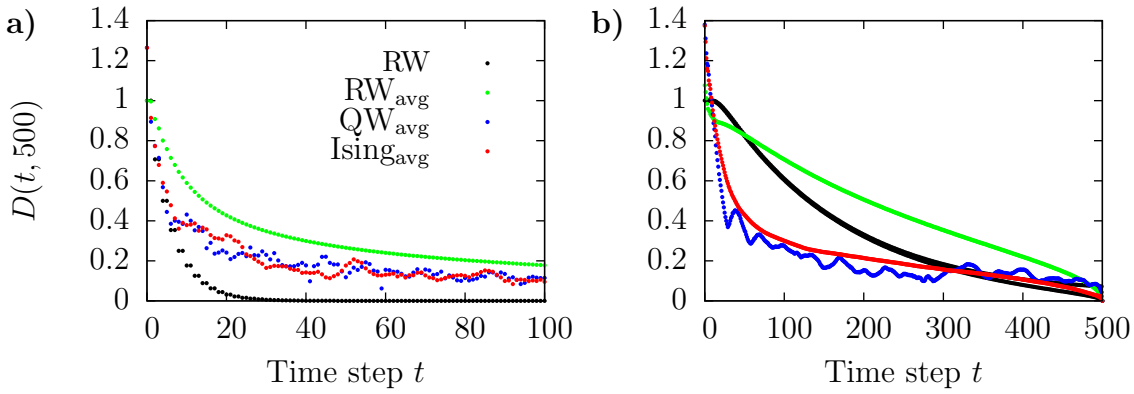

FIGURE 2.9: Total variation distance $D(t, T)$. a) 5 sites. b) 21 sites. Black represents the classical random walk and green represents the time-averaged classical random walk. Blue is the time-averaged Hadamard walk and red is the time-averaged Ising walk. Total number of time steps was 500 and periodic boundary conditions were used.

such that lower values of D mean faster convergence. The total variation distance for Ising anyons is plotted in Fig. 2.9 with the corresponding plots the random walk and the Hadamard walk. Note that the random walk distribution converges to the uniform distribution even without averaging, and for this reason both the actual and time-averaged distributions are plotted. For a small number of sites, the time-averaged probability distributions are quite similar, although the convergence of the random walk distribution is smoother than that of quantum and anyonic walks. For a larger number of sites, the differences become more apparent. The quantum and anyonic walks converge faster initially, exhibiting a quantum speedup in the convergence. The convergence of the anyonic walk is smoother than that of the usual quantum walk. One could deduce that the anyonic walk has good convergence properties, as it supersedes the convergence speed of the classical random walk and has less irregularities than the quantum walk.

2.5 Proposal for experimental setup

A possible experimental platform for simulating anyonic walks could be in Fractional Quantum Hall samples. The quasiparticles at the $\nu = 5/2$ plateau have been proposed to have non-Abelian anyonic statistics corresponding to Ising anyons. Some evidence for the statistical signatures of non-Abelian anyons have been reported in the literature recently in interference experiments, as highlighted below, but conclusive evidence is still lacking.

2.5.1 Fractional Quantum Hall Interferometry

Several wave function candidates have been proposed for the $\nu = 5/2$ Fractional Quantum Hall state, some of these with Abelian braiding statistics and some with non-Abelian statistics. The effective quasiparticle charge e^* was measured in tunneling experiments through a single quantum point contact, measuring the spectral density of shot noise fluctuations as a function of impinging current [57] and measuring the temperature scaling of the tunneling current pattern [58]. Both measurements were consistent with $e^* = e/4$, where e is the electron charge. These measurements can not distinguish between Abelian and non-Abelian statistics, since the quasiparticle charge is $e/4$ in both Abelian and non-Abelian models. To probe the statistics, an interferometer with at least two point contacts is needed.

The experiments probing quasiparticle statistics can be done using a Fabry-Perot type interferometer on top of a FQHE layer [59, 60]. An interference pattern is induced on the longitudinal conductance σ_{xx} as the side gate voltage V_s is varied. The side gate voltage controls the size of the island where bulk quasiparticles are confined, thus changing the magnetic flux which the edge quasiparticles circulate. As the magnetic flux inside the interferometer loop changes, also the Aharonov-Bohm phase acquired by quasiparticles circulating the loop changes, resulting in Aharonov-Bohm oscillations in the transmitted current through the interferometer. The period of the AB oscillations is given by $\Delta A_L = (e/e^*)\Phi_0/B$, where e^* is the charge of the tunneling quasiparticle and $\Phi_0 = hc/e$ is the magnetic flux quantum. The area of the loop is approximated to be linearly dependent on the applied side gate voltage, $\Delta A_L \propto \Delta V_s$. AB oscillations are also observed when magnetic field is varied, but these oscillations are not usually measured because varying the magnetic field changes also the area of the island, allowing less control of the experimental setup.

The current through the non-Abelian interferometer is given by [60]

$$I = (|t_1|^2 + |t_2|^2)/2 + \mathrm{Re}\{t_1^* t_2 e^{i\alpha} \langle \psi | B | \psi \rangle\}$$

where t_i are the tunneling amplitudes through constrictions 1 and 2, and B is the braid group representation associated with braiding the edge mode quasiparticle and bulk quasiparticles confined on the island. This expression holds when the quasiparticles wind around the island only once and tunneling at the point contacts is weak. It was pointed out in Refs. [61, 62] that for non-Abelian anyons, the Aharonov-Bohm oscillations are suppressed if the number of non-Abelian particles on the island is odd. The suppression of oscillations is due to the fact that for odd number of particles, the interference term in the above equation is not allowed by the fusion rules of Ising anyons. The disappearance of these oscillations was confirmed experimentally [63], but instead of complete suppression of oscillations, the period switched between the values corresponding to $e/4$ quasiparticle charge (σ anyon) and $e/2$ (ψ anyon), the $e/4$ oscillations having a larger amplitude. When the temperature was raised from 30 mK to 150 mK, the $e/4$ oscillations disappeared. The conclusion was that if the number of quasiparticles on the island is even, both $e/4$ and $e/2$ oscillations are present. As the side gate voltage changes, the area of the island also changes, and new quasiparticles may be introduced to the enclosed area. If the number of quasiparticles changes from

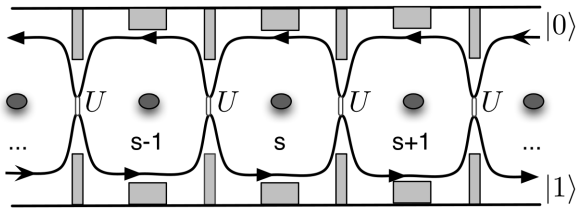

Figure 2.10: Potential physical realization using a chained version of the two point contact interferometer in Fractional Quantum Hall systems. The tunneling matrix U and dynamical and Aharanov- Bohm phases can be tuned by adjusting the gate voltages indicated by the thin and wide rectangles. The tunneling matrix U corresponds to the coin flip operator F in the quantum walk formalism.

even to odd, the $e/4$ oscillations disappear but $e/2$ oscillations persist. This interpretation was backed up by further measurements [64], where the period switching was observed over large sweeps of the side gate voltage, and the switching was aperiodic as a function of the side gate voltage, which fits the picture that the quasiparticles are randomly distributed on the island. Additionally, performing the sweeps with two different magnetic fields which differ by an energy corresponding to addition of a single localized quasiparticle, the patterns were interchanged, which supports the idea that $e/4$ oscillations are observed for even number of quasiparticles and $e/2$ oscillations for odd number of quasiparticles. The origin of $e/2$ oscillations was discussed in detail in Ref. [65], where two explanations were given: they could correspond to an $e/4$ particle going through the interferometer loop twice, or there could be ψ particles going through the interferometer loop as well. Based on their analysis, the latter option seems more plausible.

2.5.2 Experimental scheme for anyonic quantum walks

An experimental setup which implements the anyonic quantum walk scheme could be used to probe statistical properties of quasiparticles via transport measurements while keeping the magnetic field and the area of the interference region constant, contrary to previous measurements which track the interference patterns as these parameters are varied. Such an experiment would implement a multipoint contact version of the Fabry-Perot type interferometer as shown in Fig. 2.10 The experiment should be done in the weak bulk-edge coupling regime of the side gate voltage, where the Aharonov-Bohm oscillations dominate the interference pattern [65]. Since the side gate voltage should be kept low and constant, the side gate is not needed at all. However, it is good to introduce antidot top gates on the islands [66], such that quasiparticles can be injected on the islands one by one.

To measure the probability distribution of the quantum walk directly would require introducing contacts at each location corresponding to spatial sites of the quantum walk. A simplified scheme where the conductivity is only measured at the ends of the multipoint contact ladder is depicted in Fig. 2.11. In this scheme, the quantum walk is induced by bringing a voltage contact to the middle of the ladder, such that localized

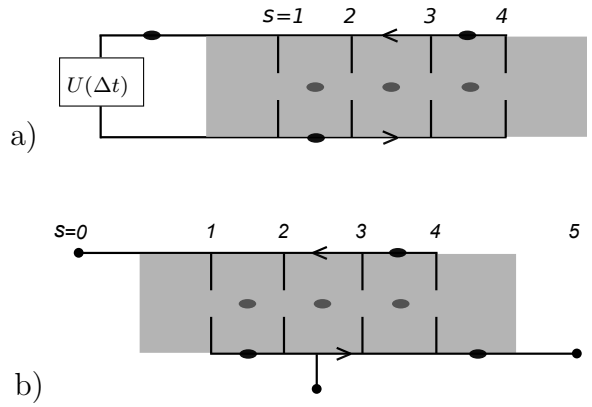

FIGURE 2.11: Measurement setup for a quantum walk in a multipoint contact interferometer. a) Non-destructive measurement. The walker interacts weakly with the measurement device and returns to the system in an altered state. The action of the measurement process in a characteristic time interval Δt is represented by the operator U, generated by the interaction between the walker and the measurement device. This introduces decoherence to the quantum walk, but the total evolution of the quantum walk + measurement device system is unitary. b) Destructive measurement. A voltage contact is brought to the middle of the chain, such that quasiparticles can be injected to the edge modes. The experiment measures the two-terminal conductivity between the initial point and either of the end point contacts. The quasiparticle configuration on the islands can be controlled with antidot gates, such that increasing the gate voltage by the chemical potential of the bulk quasiparticles creates a single quasiparticle in the bulk.

initial states with definite initial coin state $|0\rangle$ can be easily prepared. Changing the voltage in this gate by the value corresponding to the chemical potential of the edge quasiparticles creates a single edge mode which starts to propagate along the edge. The coin states are encoded by the occupation of either upper or lower edge and the tunneling matrix at the point contacts corresponds to the coin mixing operator in the quantum walk formalism. The conductivity between the initial point and the edge contacts is given by the probability for the quantum walker to reach the end sites. The measurement is assumed to be destructive, such that quasiparticles reaching the end contacts can not travel back, which corresponds to introducing absorbing boundary conditions to the quantum walk.

In the weak tunneling limit of the quantum point contacts, multiple windings around the interferometer are strongly suppressed in the signal. In the quantum walk language, the weak tunneling limit corresponds to using a coin which mixes the coin states only weakly. The Hadamard operator is strongly mixing, so implementation of the Hadamard walk would require strong coupling at the point contacts.

The initial fusion state can be controlled with the antidot gates. The antidots control the number of quasiparticles on the islands, allowing measurements with different charge configurations on the islands. Particular charge configurations can also be prepared by measuring charges on each island separately (although additional gates are probably needed). Of special interest is the all-vacuum configuration, for which the

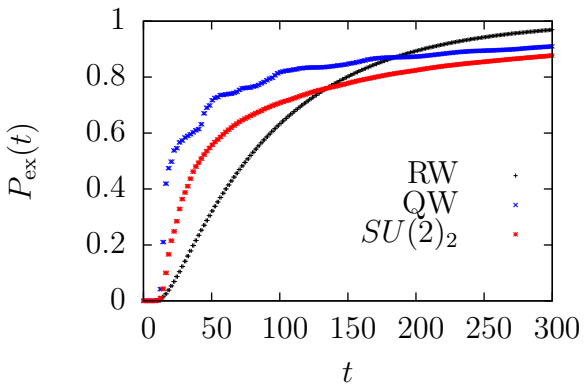

Figure 2.12: Accumulated exit probability as a function of time. The number of sites in the simulation is 21.

statistics should not play any role, and the uniform filling configuration, in which the number of localized quasiparticles is odd such that the total charge on a single island is σ.

We propose two types of measurements to be performed, with uniform and disordered charge configurations on the islands. The uniform case requires careful preparation of the initial fusion state, such that all islands are occupied by the same number of quasiparticles. Based on results on anyonic quantum walks with uniform charge configuration, the probability to reach a site far from the initial site is smaller if the walker and all stationary anyons are σ anyons. Intuitively, the conductivity should be lower in this case, but this drop in conductance can not be quantified with the quantum walk model. A toy model simulation of the anyonic walk is presented in Fig. 2.12, where the accumulated exit probability is plotted as a function of time. Assuming absorbing boundary conditions, the total exit probability at time step t is $p(s = -1, t) + p(s = N + 2, t)$. The accumulated exit probability can then be written

$$P_{\mathrm{ex}}(t) = \sum_{t'=0}^{t} p(-1, t') + p(N + 2, t'). \tag{2.27}$$

The simulation shows that initially the random walker takes the longest time to exit the lattice. The anyonic walker is faster than the random walker, but slower than the quantum walker.

In real experiments, the quasiparticle occupations on the islands are hard to control and experiments with uniform charge configurations might be unrealistic. A more implementable experiment would exploit disorder in the determination of statistics. As shown in Chapter 5, Abelian anyons localize when the results are averaged over many different occupations, while non-Abelian anyons do not. If the length of the ladder is bigger than the localization length, on average there should be no particles exiting the ladder and the average conductivity should be zero. If the particles are non-Abelian anyons, there should be some leakage current in the ends of the ladder. Unfortunately the amount of this current can not be estimated quantitavely from the

quantum walk.

Because of imperfections in the experimental preparation, there is bound to be some disorder in the system: the front gate voltages might vary across the ladder, the effective sizes of the islands are different, and distances between front gates are different. The fluctuations of the front gate voltage correspond to using a slightly different coin at every site, and such disorder has been shown to cause localization for almost all cases considered in the literature. The size of the island is proportional to the Aharonov-Bohm phase, and the distance between front gates brings an additional dynamical phase, which can both be absorbed to a random statistical phase, which has been shown to cause localization. Therefore any type of disorder in the experimental configuration implies localization for Abelian anyons, but the effective temporal randomness in the non-Abelian case causes the wave packet to diffuse, thus allowing to distinguish the pure statistical behaviour of the quasiparticles.

The main concern in our proposal is the coherence length of mobile quasiparticles. Localization is only observed if the spatial disorder is fixed during a single run of the experiment, and fluctuations occur between the runs. The observation of localization might need a ladder with several quantum point contacts, but when the length of the sample is increased, the propagating edge modes are subject to noise and the quantum coherence might be lost. The noise would introduce temporal randomness such that localization can not be observed. It is therefore important that localization is shown for values of the magnetic field which are known to support Abelian anyons.

3
Ising Anyons

The simplest anyonic quantum walk is the uniform and unitary walk, where each island is occupied by a single anyon and the walk evolves in a pure state $\big|\Psi(t)\big\rangle$. The time evolution of the spatial probability distribution for an initially localized walker particle is solved analytically as a function of number of time steps. The main question is, how likely is it to find the walker a distance $|s - s_0|$ away from the initial location? In other words, how fast does the particle propagate away when it is initially placed at a definite location. The probability to find the particle far away from its initial location can be quantified by the variance of the probability distribution of the position of the particle. The main result is that the variance depends linearly on the number of time steps t. If each island is occupied by the vacuum charge, then the walk is equivalent to the Hadamard walk, and the variance depends linearly on the square of the number of time steps. Similarly, if the anyons are Abelian, the statistical phase has a trivial effect and the walk is identical to the Hadamard walk. Thus, the mutual statistical interactions of the non-Abelian anyons slow down the propagation of the wave packet from ballistic to diffusive.

This chapter is organized as follows. In Sec. 3.1, the trace over the fusion degrees of freedom is expressed in terms of the Jones polynomial, and it is shown how the structure of the links encountered in anyonic quantum walks can be used to simplify the Jones polynomial, leading to a compact formula for the probability distribution in Eq. (3.8). The exact numerical results up to 25 time steps are presented in Sec. 3.2. The asymptotic results for the variance as $t \to \infty$ are derived in Sec. 3.3 using certain approximations. The asymptotic behaviour is shown to be related to the fraction of proper links over all links, and the fraction of proper paths is shown to be $O(1/t^2)$ in Sec. 3.4. The results presented in this chapter are reported in [L. Lehman, V. Zatloukal, J. Pachos, G. Brennen and Z. Wang. *Quantum Walks with Non-Abelian Anyons.*]

3.1 Analytical formula for probability distribution

In Sec. 2.3 it was shown that the evaluation of the anyonic term $\mathrm{Tr}\left(\mathcal{B}_{\overline{a}}^{t}\big|\Phi_0\big\rangle\big\langle\Phi_0\big|(\mathcal{B}_{\overline{a}'}^{t})^{\dagger}\right)$ for $SU(2)_k$ anyons of Chern-Simons theory is equivalent to evaluating the Jones polynomial of the link drawn by the trajectories of the anyons. Evaluation of the Jones polynomial for a generic link is exponentially hard in the number of crossings [33], and since number of crossings is equal to the number of time steps, the evaluation of the Jones polynomial is exponentially hard in time for *each* path. The calculation of the probability distribution is thus hopelessly inefficient in the general case. However, in the special case k=2, the calculation of the Jones polynomial is only polynomially hard in the number of crossings, and numerical calculations become slightly more efficient. The number of paths grows still exponentially in time and the probability distribution can only be evaluated for a small number of time steps.

This section presents one of the main results: an analytical formula for the anyonic quantum walk distribution of Ising anyons as a function of t. There is a structure to the links encountered in anyonic quantum walks that simplifies the evaluation of the Jones polynomial, such that the trace over the anyonic degrees of freedom can be expressed in terms of two simple link properties, *properness* and `arf`, as explained later.

The system's initial state is $\big|\Psi_0\big\rangle = \big|s_0\big\rangle_{\mathrm{S}}\big|\Phi_0\big\rangle_{\mathrm{F}}\big|0\big\rangle_{\mathrm{C}}$, where $\big|\Phi_0\big\rangle = B_0\big|\chi_0\big\rangle$ is the vacuum state of the N_A pairs of anyons with half the members braided to the left as depicted in Sec. 2.3. The lattice consists of N spatial sites on a line with $N-1$ islands between the sites, each island filled with a single stationary Ising anyon. The total number of anyons taking part in the walk is then $N_A = N$. Choosing the Hadamard coin $F = \frac{1}{\sqrt{2}}\begin{pmatrix}1 & 1\\ 1 & -1\end{pmatrix}$ as the coin flip operator and recalling Eq. (2.7), the probability distribution after t steps is

$$p(s,t) = \big(\rho_{\mathrm{S}}(t)\big)_{s,s} = \frac{1}{2^t}\sum_{\overline{a},\overline{a}'\rightsquigarrow s}(-1)^{z(\overline{a})+z(\overline{a}')}\,\mathrm{Tr}\left(\mathcal{B}_{\overline{a}}^{t}\big|\Phi_0\big\rangle\big\langle\Phi_0\big|(\mathcal{B}_{\overline{a}'}^{t})^{\dagger}\right). \tag{3.1}$$

The lattice is assumed to be infinite. In reality, for a given number of time steps, the size of the lattice is always chosen such that $N \geq 2t+1$, and boundary conditions need not be used.

The anyonic trace term is evaluated using link invariant polynomials as described in Sec. 2.3. Although the correspondence between the fusion trace and the Jones polynomial holds for spin-1/2 irreps of the quantum group $SU(2)_k$, the probability distribution for Ising anyons can also be calculated using the formula (2.12). As seen in Sec. 2.2, the braid generators of the $SU(2)_2$ and Ising anyon models are equivalent up to a phase and complex conjugation. To see that the probabilities are invariant, consider a phase change in the generators such that the braid word becomes $\mathcal{B}_{\overline{a}} = e^{i\phi_{\overline{a}}}\mathcal{B}_{\overline{a}}^{*}$ (* denotes complex conjugation). For the terms with $\overline{a} = \overline{a}'$ in the sum in Eq. (3.1) the braid words cancel each other and the anyonic contribution is trivial. The remaining

terms can be written

$$\begin{aligned}
&\frac{1}{2^t}\sum_{\substack{\overline{a},\overline{a}'\rightsquigarrow s\\ \text{s.t. } \overline{a}\neq\overline{a}'}}\Big[(-1)^{z(\overline{a})+z(\overline{a}')}\ \mathrm{Tr}\left(e^{i\phi_{\overline{a}}}\mathcal{B}^*_{\overline{a}}\big|\Phi_0\big\rangle\big\langle\Phi_0\big|(\mathcal{B}^*_{\overline{a}'})^\dagger e^{-i\phi_{\overline{a}'}}\right)\\
&\qquad\qquad + (-1)^{z(\overline{a}')+z(\overline{a})}\ \mathrm{Tr}\left(e^{i\phi_{\overline{a}'}}\mathcal{B}^*_{\overline{a}'}\big|\Phi_0\big\rangle\big\langle\Phi_0\big|(\mathcal{B}^*_{\overline{a}})^\dagger e^{-i\phi_{\overline{a}}}\right)\Big]\\
=\ &\frac{1}{2^t}\sum_{\substack{\overline{a},\overline{a}'\rightsquigarrow s\\ \text{s.t. } \overline{a}\neq\overline{a}'}}(-1)^{z(\overline{a})+z(\overline{a}')}\Big[\big\langle\Phi_0\big|(\mathcal{B}^*_{\overline{a}'})^\dagger\mathcal{B}^*_{\overline{a}}\big|\Phi_0\big\rangle\\
&\qquad\qquad + \big\langle\Phi_0\big|(\mathcal{B}^*_{\overline{a}})^\dagger\,\mathcal{B}^*_{\overline{a}'}\big|\Phi_0\big\rangle\Big].
\end{aligned}$$

Here $\phi_{\overline{a}} = \phi_{\overline{a}'}$ since the walker braids exactly t times during both bra- and ket-evolution, and the phase difference for each generator of Ising and $SU(2)_2$ models is $e^{i\phi} = i$. The complex conjugation can now be moved to be taken over the whole expectation values and the anyonic term becomes

$$\begin{aligned}
&\big\langle\Phi_0\big|(\mathcal{B}^*_{\overline{a}'})^\dagger\mathcal{B}^*_{\overline{a}}\big|\Phi_0\big\rangle + \big\langle\Phi_0\big|(\mathcal{B}^*_{\overline{a}})^\dagger\,\mathcal{B}^*_{\overline{a}'}\big|\Phi_0\big\rangle\\
&\qquad= \big\langle\Phi_0\big|(\mathcal{B}_{\overline{a}'})^\dagger\mathcal{B}_{\overline{a}}\big|\Phi_0\big\rangle^* + \big\langle\Phi_0\big|(\mathcal{B}_{\overline{a}'})^\dagger\,\mathcal{B}_{\overline{a}}\big|\Phi_0\big\rangle\\
&\qquad= 2\,\mathrm{Re}\Big(\big\langle\Phi_0\big|(\mathcal{B}_{\overline{a}'})^\dagger\,\mathcal{B}_{\overline{a}}\big|\Phi_0\big\rangle\Big)
\end{aligned}$$

which is exactly the same without phases and complex conjugation, and results hold equivalently for Ising and $SU(2)_2$ anyons.

Recalling Eq. (2.12), the trace over the fusion space is related to the Jones polynomial as

$$\mathrm{Tr}\left(\mathcal{B}^t_{\overline{a}}\big|\Phi_0\big\rangle\big\langle\Phi_0\big|(\mathcal{B}^t_{\overline{a}'})^\dagger\right) = \frac{(-q^{3/4})^{w(L(\overline{a},\overline{a}'))}}{d^{N_A-1}}V_{L(\overline{a},\overline{a}')}(q)$$

where the quantum dimension is $d = \sqrt{2}$ for Ising anyons, and the parameter of the Jones polynomial is $q = i$. The link corresponding to the paths of the anyons is the Markov closure of the braid word ${\mathcal{B}^t_{\overline{a}'}}^\dagger\mathcal{B}^t_{\overline{a}}$:

$$L(\overline{a},\overline{a}') \mathrel{\widehat{=}} ({\mathcal{B}^t_{\overline{a}'}}^\dagger\mathcal{B}^t_{\overline{a}})^{\mathrm{Markov}}.$$

Since the braids in the forward and backward time parts of the link have the opposite orientation (counterclockwise and clockwise respectively), and the number of crossings is equal to the number of time steps in both parts, the writhe is always zero: $w(L(\overline{a},\overline{a}')) = t - t = 0$. Thus for a uniform filling of Ising anyons the fusion trace is simply related to the Jones polynomial via

$$\mathrm{Tr}\left(\mathcal{B}^t_{\overline{a}}\big|\Phi_0\big\rangle\big\langle\Phi_0\big|(\mathcal{B}^t_{\overline{a}'})^\dagger\right) = \frac{V_{L(\overline{a},\overline{a}')}(i)}{\sqrt{2}^{N_A-1}}. \tag{3.2}$$

The probability distribution is now given by a sum over weighted Jones polynomials. At the special value $q = i$, the Jones polynomial of a link can be related to a simpler knot invariant known as the `arf` invariant [67]. Specifically,

$$V_L(i) = \begin{cases} \sqrt{2}^{\#(L)-1}(-1)^{\mathtt{arf}(L)} & \text{if } L \text{ proper}\\ 0 & \text{if } L \text{ not proper}\end{cases} \tag{3.3}$$

where the number of components $\#(L) = N_A$ here. An oriented link is *proper* if each component L_k evenly links the union of other components, such that

$$\sum_{j\neq k} lk(L_j, L_k) = 0 \bmod 2, \quad \forall j \tag{3.4}$$

holds. The linking number of two components $lk(L_j, L_k)$ is defined in Sec. 1.1.2 and can be computed in polynomial time in the number of crossings of a braid presentation. The `arf` of a knot K, which is a single component link, is equal to zero if K is equivalent to the unknot and is equal to one if K is equivalent to the trefoil knot. It can be related to the Alexander polynomial for knots Δ_K:

$$\texttt{arf}(K) = \frac{(\Delta_K(-1))^2 - 1}{8} \bmod 2$$

which can be computed in time polynomial in the crossing number of a braid presentation of the knot [68]. For multicomponent links L, the `arf` has a more complicated definition in terms of a knot that is related to the link. Since both properness and `arf` can be computed in polynomial time, the Jones polynomials at value $q = i$ can be evaluated in polynomial time [33].

The evaluation of `arf` can be simplified for links that appear in anyonic walks. If a link is *totally proper*, every component of the link links evenly with *every* other component (not just the union), or $lk(L_j, L_k) = 0 \bmod 2 \ \forall j, k$. In the special case where the link L is totally proper, there is a three local formula for the `arf` invariant:

$$\texttt{arf}(L) = \sum_i c_1(L_i) + \sum_{i<j} c_2(L_i, L_j) + \sum_{i<j<k} c_3(L_i, L_j, L_k) \bmod 2 \tag{3.5}$$

where $c_s(\Gamma)$ is the coefficient of z^{s+1} in the Alexander-Conway polynomial of the s-component sublink Γ [67]. An s-component sublink is a link obtained from the original link by removing all but s components. It is immediately clear that all totally proper links are also proper, but the converse is not necessarily true. However, the links that appear in anyonic quantum walks have a special structure such that it is true, as will be shown next. This allows to use the above formula in Eq. 3.3. It simplifies greatly the evaluation of `arf`, as one needs only to compute quantities for links with 1, 2 and 3 components.

To see that proper links are also totally proper, consider the set of all the sums $S = \{\sum_{k\neq j} lk(L_j, L_k)\}_{j=1}^n$. The condition of L being proper is that every member of S is an even integer. Separating the walker component, the sums can be written $S = \{\sum_{k\neq j} lk(L_j, L_k)\}_{j\neq w} \sqcup \{\sum_{k\neq w} lk(L_w, L_k)\}$, but since the stationary strands never braid with each other, the only term surviving from the sum in the $j \neq w$ part is $lk(L_j, L_w)$. The $j = w$ part is the sum of linking numbers of the walker component and every other component. Note that the crossings are always of the same type in the forward and backward time parts of the link diagram (and opposite to each other), and the number of crossings is always equal to the number of time steps in both parts, therefore the total linking number is zero: $\sum_{k\neq w} lk(L_w, L_k) = (t - t)/2 = 0$. Thus for the links considered here, $S = \{lk(L_j, L_w)\}_{j\neq w} \sqcup \{0\}$. But the condition that L

is totally proper is precisely that every member of the set $\{lk(L_j, L_w)\}_{j\neq w}$ is an even integer. Hence if L is proper then it is totally proper.

The structure of the anyonic walk paths allows even further simplification of the Jones polynomial. The c_1 term in `arf` counts the number of tangles in each component, and tangles can only form when a particle makes a loop and goes through it. Such a process would correspond to turning backwards in time, or braiding the particle with its antipartner in a certain way and then fusing them. These processes do not appear in paths, so there is no self-linking: $c_1 = 0$.

Furthermore, the term $\sum_{i<j} c_2(L_i, L_j)$ for the links in anyon walks is an even number. For that it is only necessary to consider links involving the walker L_w and any other component L_j since the non-walker components are disjoint. Such a link is the braid closure of a braid in the two component braid group $\mathcal{B}_2$ with one generator b so that link can be written, $(L_w, L_j) = (b^m)^{\text{Markov}}$ where $m = 2 \times lk(L_w, L_j)$. The two-point invariant can be computed using the defining skein relation for the Alexander-Conway polynomial

$$\nabla_{\ell_+} - \nabla_{\ell_-} = z\nabla_{\ell_0}. \tag{3.6}$$

If one of the components is unlinked from the others then it can be removed with a multiplicative factor: $\nabla_O = 1$. The polynomial for any link L can be written as $\nabla_L(z) = \sum_{i=0}^{\infty} a_i z^i$. For pairwise component links (L_w, L_j) the Alexander-Conway polynomial can be expressed as

$$\nabla_{(L_w,L_j)} = f_{|m|}(z) + f_{|m|-1}(z),$$

where these functions satisfy the Alexander-Conway skein relation: $f_{|m|}(z) = zf_{|m|-1}(z) + f_{|m|-2}(z)$. This can be verified by writing the skein relation for the Alexander-Conway polynomial, noting that the deformations just remove one or two of the crossings such that the new links can be written as $(b^{m-1})^{\text{Markov}}$ and $(b^{m-2})^{\text{Markov}}$, and using the definition of the Alexander-Conway polynomial in terms of the function $f_{|m|}(z)$. The recursion relation for the function $f_{|m|}(z)$ can be solved using Mathematica to get the result as

$$\begin{aligned} f_{|m|}(z) &= \tfrac{1}{2^{m+1}\sqrt{z^2+4}}\Big[z\Big(\big(z+\sqrt{z^2+4}\big)^m - \big(z-\sqrt{z^2+4}\big)^m\Big) \\ &\quad +\sqrt{z^2+4}\Big(\big(z+\sqrt{z^2+4}\big)^m + \big(z-\sqrt{z^2+4}\big)^m\Big)\Big]. \end{aligned}$$

Expanding the Alexander-Conway polynomial in powers of z and substituting $m = 2lk(L_w, L_j)$, the expression for c_2 can now be read from the coefficient of the cubic term:

$$c_2(L_w, L_j) = lk(L_w, L_j)(lk(L_w, L_j)^2 - 1)/6. \tag{3.7}$$

Note that the linking numbers are always even, $lk(L_w, L_j) = 2n_j$ with n_j an integer, so the sum can be written as

$$\begin{aligned} \textstyle\sum_{j<k} c_2(L_j, L_k) &= \tfrac{8}{6}\textstyle\sum_{j\neq w} n_j^3 - \tfrac{8}{6}\sum_{j\neq w} n_j \\ &= 8\textstyle\sum_{j\neq w}\binom{n_j+1}{3} \quad \in 2\mathbb{N} \end{aligned}$$

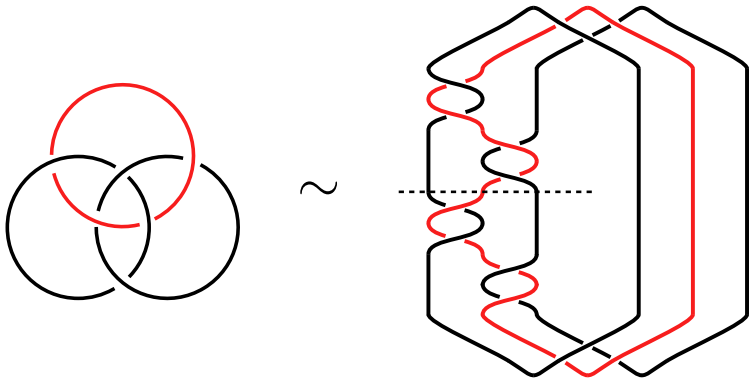

FIGURE 3.1: Borromean rings and the corresponding quantum walk path. These links are related via Reidemeister moves.

using the facts that the sum of the linking numbers is zero, so that $\sum_{j\neq w} n_j = 0$, and the binomial coefficient is always an integer.

Finally, the triple component invariant $c_3(L_r, L_s, L_t)$ is known as the Milnor invariant. It counts the number of Borromean rings in three-component sublinks [69], and it is the only term that has a nontrivial contribution to the `arf` of the links. Borromean rings are a three-component link where each pair of components are disjoint to each other, but together they are inseparable. It can be shown via Reidemeister moves that the Borromean rings are isotopic to the anyon walk path shown in Fig. 3.1. If b_1 and b_2 are the generators of the three-strand braid group, then this path corresponds to the braid word $B = (b_1^\dagger)^2(b_2^\dagger)^2 b_1^2 b_2^2$. Note that at the last time step the walker moves in different directions in the forward and backward time parts, thus this path is not well defined and the first Borromean rings start to form after 5 time steps of anyonic quantum walk evolution.

To evaluate the Milnor invariant c_3, it is helpful to consider the relation between fusion trace and the Jones polynomial. First, for any triple of components without the walker, the invariant is always zero: $c_3(L_r, L_s, L_t) = 0$; $r, s, t \neq w$. Picking two components r and s, the Jones polynomial for the sublink (L_r, L_w, L_s) with the walker component can be written

$$V_{(L_r,L_w,L_s)}(i) = \sqrt{2}^2(-1)^{\mathtt{arf}(L_r,L_w,L_s)}.$$

Since the original link is totally proper, also the sublink is totally proper. Using the formula (3.5) for `arf`, and noting again that $c_1 = 0$ and $c_2 = 0$, the Jones polynomial simplifies to $V_{(L_r,L_w,L_s)}(i) = 2(-1)^{c_3(L_r,L_w,L_s)}$. Now consider the 3-strand braid group with generators b_1 and b_2, and define braid words $B_{\bar{a}}$ and $B_{\bar{a}'}$ such that the 3-component sublink (L_r, L_w, L_s) corresponds to the Markov closure of the braid word $B_{\bar{a}'}^\dagger B_{\bar{a}}$. Then the fusion trace over this braid word is related to the Jones polynomial of the corresponding link as

$$\mathrm{Tr}\left(B_{\bar{a}}\big|\Phi_0\big\rangle\big\langle\Phi_0\big|B_{\bar{a}'}^\dagger\right) = \frac{(-i^{3/4})^{w(L_r,L_w,L_s)}}{d^{N_A-1}} V_{(L_r,L_w,L_s)}(i) = (-1)^{c_3(L_r,L_w,L_s)}$$

where total properness implies $w = 0$. The braid words $B_{\overline{a}}$ and $B^{\dagger}_{\overline{a}'}$ are formed by taking the original braid words $\mathcal{B}^t_{\overline{a}}$ and $(\mathcal{B}^t_{\overline{a}})^{\dagger}$, picking only the generators which correspond to braiding with components r and t, and relabelling the generators as b_1 and b_2. Thus, the evenness of $c_3(L_r, L_w, L_s)$ is determined by the trace over the generators of the 3-strand braid group. For Ising anyons, the representations for these generators are

$$b_1 = -e^{-i\pi/8}\begin{pmatrix} 1 & 0 \\ 0 & i \end{pmatrix} = -e^{i\pi/8}e^{-i\pi\sigma^z/4}$$
$$b_2 = -\frac{e^{i\pi/8}}{\sqrt{2}}\begin{pmatrix} 1 & -i \\ -i & 1 \end{pmatrix} = -e^{i\pi/8}e^{-i\pi\sigma^x/4}.$$

where $\sigma^{x,z}$ are the Pauli operators. Note that if the walker is initially in the middle, $r < w < s$, the generators b_1 and b_2 always appear in pairs, since the walker has to return to the middle before braiding with the other strand. Noting that $b_1^2 = e^{-i\pi/4}\sigma^z$ and $b_2^2 = e^{-i\pi/4}\sigma^x$, the calculation of the trace reduces to analysis of Pauli operators. Using the commutation relations of Pauli operators and the identities $(\sigma^x)^2 = (\sigma^x)^2 = \mathbb{I}$, the string of braid words is found to be proportional to the identity matrix, with the sign determining evenness of $c_3(L_r, L_w, L_s)$. If the walker is not between strands r and s initially or at the final step, there is an extra generator in the beginning or end of the braid word, but the effect in both cases is trivial under tracing. Thus, for a given total link $L(\overline{a}, \overline{a}')$, the sum $\sum_{i<j<k} c_3(L_i, L_j, L_k) \bmod 2$ is calculated by forming the 3-strand braid words corresponding to all pairs of stationary strands and the walker strand, grouping the squares of generators b_1 and b_2, and calculating the sign of the string of Pauli operators.

In summary, the analysis above allows to express the Jones polynomial of the link corresponding to a path $(\overline{a}, \overline{a}')$ in a very compact form, and the probability distribution at time step t can now be written

$$p(s,t) = \sum_{\overline{a},\overline{a}' \rightsquigarrow s} \begin{cases} (-1)^{z(\overline{a})+z(\overline{a}')+\tau(\overline{a},\overline{a}')}/2^t & L \text{ proper} \\ 0 & L \text{ not proper} \end{cases} \tag{3.8}$$

where the sum of Milnor invariants over sublinks is $\tau(\vec{a}, \vec{a}') = \sum_{r<s<t} c_3(L_r, L_s, L_t)$. When all links are proper and $\tau(\overline{a}, \overline{a}')$ is even, then $p(s,t)$ becomes equal to $p_{\mathrm{QW}}(s,t)$, the Hadamard walk distribution. When all nonmirror paths (i.e., $\overline{a} \neq \overline{a}'$) are nonproper, then $p(s,t)$ becomes equal to $p_{\mathrm{RW}}(s,t)$, the classical random walk distribution.

3.2 Numerical results

In the previous section, it was shown how the Jones polynomial simplifies for links in anyonic quantum walks, which allowed a compact expression for the spatial probability distribution of the walker at time step t, see Eq. 3.8. The anyonic contribution to each path is given by properness of the corresponding link and the sum of the Milnor invariants $\tau(\overline{a}, \overline{a}')$. It was also shown that the evaluation of the Milnor invariants c_3 reduces to evaluation of trace over Pauli operators. The probability distribution for a given time step can thus be evaluated by implementing the following algorithm:

1. Form all the pairs of paths leading to site s by taking all vectors $\overline{a}$ and $\overline{a}'$ of length t, such that they satisfy $s = s_0 + 2\sum_{t'=1}^{t} a_{t'} - t$ and have identical last elements, $a_t = a'_t$. The number of such paths is $\binom{t-1}{H_{s,t}-1}^2 + \binom{t-1}{H_{s,t}}^2$, where $H_{s,t} = (s - s_0 + t)/2$.

2. Check if the path is proper, ie. $\sum_k (\#b_k(\overline{a}) - \#b_k^\dagger(\overline{a}'))/2 = 0$ where $\#b_k(\overline{a})$ is the number of generators b_k in the braid word $B_{\overline{a}}^t$.

3. If the path is proper, calculate $z(\overline{a}) + z(\overline{a}') = \sum_{t'=1}^{t-1}(a_t a_{t+1} + a'_t a'_{t+1})$. Otherwise proceed to next path.

4. Calculate $\tau(\overline{a}, \overline{a}')$ as described in the previous section.

5. Calculate $(-1)^{z(\overline{a})+z(\overline{a}')+\tau(\overline{a},\overline{a}')}/2^t$ and sum over all paths.

Note that this method gives only the spatial probability distribution, and the information about coin and fusion degrees of freedom is lost.

The efficiency of the calculations can be enhanced by taking into account two symmetries of the link invariants. First, exchanging the path indices $\overline{a}$ and $\overline{a}'$ is equivalent to turning the link around on the plane, and reversing each crossing. Such a procedure does not change the properness of the link or the number of Borromean rings in the sublinks, so that the summation can be done only over distinct pairs of paths. Second, considering the paths leading to $s_0 - s$ and $s_0 + s$, the links for these two cases can also be obtained from each other by turning the link around the axis orthogonal to the first one and reversing the crossings. In this case the coin terms $(-1)^{z(\overline{a})+z(\overline{a}')}$ will be different. The coin terms for $s_0 + s$ can be obtained from the paths leading to $s_0 - s$ by considering consecutive zeros instead of consecutive ones. Thus it suffices to consider only sites $s_0 - t \leq s \leq s_0$.

The numerical results for Ising anyons are presented in Fig. 3.2, where the spatial probability distribution has been plotted for $t = 0$, 10, 20 and 25 (calculations were done for every time step up to 25). At 25 time steps, the calculations are simulating the time evolution of 52 anyons (and their antipartners involved in the tracing).

The variance $\sigma^2(t) = \langle (s - s_0)^2 \rangle$, where the expectation value is $\langle O(s) \rangle \equiv \sum_s O(s) \times p(s,t)$, is plotted in Fig. 3.3, and it quickly approaches the linear random walk variance. The total variation distance to the random walk distribution is $||p(s,25) - p_{\mathrm{RW}}(s,25)|| = 0.04$ and to the Hadamard walk distribution $||p(s,25) - p_{\mathrm{QW}}(s,25)|| = 0.34$.

3.3 Asymptotics in time

The numerical results for the uniform filling of Ising anyons, shown in Fig. 3.3, suggest that the variance of the walker approaches that of the classical random walk, $\sigma_{\mathrm{Ising}}(t) \to t$. Here it is shown, using certain well justified approximations, that the variance of the non-Abelian anyonic walker is indeed linearly dependent (with coefficient 1) on the number of time steps in the asymptotic limit $t \to \infty$.

Comparing the formulas for the spatial probability distribution of the usual Hadamard walk and the non-Abelian anyonic walk, Eqs. (1.60) and (3.8) respectively, the

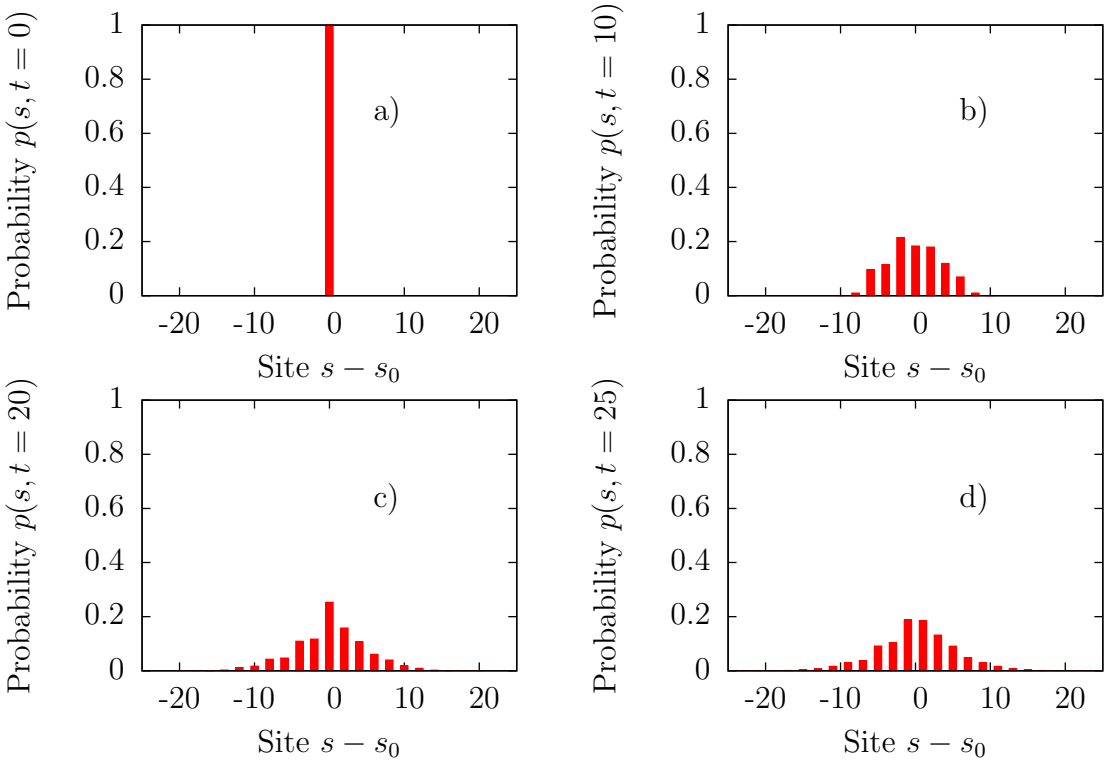

Figure 3.2: Time evolution of the probability distribution of the Ising anyon walk. a)–d) for 1, 10, 20 and 25 time steps respectively.

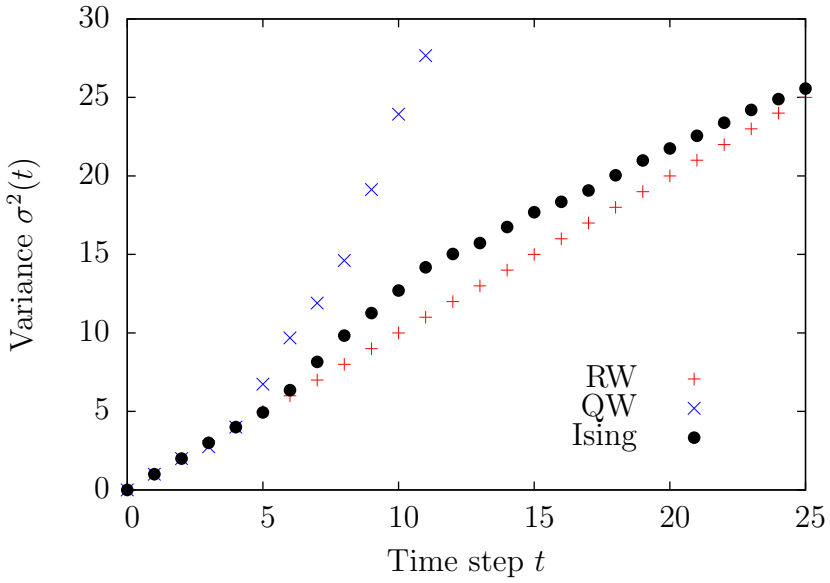

Figure 3.3: Numerical results for the variance of the spatial distribution $p(s, t)$ for the Ising anyonic walk and the corresponding classical and quantum walk evolutions with the same initial state.

amplitudes for each path are similar except the anyonic expression includes properness and the sum over Milnor invariants τ. The amplitudes in the Hadamard walk can only take values $\{1,-1\}$ but the amplitudes in the anyonic walk can take values $\{1,0,-1\}$. If the link corresponding to a path is not proper, the amplitude for such a path is zero since the Jones polynomial for the link is zero. Thus, the paths for which the amplitude is zero do not contribute to the probability at all, and the effect of the Jones polynomial is that it projects to the set of paths which have a proper link. As it turns out, at large time scales most of the paths are not associated with proper links.

The fraction of proper paths measures how often one gets a proper path, and is defined by

$$p_P(s,t) = \frac{N_P(s,t)}{\sum_{s'} N(s',t)} \tag{3.9}$$

where $N_P(s,t)$ is the number of proper paths leading to site s at time t, and $N(s,t)$ is the number of all paths leading there. The fraction p_P can be viewed as the statistical probability for a proper path to occur at site s, when the sample space is the set of all paths (on any site). The probability distribution $p(s,t)$ can be written in terms of p_P. In order to do this, first note that the probability distribution can always be separated to a classical random walk term and a quantum term,

$$p(s,t) = p_{\mathrm{RW}}(s,t) + \sum_{\substack{\overline{a},\overline{a}' \rightsquigarrow s \\ \text{st. } \overline{a}\neq\overline{a}'}} \begin{cases} (-1)^{z(\overline{a})+z(\overline{a}')+\tau(\overline{a},\overline{a}')}/2^t & L \text{ proper} \\ 0 & L \text{ not proper} \end{cases} \tag{3.10}$$

where $p_{\mathrm{RW}}(s,t) = \binom{t}{H_{s,t}}/2^t$ is the random walk probability to be at site s at time t, and the summation in the second term is only done over paths which are not identical. This is a consequence of the fact that the trace over the coin and fusion spaces is 1 for all identical paths, and the number of pairs of identical paths is equal to the number of paths leading to s at t in the random walk. Denoting $N_{P,\pm}$ the number of proper paths for which $(-1)^{z(\overline{a})+z(\overline{a}')+\tau(\overline{a},\overline{a}')} = \pm 1$ and $\overline{a} \neq \overline{a}'$ hold, the distribution is written

$$p(s,t) = p_{\mathrm{RW}}(s,t) + \frac{N_{P,+}(s,t) - N_{P,-}(s,t)}{2^t}. \tag{3.11}$$

Furthermore, if one assumes that properness is statistically uncorrelated with the value of $z(\overline{a}) + z(\overline{a}') + \tau(\overline{a},\overline{a}')$, then

$$\begin{aligned} N_{P,+} - N_{P,-} &= \left(\frac{N_{P,+}}{\sum N} - \frac{N_{P,-}}{\sum N}\right)\sum N \\ &= (p_{P,+} - p_{P,-})\sum N \\ &\approx p_P(p_+ - p_-)\sum N \\ &= p_P(N_+ - N_-) \end{aligned}$$

where the dependence on s and t is left out to clarify the notation, and $p_\pm(s,t) = N_\pm(s,t)/(\sum_{s'} N(s',t))$ is fraction of paths for which $(-1)^{z(\overline{a})+z(\overline{a}')+\tau(\overline{a},\overline{a}')} = \pm 1$ and $\overline{a} \neq \overline{a}'$ hold, but properness is not required. The statistical probability that the path is

proper and $(-1)^{z(\overline{a})+z(\overline{a}')+\tau(\overline{a},\overline{a}')} = 1$ can be written in terms of conditional probability: $p_{P,+} = p_P\, p_{+|P} \approx p_P\, p_+$, where the assumption about statistical independence has been used: $p_{+|\mathrm{P}} \approx p_+$.

Using the approximation above, the probability distribution can be written

$$p(s,t) \approx \tilde{p}(s,t) = p_{\mathrm{RW}}(s,t) + p_P(s,t)\,\frac{N_+(s,t) - N_-(s,t)}{2^t}. \tag{3.12}$$

Furthermore, by noting that the usual Hadamard walk distribution can also be written as $p_{\mathrm{QW}}(s,t) = p_{\mathrm{RW}}(s,t) + (N_+(s,t) - N_-(s,t))/2^t$, this reduces to the simple form:

$$\tilde{p}(s,t) = p_{\mathrm{RW}}(s,t) + p_P(s,t)\,(p_{\mathrm{QW}}(s,t) - p_{\mathrm{RW}}(s,t)). \tag{3.13}$$

The formula above has the intuitive property that it converges to the random walk distribution when $p_P = 0$ and to the Hadamard walk distribution when $p_P = 1$. In the former case, the quantum term becomes identically zero, and in the latter the quantum term is identical to Hadamard walk term when all the paths are proper (and $\tau = 0$), as is the case without approximation. The validity of the approximation on statistical independence can be estimated by expressing the probability as

$$p(s,t) = \tilde{p}(s,t) + E_{\mathrm{P}}(s,t) \tag{3.14}$$

where the analytical error function is defined as

$$E_{\mathrm{P}}(s,t) = \big(N_{P,+}(s,t) - N_{P,-}(s,t) - p_P(s,t)(N_+(s,t) - N_-(s,t))\big)/2^t. \tag{3.15}$$

Equation (3.13) turns out to be very helpful when estimating the variance of the probability distribution as a function of time steps. More specifically, the behaviour of the variance depends on time dependence of the fraction of proper paths $p_P(s,t)$. The variance can now be written

$$\sigma^2(t) = \sigma^2_{\mathrm{RW}}(t) + Q(t) + E(t) \equiv \tilde{\sigma}^2(t) + E(t) \tag{3.16}$$

where the quantum and error terms are given respectively as

$$\begin{aligned} Q(t) = &\sum_s p_P(p_{\mathrm{QW}} - p_{\mathrm{RW}})s^2 - \sum_s p_{\mathrm{RW}} s \Big(\sum_{s'} p_P(p_{\mathrm{QW}} - p_{\mathrm{RW}})s'\Big) \\ &- \Big(\sum_s p_P(p_{\mathrm{QW}} - p_{\mathrm{RW}})s\Big)^2 \end{aligned} \tag{3.17}$$

$$E(t) = \sum_s E_{\mathrm{P}} s^2 - \big(\sum_s E_{\mathrm{P}} s\big)^2 - \sum_s E_{\mathrm{P}} s \Big(\sum_{s'} \big(p_{\mathrm{RW}} + 2p_P(p_{\mathrm{QW}} - p_{\mathrm{RW}})\big)s'\Big) \tag{3.18}$$

and the variance is approximated as $\sigma^2(t) \approx \tilde{\sigma}^2(t) = \sigma^2_{\mathrm{RW}}(t) + Q(t)$ assuming statistical independence between properness and $z(\overline{a}) + z(\overline{a}') + \tau(\overline{a},\overline{a}')$.

Next it is shown that the term $Q(t)$ is bounded from above and below by a constant function, such that the variance behaves asymptotically similar to the variance of the random walk. A manipulation gives

$$Q(t) = \sum_s p_P(s,t\,)\big(p_{\mathrm{QW}} - p_{\mathrm{RW}}\big)\; s\,\big(s - \sum_{s'} \tilde{p}(s',t)s'\big). \tag{3.19}$$

The individual terms are bounded as follows:

$$-1 \leq p_{\mathrm{QW}}(s,t) - p_{\mathrm{RW}}(s,t) \leq 1$$

$$-t \leq s \leq t$$

choosing $s_0 = 0$, and $0 \leq p_P(s,t\,) \leq 1$. It can be shown that the last term is bounded by

$$-X_1(t) \leq s - \sum_{s'} \tilde{p}(s',t)s' \leq X_1(t)$$

$$X_1(t) = t\big(2 + \sum_{s'} p_P(s',t)\big)$$

And taking the extremes of each term yields the bounds

$$-X(t) \leq Q(t) \leq X(t)$$

$$X(t) = t^2 \sum_{s} p_P(s,t)\big(2 + \sum_{s'} p_P(s',t)\big)$$

where $X(t) \geq 0\ \forall t$. The sum over fraction of proper paths can be evaluated as follows. Recall $N_P(s,t)$ is the number of proper paths leading to site s at time t. It can be written as $N_P(s,t) = p'_P(s,t)\,N(s,t)$, where $p'_P(s,t) = N_P(s,t)/N(s,t)$ is the probability for proper paths, when the sample space is the set of all paths leading to (s,t). As argued in the next section, this probability is highest at the initial site, $p'_P(s,t) \leq p'_P(s_0,t)$. This allows to express the sum as

$$\sum_s p_P(s,t) = \frac{\sum_s N_P(s,t)}{\sum_{s'} N(s',t)} \leq \frac{p'_P(s_0,t)\sum_s N(s,t)}{\sum_{s'} N(s',t)} = p'_P(s_0,t). \tag{3.20}$$

Furthermore,

$$X(t) \leq t^2\, p'_P(s_0,t)\big(2 + p'_P(s_0,t)\big).$$

As shown in the next section, $p'_P(s_0,t) \leq \frac{C}{t^2}$. Thus $X(t) = O(1)$ as $t \to \infty$ and

$$\tilde{\sigma}^2(t) = \sigma^2_{\mathrm{RW}} + O(1) \tag{3.21}$$

3.4 Density of proper paths

The fraction $p_P(t)$ is plotted in Fig. 3.4 which shows clearly that most of the paths are not proper. This means that actually only a small subset of the paths contribute to the walk, while most amplitudes are zero. The highest fraction of paths is found at $t = 7$, where about every tenth path is proper.

It will now be shown that $p_P(s_0,t)$, the probability of a randomly chosen link L to be proper (mirror paths excluded), is bounded from above by a function $\frac{C}{t^2}$ under certain assumptions. (The prime in $p'_P(s_0,t)$ used to denote a different sample space is dropped in this section.) This is done by considering the number of links with even linking numbers and deriving $p_P(s_0,t)$ as the proportion of these links with respect to

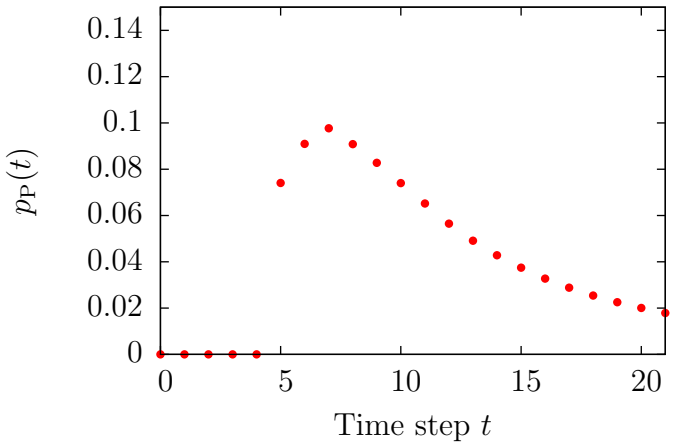

Figure 3.4: The fraction of proper paths. Here the fraction is calculated over all sites, ie. $p_P(t) = \frac{\sum_s N_P(s,t)}{\sum_s N(s,t)}$. Note that only nonidentical path pairs are taken into account. For a few initial steps, all legit path pairs are identical and $N(s,t) = 0$, and in these cases it has been defined that $p_P = 0$. The total number of non-identical paths for a given site is $N(s,t) = \binom{t-1}{H_{s,t}}^2 + \binom{t-1}{H_{s,t}-1}^2 - \binom{t}{H_s}$.

all links. The result holds for paths which end up on the initial site but numerical results suggest that $p_{\text{prop}}(s,t) < p_{\text{prop}}(s_0,t)$ if $s \neq s_0$, provided s is not too close to the boundaries at $s_0 \pm t$. In particular, it is true inside the domain $\frac{s_0-s}{t} = [-\frac{1}{\sqrt{2}}, \frac{1}{\sqrt{2}}]$.

Suppose a path $(\overline{a}, \overline{a}')$ leading after t steps to the position s_0 links with link components L_j, $j \in \{l, ..., r\}$ (Fig.3.5). For the corresponding link L to be proper, all the linking numbers $lk(L_w, L_l), ..., lk(L_w, L_r)$ must be even. Let $p_{\text{e}}(t,j)$ be the probability that $lk(L_w, L_j)$ is even. Assume that for large enough (fixed) t, the probabilities $p_{\text{e}}(t,j)$ can be treated as independent. This is justified inside the interval $\frac{s_0-s}{t} = [-\frac{1}{\sqrt{2}}, \frac{1}{\sqrt{2}}]$, where the number of paths that contribute to the anyonic walk density at each point s is exponential in t. The linking number of the walker with any particular component can change even/odd parity by a simple deformation and within the typical width (i.e. number of components touched by the walker) of the path there are an exponential number of such deformations. Hence the linking numbers of the walker with those components are well approximated as independent quantities, and the probability for the link L to be proper can be written as

$$p_P(s_0,t) = p_{\text{e}}(t,l) \cdot ... \cdot p_{\text{e}}(t,r) \ . \tag{3.22}$$

Denoting the maximum of the individual strand probabilities as

$$\rho \equiv \max_j p_{\text{e}}(t,j) \ , \tag{3.23}$$

where j runs over all link components L_j that braid with some t step long path leading to s_0, this can be estimated from above as

$$p_P(s_0,t) \leq \rho^w \ , \tag{3.24}$$

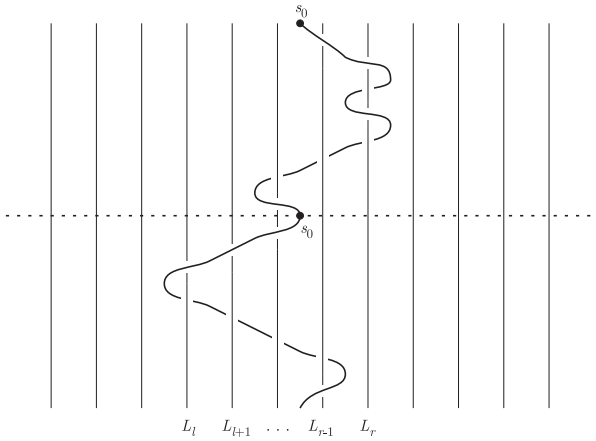

FIGURE 3.5: A generic path reaching after t steps (here $t = 8$) the position s_0. The path braids with all the link components $L_l, ..., L_r$, and its width is $w = r - l + 1 = 5$.

where $w = r - l + 1$ is called the *width* of the link.

The idea of the proof is to count all the paths whose width is exactly w, and calculate the probability of each such path having an even linking number over every strand. This gives an upper bound on the total number of paths as given in Eq. (3.31). This formula can be evaluated by subsituting the number of paths which touch a given diagonal given by Eq. (3.27), to yield the final result in Eq. (3.39).

The paths $(\overline{a}, \overline{a}')$ relevant for a walk of t steps must satisfy $a_t = a'_t$. Consider the paths leading to s_0 (assume t is even), for which $a_t = a'_t = 1$. It is useful to depict a half-path $\overline{a}$ as a lattice path on a $n - 1 \times n$ lattice ($n = \frac{t}{2}$) with allowed steps $\uparrow$ and $\rightarrow$ (Fig.3.6). The number of all such paths is [70]

$$\binom{2n-1}{n-1} \equiv \#(all) \ . \tag{3.25}$$

The number of lattice paths that touch the diagonal $y = x + w, w \in \{1, ..., n\}$ in an $n - 1$ by n lattice is

$$\binom{2n-1}{n-w} \equiv \#(w) \ . \tag{3.26}$$

Consider the set $\mathcal{P}_w$ of lattice paths that touch the diagonal $y = x + w$ but do not touch the further diagonal $y = x + w + 1$. The sets $\mathcal{P}_w$ are for distinct $w \in \{1, ..., n\}$ disjoint. The number of paths in $\mathcal{P}_w$ is

$$|\mathcal{P}_w| = \#(w) - \#(w+1) = \binom{2n-1}{n-w} - \binom{2n-1}{n-w-1} \ . \tag{3.27}$$

Here the convention that $\binom{m}{k} = 0$ if $k < 0$ is used. Furthermore, the union $\bigcup_{w=1}^{n} \mathcal{P}_w$ comprises all the paths on $n - 1$ by n lattice, which follows from

$$\begin{array}{rcl} \sum_{w=1}^{n} |\mathcal{P}_w| & = & \sum_{w=1}^{n} \left(\binom{2n-1}{n-w} - \binom{2n-1}{n-w-1} \right) \\ & = & \binom{2n-1}{n-1} \\ & = & \#(all). \end{array} \tag{3.28}$$

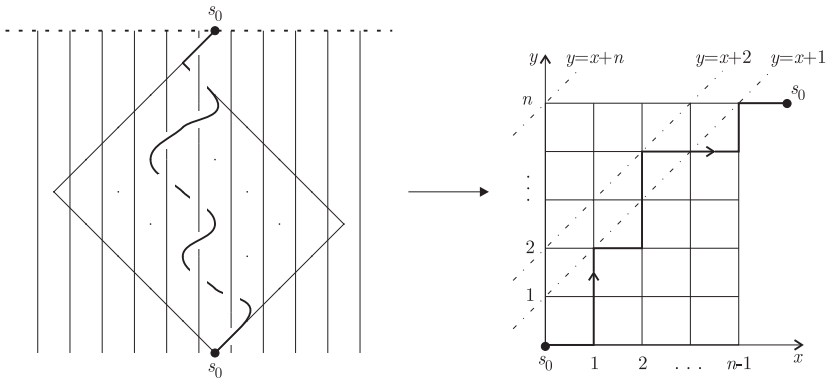

FIGURE 3.6: Any half-path (i.e. either "bra" or "ket" history of the walker) can be thought of as being realized on a two dimensional lattice, where only the steps $\uparrow$ and $\rightarrow$ are allowed. If the number of steps t is fixed (presume t even), the position reached after t steps $s = s_0$ and the last coin outcome $a_t = 1$, all the possible half-paths can be drawn on a lattice $n-1$ by n, where $n = \frac{t}{2}$. The figure on the right shows one such path. The lattice paths that touch the diagonal $y = x + w$ $(1 \leq w \leq n)$, but don't touch $y = x + w + 1$, braid with at least w link components. "At least", because they certainly braid with the w components to the left of s_0, but they might be (and typically are) spread to the right of s_0 as well.

A path $(\overline{a}, \overline{a}')$ consists of two lattice paths, the "bra" and "ket" parts $\overline{a}$ and $\overline{a}'$, where $\overline{a} \in \mathcal{P}_w$ and $\overline{a}' \in \mathcal{P}_{w'}$ for some $w, w' \in \{1, ..., n\}$, i.e. $(\overline{a}, \overline{a}') \in \mathcal{P}_w \times \mathcal{P}_{w'}$. The full path touches the diagonals w and w' during the bra and ket evolution respectively and the width of the path $(\overline{a}, \overline{a}')$ is at least $\max\{w, w'\}$ (if the other path extends to the left and the other to the right then the total width is $w + w'$). Now let ρ be the maximum probability that the linking number of a single strand is even, as defined in Eq. (3.23). Dividing the paths into sets of different widths, the number of proper paths can be estimated from above as

$$N_P(s_0, t) = \sum_{w=1}^{n} \rho^w \times \#(\overline{a}, \overline{a}' \mid \text{width } w) \; . \tag{3.29}$$

In the following, it does not matter how large ρ is as long as $\rho < 1$.

The number of paths with width w can be evaluated by considering all the combinations of bra and ket paths whose other part has at least width w and the other part can vary from 1 to w. This is illustrated in Fig. 3.7 which shows the different sets of paths for a given width w. The total number of paths with width w can thus be written

$$\#(\overline{a}, \overline{a}' \mid \text{width } w) = |\mathcal{P}_w|^2 + 2 \sum_{j=1}^{w-1} |\mathcal{P}_w||\mathcal{P}_j| - |\mathcal{P}_w|$$

The upper bound for the density of proper paths $p_P(s_0, t)$ can now be written as the

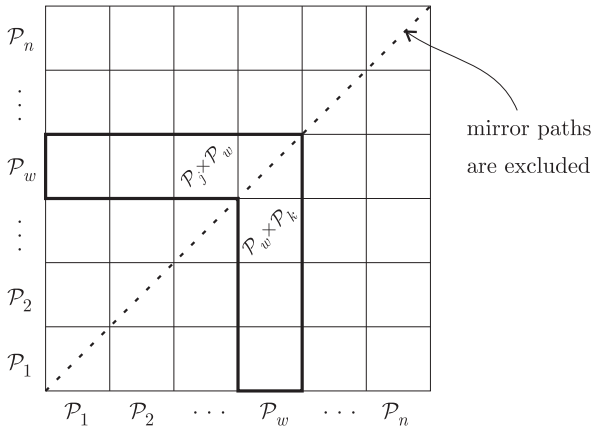

FIGURE 3.7: The set of paths that after t steps reach the position $s = s_0$, with the last coin outcome fixed. The axes correspond to bra and ket paths and a point corresponds to a full path $(\overline{a}, \overline{a}')$. The number of paths with width $\{w \dots 2w-1\}$ is $\#(\overline{a}, \overline{a}' \mid \text{width } w) = |\mathcal{P}_w|^2 + 2\sum_{j=1}^{w-1} |\mathcal{P}_w||\mathcal{P}_j| - |\mathcal{P}_w|$, where the mirror paths $\overline{a} = \overline{a}'$ are excluded.

number of proper paths divided by the number of all paths:

$$p_P(s_0,t) \leq \frac{N_P(s_0,t)}{N(s_0,t)} \tag{3.30}$$

$$= \frac{2\left(\sum_{w=1}^{n} \rho^w \left(|\mathcal{P}_w|^2 + 2\sum_{j=1}^{w-1} |\mathcal{P}_w||\mathcal{P}_j| - |\mathcal{P}_w|\right)\right)}{2\big(\#(all)^2 - \#(all)\big)} \ . \tag{3.31}$$

The number 2 in both the nominator and the denominator is due to the fact that both types of paths – with $a_t = a'_t = 0$ and $a_t = a'_t = 1$ – are counted, and the symmetry between the two situations is used. Also, the mirror paths have been excluded.

Before substituting to (3.31), rewrite (3.27) as

$$\begin{aligned} |\mathcal{P}_w| &= \tfrac{(2n-1)!}{(n-w-1)!(n+w-1)!}\left(\tfrac{1}{n-w} - \tfrac{1}{n+w}\right) \\ &= \tfrac{w}{n}\tbinom{2n}{n-w} \end{aligned} \tag{3.32}$$

and (3.25) as

$$\#(all) = \frac{(2n-1)!}{n!(n-1)!} = \frac{1}{2}\binom{2n}{n} \ . \tag{3.33}$$

Now (3.31) reads

$$p_P(s_0,t) \leq \frac{\frac{1}{2}\binom{2n}{n}}{\frac{1}{2}\binom{2n}{n}-1} \frac{\sum_{w=1}^{n} \rho^w \left(\binom{2n}{n-w}^2 - |\mathcal{P}_w| + 2\sum_{j=1}^{w-1} |\mathcal{P}_w||\mathcal{P}_j|\right)}{\frac{1}{2}\binom{2n}{n}\frac{1}{2}\binom{2n}{n}} \ ,$$

which can be estimated from above using the relation between binomial coefficients

$\binom{2n}{n-w} \leq \binom{2n}{n}$ to get:

$$\begin{aligned} p_P(s_0,t) &\leq \frac{\frac{1}{2}\binom{2n}{n}}{\frac{1}{2}\binom{2n}{n}-1} \frac{\sum_{w=1}^{n} \rho^w \left(\frac{w^2}{n^2} + 2\sum_{j=1}^{w-1} \frac{w}{n}\frac{j}{n}\right)}{\frac{1}{2}\frac{1}{2}} \\ &= \left(1+\frac{1}{\frac{1}{2}\binom{2n}{n}-1}\right) \frac{4}{n^2} \sum_{w=1}^{n} \rho^w \left(w^2 + 2w\sum_{j=1}^{w-1} j\right) \\ &= \left(1+\frac{1}{\frac{1}{2}\binom{2n}{n}-1}\right) \frac{4}{n^2} \sum_{w=1}^{n} \rho^w w^3 \ , \end{aligned} \tag{3.34}$$

where the formula $\sum_{j=1}^{w-1} j = \frac{1}{2}w(w-1)$ has been used. For $n \geq 2$ (i.e. $t \geq 4$)

$$\frac{1}{\frac{1}{2}\binom{2n}{n}-1} \leq \frac{1}{\frac{1}{2}\binom{4}{2}-1} = \frac{1}{5} \ . \tag{3.35}$$

Thus

$$\begin{aligned} p_P(s_0,t) &\leq \frac{6}{5}\frac{4}{n^2}\sum_{w=1}^{n} \rho^w w^3 \\ &< \frac{6}{5}\frac{4}{n^2}\sum_{w=1}^{\infty} \rho^w w^3. \end{aligned} \tag{3.36}$$

The infinite sum on the right hand side converges for all $\rho \in [0,1)$ and one can find that

$$\sum_{w=1}^{\infty} \rho^w w^3 = \frac{\rho(1+4\rho+\rho^2)}{(1-\rho)^4} \ . \tag{3.37}$$

The following upper bound (recall $n = t/2$) is finally obtained:

$$p_P(s_0,t) \leq \frac{1}{t^2}\frac{6\cdot 4\cdot 4}{5}\frac{\rho(1+4\rho+\rho^2)}{(1-\rho)^4} \tag{3.38}$$

$$= \frac{C}{t^2} \ , \tag{3.39}$$

where C is independent of time (number of steps) t.

4

Anyonic U^2 Quantum Walk

In the previous chapter, evaluation of the Jones polynomial could be done in polynomial time in the number of time steps for Ising anyons, which correspond to spin-1/2 irreps of $SU(2)_2$. For higher values of k, the Jones polynomial for spin-1/2 irreps is exponentially hard to evaluate in the number of time steps, and numerical calculations freeze after only a handful of time steps. In this chapter, the anyonic quantum walk model is simplified such that numerical calculations can be carried out for $SU(2)_k$ anyons for any level k for fairly long times. By using a certain approximation, it is also possible to obtain analytical expressions of probability distributions for a few special values of k.

The model considered here is a variant of the so called U^n quantum walk [71]. In this model, the walker takes n discrete steps as in the usual quantum walk, after which the coin degree of freedom is traced out and reset before the next step. The walk proceeds thus with the tracing carried out every n steps. The density matrix of the position space carries information about the history of the walk, but entanglement between space and coin is lost in the tracing. The tracing process thus introduces decoherence in the walk, and the memory stored in the coin degrees of freedom is lost. In the anyonic version, the loss of memory simplifies the calculations significantly, as the number of degrees of freedom to keep track of is small.

As the total state evolution in the U^n walk is not unitary, it is interesting to see whether this walk exhibits quantum properties. In unitary quantum walks, the Shannon entropy of the probability distribution grows on average, but might decrease at individual time steps. This is due to the breakdown of majorization ordering of probability distributions. In the U^n model the majorization ordering is still valid like in classical random walks. Surprisingly, the variance does not behave like in classical random walks, but is proportional to the square of the number of time steps for any $n \geq 2$ [72] ($n = 1$ corresponds to the classical random walk).

The U^n model can be thought to describe the dynamics for systems where coherence

time of the joint coin+space system is finite but the coherence time of spatial degrees of freedom is long, such as a two-level atom in a cavity driven by laser field [73, 74]. The laser field adds noise to the system, and the level of noise can be controlled easily, allowing the investigation of quantum to classical transition. The dynamics is fairly robust against the noise, since the classical behaviour is only obtained when tracing is carried out on every time step.

As seen in the previous chapter, anyonic quantum walks with $SU(2)_2$ anyons behave effectively classically, in the sense of asymptotic dependence of the variance. This suggests to ask whether similar behaviour is seen also in U^n walks. Additionally, numerical results for $SU(2)_k$ anyons for higher k show that the probability distribution at small number of time steps resembles that of the non-anyonic quantum walk as k increases, but the calculations become very inefficient when k and t are large. The U^n model allows efficient calculations for any level of k and the anyon models are therefore easy to compare.

The first section introduces the anyonic version of the $U^{n=2}$ quantum walk. Calculation of the CP map elements using the Kauffman bracket is discussed in Sec. 4.2 and numerical results are presented in Sec. 4.3. In Sec. 4.4 the Kraus generators of the CP map are approximated by circulant matrices and these results are used in Sec. 4.5 to derive the asymptotic probability distribution for the special level $k = 2$. The results presented in this chapter are reported in [L. Lehman, D. Ellinas and G. Brennen. *Quantum Walks of $SU(2)_k$ Anyons on a Ladder.*]

4.1 Anyonic U^2 model

The anyonic U^2 quantum walk is a straightforward modification of the unitary anyonic quantum walk. The system evolves unitarily according to the time evolution operator U^2, after which other than spatial degrees of freedom are traced out. In the original U^2 model, these are just the coin degrees of freedom, but in the anyonic case the fusion space must traced out as well. This constitutes one step of the walk. The coin and fusion states are then reset to their initial values, and the procedure is repeated $t/2$ times to yield a walk that corresponds to t time steps of the unitary quantum walk. The effect of resetting the coin and fusion degrees of freedom is that the quantum correlations between position states and coin and fusion states are erased, and decoherence is introduced in the time evolution. Total probability is still conserved in this model, so that renormalization of the density matrix is not necessary.

One might ask what is the physical meaning of tracing and resetting the coin and the fusion DOFs. Discarding the information of these states should be understood as decoupling and recoupling again the position from other DOFs, such that all the entanglement between the states is removed during this operation. Note that if the other degrees of freedom were measured, the total state would collapse to the state which is consistent with the measurement, which would also be reflected in the density matrix of position. In the U^2 model the position density matrix does not however change during the decoupling. Therefore the correct interpretation is that position is decoupled from other DOFs, the information about the other DOFs is discarded, and

the other DOFs are prepared again with a precisely known initial state. In a practical setup, the experimenter should find a way to prepare the other DOFs in a definite state without affecting the position DOFs in any way.

The main advantage of using this model is that it allows numerical calculations for high number of time steps for spin-1/2 irreps of the quantum groups $SU(2)_k$ for any level of k. This becomes possible because the information about fusion degrees of freedom is kept only for two consecutive steps of the walk, and the number of degrees of freedom to keep track of does not grow with the number of time steps as it does in the unitary anyon walk. The evaluation of the fusion trace can be done by analyzing the Kauffman bracket of link diagrams with just four crossings, which can be carried out analytically.

In the usual quantum walk protocol, the quantum speedup is understood to originate from the entanglement between position states and coin states. The system evolves coherently and the correlations between the position states and coin states preserve the memory in the system, hence the system dynamics is highly non-Markovian. If the walk is subject to decoherence, the correlations between the position and the coin become degraded and some of the memory in the system is lost. The loss of memory happens because the state of the coin is erased and reset on every nth step, for example by doing a measurement on the coin and preparing it over again in the initial state. After resetting the coin, the system is in a product state and the correlations between the position and coin are lost. Remarkably even in the U^2 model there is enough coherence left in the system to provide for quadratic speed up over the classical random walk. Specifically, it was shown in Ref. [72] that the variance asymptotically scales like $\sigma(t)^2 = K_2 t^2 + K_3 t$ for some constants K_2, K_3.

The setup for the U^2 walk is similar to the unitary walk. The one-dimensional lattice is assumed to be infinite such that the walker may propagate freely in both directions. The initial density matrix of the coin is $\big|c_0\big\rangle\big\langle c_0\big| = \big|0\big\rangle\big\langle 0\big|$ and the Hadamard coin is chosen as the coin flip operator F. The initial state of the anyons is $\big|\Phi_0\big\rangle\big\langle\Phi_0\big| = B_0\big|\chi_0\big\rangle\big\langle\chi_0\big|B_0^\dagger$, such that the tracing corresponds to Markov tracing as explained in Sec. 2.3. The trace over the fusion degrees of freedom can then be expressed in terms of the Kauffman bracket $\big\langle L\big\rangle(A)$, as expressed in Eq. (2.13):

$$\mathrm{Tr}(\mathcal{B}_1\big|\Phi_0\big\rangle\big\langle\Phi_0\big|\mathcal{B}_2^\dagger) = \big\langle\Phi_0\big|\mathcal{B}_2^\dagger\mathcal{B}_1\big|\Phi_0\big\rangle = \frac{\big\langle L(\mathcal{B}_1,\mathcal{B}_2)\big\rangle(A)}{d^{\#(L)-1}} \tag{4.1}$$

where $L(\mathcal{B}_1,\mathcal{B}_2) = (\mathcal{B}_2^\dagger\mathcal{B}_1)^{\mathrm{Markov}}$ is the link obtained by taking the Markov closure of the braid word $\mathcal{B}_2^\dagger\mathcal{B}_1$, $d = 2\cos\frac{\pi}{k+2}$ is the quantum dimension of the anyons, $\#(L)$ is the number of distinct components (strands) in the link L, and the value of the parameter for $SU(2)_k$ anyons is $A = ie^{i\pi/2(k+2)}$.

The dynamics of the system can be written in terms of a superoperator $\mathcal{E}$ acting

on the density operator $\rho_{\rm S}(t)$ for the spatial degrees of freedom of the walker:

$$\begin{aligned}\rho_{\rm S}(t+2) &= \mathcal{E}(\rho_{\rm S}(t)) \qquad (4.2)\\ &= \sum_{f,c}\Big[\big(\mathbb{I}_{\rm S}\otimes\langle f|\otimes\langle c|\big)\big(\mathcal{SF}\big)^2\Big]\,\rho_{\rm S}(t)\otimes|\Phi_0\rangle\langle\Phi_0|\otimes|c_0\rangle\langle c_0|\\ &\quad\times\Big[\big((\mathcal{SF})^2\big)^\dagger\big(\mathbb{I}_{\rm S}\otimes|f\rangle\otimes|c\rangle\big)\Big]\\ &= \sum_{f,c}\Big[\big(\mathbb{I}_{\rm S}\otimes\langle f|\otimes\langle c|\big)\big(\mathcal{SF}\big)^2\big(\mathbb{I}_{\rm S}\otimes|\Psi_0\rangle\otimes|c_0\rangle\big)\Big]\,\rho_{\rm S}(t)\\ &\quad\times\Big[\big(\mathbb{I}_{\rm S}\otimes\langle\Phi_0|\otimes\langle c_0|\big)\big((\mathcal{SF})^2\big)^\dagger\big(\mathbb{I}_{\rm S}\otimes|f\rangle\otimes|c\rangle\big)\Big]\\ &\equiv \sum_{f,c}E_{fc}\,\rho_{\rm s}(t)\,E_{fc}^\dagger \qquad (4.3)\end{aligned}$$

where the Kraus generators have been defined as

$$E_{fc} = \big(\mathbb{I}_{\rm S}\otimes\langle f|\otimes\langle c|\big)\,\big(\mathcal{SF}\big)^2\,\big(\mathbb{I}_{\rm S}\otimes|\Psi_0\rangle\otimes|c_0\rangle\big). \qquad (4.4)$$

Substituting the expressions for the coin flip operator (2.1) and the conditional shift (2.2) the double step operator is written

$$\begin{aligned}(\mathcal{SF})^2 \;=\; &\sum_s\Big(|s-2\rangle\langle s|\otimes b_{s-2}b_{s-1}\otimes P_0FP_0F \;+\; |s\rangle\langle s|\otimes b_s^2\otimes P_0FP_1F\\ &+\;|s\rangle\langle s|\otimes b_{s-1}^2\otimes P_1FP_0F \;+\; |s+2\rangle\langle s|\otimes b_{s+1}b_s\otimes P_1FP_1F\Big).\end{aligned} \qquad (4.5)$$

It is clear from this equation that the double step operator shifts the coefficients of the density matrix by two rows or columns, or not at all. By inserting this expression to the superoperator and using the completeness of the fusion and coin bases, $\sum_f\langle f|b_s|\Phi_0\rangle\langle\Phi_0|b_{s'}^\dagger|f\rangle = \langle\Phi_0|b_{s'}^\dagger b_s|\Phi_0\rangle$ and $\sum_c\langle c|P_aFP_bF|c_0\rangle\langle c_0|F^\dagger P_{a'}F^\dagger P_{b'}|c\rangle = \delta_{a,b'}$ $\times\langle c_0|H^\dagger P_{a'}F^\dagger P_aFP_bF|c_0\rangle$, the action of the superoperator on a general element $|s\rangle\langle s'|$ of the spatial density matrix can be written as a sum of 7 terms:

$$\begin{aligned}\mathcal{E}(|s\rangle\langle s'|) \;=\; &\tfrac14\Big[|s-2\rangle\langle s'-2|\,\langle\Phi_0|b_{s'-1}^\dagger b_{s'-2}^\dagger b_{s-2}b_{s-1}|\Phi_0\rangle\\ &+\;|s-2\rangle\langle s'|\,\langle\Phi_0|b_{s'}^{\dagger2}b_{s-2}b_{s-1}|\Phi_0\rangle \;+\; |s\rangle\langle s'-2|\,\langle\Phi_0|b_{s'-1}^\dagger b_{s'-2}^\dagger b_s^2|\Phi_0\rangle\\ &+\;|s\rangle\langle s'|\,\Big(\langle\Phi_0|b_{s'}^{\dagger2}b_s^2|\Phi_0\rangle \;+\; \langle\Phi_0|b_{s'-1}^{\dagger2}b_{s-1}^2|\Phi_0\rangle\Big)\\ &-\;|s\rangle\langle s'+2|\,\langle\Phi_0|b_{s'}^\dagger b_{s'+1}^\dagger b_{s-1}^2|\Phi_0\rangle \;-\; |s+2\rangle\langle s'|\,\langle\Phi_0|b_{s'-1}^{\dagger2}b_{s+1}b_s|\Phi_0\rangle\\ &-\;|s+2\rangle\langle s'+2|\,\langle\Phi_0|b_{s'}^\dagger b_{s'+1}^\dagger b_{s+1}b_s|\Phi_0\rangle\Big].\end{aligned} \qquad (4.6)$$

where the initial coin state is $|c_0\rangle = |0\rangle$ and the Hadamard coin has been chosen as the coin flip operator F such that $\langle c_0|F^\dagger P_{a'}F^\dagger P_aFP_bF|c_0\rangle = \pm\frac14$.

Equation (4.6) shows that for any element of the initial spatial density matrix, there are only seven nonzero elements of the superoperator $\mathcal{E}$. Writing the density matrix in a vectorized form, the superoperator can be written as a matrix: $\vec{\rho}\,' = \sum_{f,c}\big(E_{fc}\otimes E_{fc}^\dagger\big)\vec{\rho}$,

where the superoperator matrix $\sum_{f,c}\left(E_{fc}\otimes E_{fc}^{\dagger}\right)$ is a band matrix with seven diagonal bands, and the rest of the elements are zero. Starting from the initial position density matrix $\rho_{\mathrm{s}}(0)=\left|s_0\right\rangle\!\left\langle s_0\right|$, the position density matrix after t time steps is obtained by applying the superoperator t times:

$$\rho_{\mathrm{S}}(t)=\mathcal{E}^{t}\big(\rho_{\mathrm{S}}(0)\big). \tag{4.7}$$

The probability distribution at time step t is then given by the diagonal elements of the final spatial density matrix $\rho_{\mathrm{S}}(t)$.

4.2 CP map elements

The construction of the superoperator $\mathcal{E}$ for non-Abelian anyons requires calculation of the eight expectation values in Eq. (4.6) for all values of s and s'. These expectation values are related to the Kauffman bracket via Eq. (4.1). The defining properties of the Kauffman bracket are given by the uncrossing relation and two relations for removing loops from the bracket:

$$\left\langle \times \right\rangle = A\left\langle \)\(\right\rangle + A^{-1}\left\langle \asymp \right\rangle \tag{4.8}$$

$$\left\langle L\cup \bigcirc \right\rangle = -(A^2+A^{-2})\left\langle L\right\rangle \tag{4.9}$$

$$\left\langle \bigcirc \right\rangle = 1. \tag{4.10}$$

The value of the Kauffman bracket for a specific braid word can be calculated by forming the link diagram that corresponds to the braid presentation and Markov closure of the word. The unique link diagrams for one braid word are drawn for illustration in Fig. 4.1. The value of the bracket polynomial is then obtained by applying the relations (4.8) and (4.9) to the link diagram, removing all crossings and loops in the diagram except one. The bracket of a single loop is trivial, so the remaining coefficient is the value of the bracket polynomial. Using the skein relations above, the following formulas for removing loops can be derived

$$\left\langle \right\rangle = -A^{-3}\left\langle \ \right\rangle \tag{4.11}$$

$$\left\langle \right\rangle = -A^{3}\left\langle \ \right\rangle \tag{4.12}$$

$$\left\langle \right\rangle = -A^{3}\left\langle \ \right\rangle \tag{4.13}$$

$$\left\langle \right\rangle = -A^{-3}\left\langle \ \right\rangle \tag{4.14}$$

For $\mathrm{SU}(2)_k$ anyons, the value of the parameter is $A=ie^{i\pi/2(k+2)}$, and the quantum dimension satisfies $d=-(A^2+A^{-2})=2\cos(\frac{\pi}{k+2})$. For $s'-s$ large, the forward and backward braid words never touch the same strands, the links corresponding to forward and back evolution are disjoint, and the value of the Kauffman bracket polynomial is equal for all s and s'. Thus, the calculation of a general element $\left\langle\Phi_0\right|B(s,s')\left|\Phi_0\right\rangle$

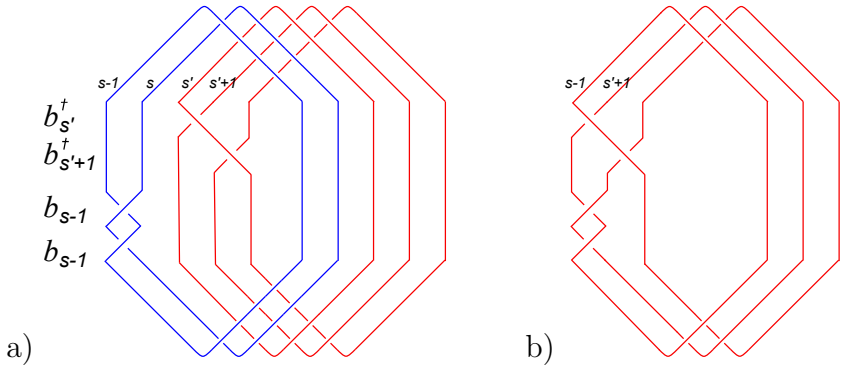

FIGURE 4.1: Two links corresponding to the expectation value $\langle\Phi_0|b^\dagger_{s'}b^\dagger_{s'+1}b^2_{s-1}|\Phi_0\rangle$. a) Case $s'-s=1$. The forward braids b^2_{s-1} and the backward braids $b^\dagger_{s'}b^\dagger_{s'+1}$ act on separate sets of strands, therefore the links corresponding to the forward and backward braids are disjoint. The links corresponding to $s'-s\leq -4$, $s'-s\geq 1$ are all disjoint and the values of the Kauffman brackets are the same. b) Case $s'-s=-1$. The forward and backward braids now form a joint link.

involves only the calculation of the disjoint element and a few cases where $s'-s$ is small. The unique values of five of the expectation values are given in Table 4.1. The remaining elements are given by

$$\langle\Phi_0|b^{\dagger 2}_{s'-1}b^2_{s-1}|\Phi_0\rangle = \langle\Phi_0|b^{\dagger 2}_{s'}b^2_{s}|\Phi_0\rangle$$

and the conjugate transpose elements

$$\langle\Phi_0|b^\dagger_{s'-1}b^\dagger_{s'-2}b^2_{s}|\Phi_0\rangle = \left(\langle\Phi_0|b^{\dagger 2}_{s}b_{s'-2}b_{s'-1}|\Phi_0\rangle\right)^*$$

and

$$\langle\Phi_0|b^{\dagger 2}_{s'-1}b_{s+1}b_{s}|\Phi_0\rangle = \left(\langle\Phi_0|b^\dagger_{s}b^\dagger_{s+1}b^2_{s'-1}|\Phi_0\rangle\right)^*.$$

4.3 Numerical results

One interesting feature of the U^2 anyonic walk is that the effect of braiding statistics is trivial for Abelian anyons. If all the stationary anyons are of the same type, the walker always picks the same phase $e^{i\phi/2}$ when braiding with them, such that

$$\langle\Phi_0|\mathcal{B}|\Phi_0\rangle = e^{-i\phi/2}e^{-i\phi/2}e^{i\phi/2}e^{i\phi/2} = 1. \tag{4.15}$$

This is similar to the fully coherent anyonic quantum walk, where the wave function always picks the phase $e^{i\phi t/2}$ during the forward time evolution and phase $e^{-i\phi t/2}$ during backward time evolution, such that the overall effect is trivial. Another way to think about the Abelian walk is to look at the case $k=1$ in Chern-Simons theory. There are only two charges $\{0,\frac{1}{2}\}$ in this model, the fusion channels are unambiguous: $j_1\times j_2 = j$, and the quantum dimension is $d=1$, so this model is Abelian. Substituting $A = ie^{-i\pi/6}$

$s\prime - s$	$\langle\Phi_0\vert b^\dagger_{s'-1}b^\dagger_{s'-2}b_{s-2}b_{s-1}\vert\Phi_0\rangle$	$\langle\Phi_0\vert b^\dagger_{s'}b^\dagger_{s'+1}b_{s+1}b_s\vert\Phi_0\rangle$
-2	d^{-4}	d^{-4}
-1	d^{-2}	d^{-2}
0	1	1
1	d^{-2}	d^{-2}
2	d^{-4}	d^{-4}
$\leq -3,\ \geq 3$	d^{-4}	d^{-4}

$s\prime - s$	$\langle\Phi_0\vert b^{\dagger 2}_{s'}b_{s-2}b_{s-1}\vert\Phi_0\rangle$	$\langle\Phi_0\vert b^\dagger_{s'}b^\dagger_{s'+1}b^2_{s-1}\vert\Phi_0\rangle$
-3	$-A^6(A^4+A^{-4})/d^3$	$-A^{-6}(A^4+A^{-4})/d^3$
-2	d^{-2}	d^{-2}
-1	d^{-2}	d^{-2}
0	$-A^6(A^4+A^{-4})/d^3$	$-A^{-6}(A^4+A^{-4})/d^3$
$\leq -4,\ \geq 1$	$-A^6(A^4+A^{-4})/d^3$	$-A^{-6}(A^4+A^{-4})/d^3$

$s\prime - s$	$\langle\Phi_0\vert b^{\dagger 2}_{s'}b^2_s\vert\Phi_0\rangle$
-1	$(A^4+A^{-4})^2/d^2$
0	1
1	$(A^4+A^{-4})^2/d^2$
$\leq -2,\ \geq 2$	$(A^4+A^{-4})^2/d^2$

Table 4.1: The values of the braid group elements involved in the evolution CP map. These are obtained by calculating the normalized Kauffman brackets.

to the values of the brackets in Table 4.1 gives $\langle\Phi_0\vert\mathbb{B}(s,s')\vert\Phi_0\rangle = 1$ for all brackets, confirming that the Abelian walk gives the same dynamics as the original U^2 quantum walk. The variance of the U^2 walk for Abelian anyons is plotted in Fig. 4.2a). It shows the known fact [71] that the original U^2 walk propagates slower than the fully coherent quantum walk, but qualitatively the behaviour is still the same: the variance depends quadratically on time. The best fit for the variance of the $k = 1$ walk is given by $\sigma^2 = 0.125\,t^2 + 0.75\,t$.

The numerical results for the time evolution of the variance $\sigma^2(t)$ for various choices of k are plotted in Fig. 4.2b) up to $t = 100$ iterations of the superoperator, corresponding to 200 quantum walk steps. For $k = 2$, the variance follows exactly the linear line $\sigma^2 = t$. It is interesting to note that this behaviour is exactly the same as was shown for the fully coherent walk with $k = 2$ in the previous chapter. For the rest of the values of k, there is surprisingly small difference in the variance, with the slope of the variance slightly increasing as a function of k. For $k = 3$ and $k = 4$ (not shown in the figure) the slope of the variance is slightly smaller than 1, $k = 3$ having the smallest slope (best fit 0.9877). The highest variance is obtained when $k \to \infty$, which corresponds to choice of the parameters $A = i$ and $d = 2$, with slope 1.0665. It should be noted that in the fully coherent anyonic quantum walk model, taking the limit $k \to \infty$ leads to

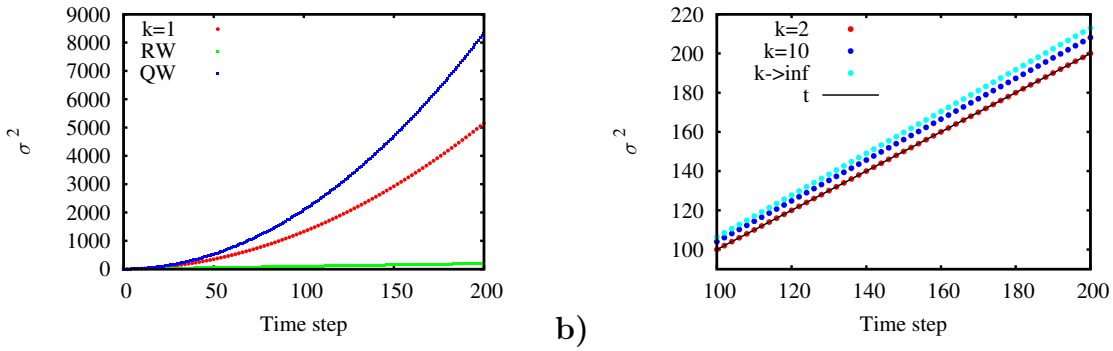

FIGURE 4.2: The variance σ^2 of the two-step walk as a function of time t for various anyon models indexed by k. The scaling of the sites and time steps is chosen such that one iteration of the superoperator $\mathcal{E}$ corresponds to two iterations of the quantum walk time evolution operator, and at each iteration of $\mathcal{E}$ the walker shifts twice. a) Case $k = 1$ corresponds to the Abelian walk, which also coincides with the original U^2 quantum walk. Plotted for comparison are the variance of the classical random walk (RW) and the ordinary quantum walk (QW) with the same initial coin state and coin flip matrix. b) Non-Abelian $SU(2)_k$ models zoomed to the last 100 time steps. Also plotted is the linear curve $\sigma^2 = t$ which corresponds to the classical random walk.

the conventional SU(2) algebra, and the braiding generators are a non-Abelian representation of the permutation group. However when decoherence was introduced in the system, the braid words that contribute to the walk have different structure than in the fully coherent model. In the fully coherent model, the diagonal elements of the spatial degree of freedom of the walker correspond to a sum over all paths where the walker strand and necessarily all other strands return their initial position after forward and backward time evolution. Hence each of these paths is a trivial permutation in the fusion space and has no effect on the diagonal elements of the quantum walk. In the U^2 model however, the links do not have a dedicated walker strand as can be seen from Fig. 4.1. The nontrivial character of the $k \to \infty$ model thus follows from the fact that the links are not identity permutations and hence expectation values in Table 4.1 are not equal to 1, as they would be in the fully coherent walk. The key difference is that only for a highly non-Markovian environment does the $k \to \infty$ case reduce to the normal quantum walk for only if one includes memory of all previous steps does the fusion degree of freedom become disentangled with the spatial degree of freedom.

4.4 Approximation by circulant matrices

In the previous section, the superoperator that describes how the spatial density matrix transforms in a single step of the walk was derived exactly, and numerical results were obtained by repeatedly applying the superoperator to the density matrix. Although the numerics showed clear diffusive behaviour for all values of k, no expression for the density matrix after evolution by an arbitrary number of steps was obtained. In the following, the Kraus operators E_{fc} are approximated by circulant matrices which have

uniform coefficients on each diagonal, and the Kraus operators are diagonalized for $k = 2, 4$ via Fourier transform to find arbitrary powers of the superoperator $\mathcal{E}$ in a compact form.

A matrix $C = (c_{ij})$ of order n is called a circulant matrix [75] if $c_{ij} = a_{i-j(\bmod n)}$. The entries of any row or column $a \equiv (a_0, a_1, ..., a_{n-1})$ determine the entire circulant matrix which is denoted $C_n = circ(a) = circ(a_0, a_1, ..., \alpha_{n-1})$, and in matrix form it reads

$$C_n = \begin{pmatrix} a_0 & a_{n-1} & a_{n-2} & \cdots & a_1 \\ a_1 & a_0 & a_{n-1} & \cdots & a_2 \\ a_2 & & a_0 & \cdots & a_3 \\ \vdots & \vdots & \vdots & \ddots & \vdots \\ a_{n-1} & a_{n-2} & a_{n-3} & \cdots & a_0 \end{pmatrix}. \tag{4.16}$$

Alternatively circulant matrices can be written in terms of an elementary circulant matrix $\widehat{h} = \sum_{m\in\{0,1,...,n-1\}} \big|m\big\rangle\big\langle m+1\big| = circ(0, 1, ..., 0)$, as $C_n = circ(a_0, a_1, ..., \alpha_{n-1}) = p(\widehat{h})$ where p is the polynomial $p(z) := a_0 + a_1 z + \cdots a_{n-1} z^{n-1}$. The elementary circulant matrix and its inverse are written explicitly as

$$\widehat{h} = \sum_n \big|n+1\big\rangle\big\langle n\big| = \begin{pmatrix} 0 & & & & 1 \\ 1 & 0 & & & \\ & 1 & 0 & & \\ & & 1 & \ddots & \\ & & & 1 & 0 \end{pmatrix}, \tag{4.17}$$

$$\widehat{h}^{-1} = \sum_n \big|n-1\big\rangle\big\langle n\big| = \begin{pmatrix} 0 & 1 & & & \\ & 0 & 1 & & \\ & & 0 & 1 & \\ & & & \ddots & 1 \\ 1 & & & & 0 \end{pmatrix}, \tag{4.18}$$

and they generate the abelian group $\{\widehat{h}^a\}_{a\in\mathbb{Z}_N} \simeq \mathbb{Z}_N$, share the property $\widehat{h}^\dagger = \widehat{h}^{-1} = \sum_{s\in\mathbb{Z}_N} \big|s+1\big\rangle\big\langle s\big|$, where $\widehat{h}^n = \mathbf{1}$. Matrix $\widehat{h}$ is diagonalized by the finite Fourier transform unitary matrix F, with elements $F_{ab} = \frac{1}{\sqrt{n}}\omega^{ab}$, $\omega = e^{i2\pi/n}$, as $F^\dagger \widehat{h} F = \widehat{g}$, where $\widehat{g} = diag(1, \omega, ..., \omega^{n-1})$. Any circulant matrix is then canonically decomposed as $C_n = circ(a_0, a_1, ..., \alpha_{n-1}) = F^\dagger diag(p(1), p(\omega), ..., p(\omega^{n-1}))F$. A *banded* circulant matrix is a circulant matrix for which only a connected subset in the sequence $a = (a_j)_{j=0}^{n-1}$ is nonzero.

The Kraus generators of the U^2 anyon walk are not circulant matrices, but they can be approximated as such. Substituting Eq. (4.5) to (4.4), the Kraus generators are written explicitly as

$$\begin{aligned} E_{fc} = \sum_s \Big[& C_c^{00} \left\langle f\middle|b_s b_{s+1}\middle|\Phi_0\right\rangle \big|s\big\rangle\big\langle s+2\big| + \left\langle f\right| \left(C_c^{01} b_s^2 + C_c^{10} b_{s-1}^2\right) \big|\Phi_0\big\rangle \big|s\big\rangle\big\langle s\big| \\ & + C_c^{11} \left\langle f\middle|b_{s+1} b_s\middle|\Phi_0\right\rangle \big|s+2\big\rangle\big\langle s\big| \Big] \end{aligned} \tag{4.19}$$

where the coin term has been defined as $C_c^{ab} := \langle c|P_aFP_bF|c_0\rangle$. The matrix expression of the generators is

$$E_{fc} = \begin{pmatrix} d_{fc}(0) & & a_{fc}(0) & \cdots & b_{fc}(N-2) & \\ & d_{fc}(1) & & a_{fc}(1) & & b_{fc}(N-1) \\ b_{fc}(0) & & d_{fc}(2) & & \ddots & \\ & b_{fc}(1) & & \ddots & \ddots & a_{fc}(N-3) \\ a_{fc}(N-2) & \cdots & \ddots & & \ddots & \\ & a_{fc}(N-1) & & b_{fc}(N-3) & & d_{fc}(N-1) \end{pmatrix}, \tag{4.20}$$

where

$$a_{fc}(s) = C_c^{00}\langle f|b_sb_{s+1}|\Phi_0\rangle, \tag{4.21}$$
$$b_{fc}(s) = C_c^{11}\langle f|b_{s+1}b_s|\Phi_0\rangle, \tag{4.22}$$
$$d_{fc}(s) = C_c^{01}\langle f|b_s^2|\Phi_0\rangle + C_c^{10}\langle f|b_{s-1}^2|\Phi_0\rangle. \tag{4.23}$$

Although the matrix E_{fc} is not a circulant matrix, it can be turned to a circulant matrix if the s-dependence of parameters $a_{fc}(s)$, $b_{fc}(s)$, $d_{fc}(s)$ is suppressed in some meaningful way, so that the sequences of these parametrers get approximated by some respective sequences $\widetilde{a}_{fc}$, $\widetilde{b}_{fc}$ and $\widetilde{d}_{fc}$. This suppression of the s-dependence also leads to circulant form for E_{fc}. The advantage of having the Kraus generators being circulant matrices stems from the fact that the spectral decomposition problem of such matrices is solved, and therefore the walk superoperator and its powers can be expressed in terms of the orthogonal eigenprojections of the generators.

A viable approximation for the Kraus generators is given by their optimal circulant matrix. For the construction of the optimal circulant matrix it has been recommended [76] (after preliminary transformations such as changing the order of the rows and multiplying them with suitable constants), to apply the following: by imposing periodicity i.e. $d_{j+N,k} = d_{j,k}$, form the arithmetic averages of the elements along the diagonals i.e. $a_j = \frac{1}{N}\sum_{k=0}^{N-1} d_{j+k,k}$, and construct in this way the circulant $C = circ(a_0, a_1, ...ma_{N-1})$. On the other hand an optimal circulant approximation of some Toeplitz matrix T (see e.g. Strang's suggestion in [77]) is constructed by determining the nearest circulant with respect to Frobenius matrix norm for matrix T, i.e. by solving the optimization problem $\min_{C:\text{circulant}} \|T - C\|_F$ [78]. The resulting circulant coincides with the one obtained by the method of arithmetic averages [76], applied to T.

The arithmetic averages of $a_{fc}(s)$, $b_{fc}(s)$ and $d_{fc}(s)$ are given by

$$a_{fc}(s) \approx \widetilde{a}_{fc}(s) = \frac{1}{N}Tr(\widehat{h}^2 E_{fc}) \tag{4.24}$$
$$d_{fc}(s) \approx \widetilde{d}_{fc}(s) = \frac{1}{N}Tr(E_{fc}) \tag{4.25}$$
$$b_{fc}(s) \approx \widetilde{b}_{fc}(s) = \frac{1}{N}Tr(\widehat{h}^{-2} E_{fc}) \tag{4.26}$$

where $\widehat{h}$ is the elementary circulant matrix. This is explicitly written as

$$\widetilde{a}_{fc} = \frac{C_c^{00}}{N}\sum_s \big\langle f\big|b_s b_{s+1}\big|\Phi_0\big\rangle, \tag{4.27}$$

$$\widetilde{d}_{fc} = \frac{C_c^{01}}{N}\sum_s \big\langle f\big|b_s^2\big|\Phi_0\big\rangle + \frac{C_c^{10}}{N}\sum_s \big\langle f\big|b_{s-1}^2\big|\Phi_0\big\rangle \tag{4.28}$$

$$\widetilde{b}_{fc} = \frac{C_c^{11}}{N}\sum_s \big\langle f\big|b_{s+1} b_s\big|\Phi_0\big\rangle, \tag{4.29}$$

Denote E_{fc}^w the matrices obtained from E_{fc} by substituting the s-dependent terms with their averages:

$$E_{fc}^w = \widetilde{a}_{fc}\sum_s \big|s\big\rangle\big\langle s+2\big| + \widetilde{d}_{fc}\sum_s \big|s\big\rangle\big\langle s\big| + \widetilde{b}_{fc}\sum_s \big|s+2\big\rangle\big\langle s\big| \tag{4.30}$$

$$= \widetilde{a}_{fc}\widehat{h}^2 + \widetilde{d}_{fc}\mathbb{I} + \widetilde{b}_{fc}\widehat{h}^{-2}. \tag{4.31}$$

The map given by the new Kraus generators E_{fc}^w is not trace preserving, so the generators have to be normalized to obtain well defined generators $\widetilde{E}_{fc}$ which satisfy the trace preserving condition $\sum_{f,c}\widetilde{E}_{fc}^\dagger\widetilde{E}_{fc} = \mathbb{I}$. The normalization is given by $\sum_{fc} E_{fc}^{w\dagger}E_{fc}^w \equiv M$, so the new trace preserving circulant Kraus generators are defined $\widetilde{E}_{fc} = \big(\sum_{f,c} E_{fc}^{w\dagger}E_{fc}^w\big)^{-1/2} E_{fc}^w \equiv \Lambda\, E_{fc}^w$ with $\Lambda = M^{-1/2}$. A calculation gives

$$M = \kappa_1\,\mathbb{I} + \kappa_2\,\widehat{h}^2 + \kappa_2^*\,\widehat{h}^{-2} \tag{4.32}$$

where

$$\kappa_1 = \sum_{f,c}\big(|\widetilde{a}_{fc}|^2 + |\widetilde{d}_{fc}|^2 + |\widetilde{b}_{fc}|^2\big)\frac{1}{4}\Big(\frac{1}{N^2}\sum_{j,j'}\big\langle\Phi_0\big|b_{j'+1}^\dagger b_{j'}^\dagger b_j b_{j+1}\big|\Phi_0\big\rangle + \frac{2}{N^2}\sum_{j,j'}\big\langle\Phi_0\big|b_{j'}^{\dagger 2}b_j^2\big|\Phi_0\big\rangle + \frac{1}{N^2}\sum_{j,j'}\big\langle\Phi_0\big|b_{j'}^\dagger b_{j'+1}^\dagger b_{j+1}b_j\big|\Phi_0\big\rangle\Big) \tag{4.33}$$

$$\kappa_2 = \frac{1}{4}\Big(\frac{1}{N^2}\sum_{j,j'}\big\langle\Phi_0\big|b_{j'}^\dagger b_{j'+1}^\dagger b_{j-1}^2\big|\Phi_0\big\rangle + \frac{1}{N^2}\sum_{j,j'}\big\langle\Phi_0\big|b_{j'}^{\dagger 2}b_j b_{j+1}\big|\Phi_0\big\rangle\Big). \tag{4.34}$$

The matrix M is a circulant band matrix which can be diagonalized via discrete Fourier transform F:

$$F^\dagger M F = \sum_l\big(\kappa_1 + \kappa_2\omega^{2l} + \kappa_2^*\omega^{-2l}\big)\big|l\big\rangle\big\langle l\big|.$$

The matrix $F^\dagger MF$ is a diagonal matrix with all diagonal values nonzero, so its inverse exists. The normalization operator Λ can now be defined as $\Lambda = F(F^\dagger MF)^{-1/2}F^\dagger$, where $(F^\dagger MF)^{-1/2} = \sum_l\big(\kappa_1 + \kappa_2\omega^{2l} + \kappa_2^*\omega^{-2l}\big)^{-1/2}\big|l\big\rangle\big\langle l\big|$. A simple check verifies that $\Lambda^2 M = I$ and $\Lambda = M^{-1/2}$ as desired.

4.5 Asymptotics

Unfortunately, the normalized generators $\widetilde{E}_{fc} = \Lambda E_{fc}$ contain all even powers of the matrices $\hat{h}$ for general values of the Chern-Simons parameter k and do not admit a helpful form. However, for the special values $k = 2, 4$ there is a significant simplification. Notice that each of the terms in expressions for κ_1, κ_2 in Eqs. (4.33) and (4.34) is an averaged Kauffman bracket. For large N most of these brackets will correspond to disjoint links, i.e. the links formed by two step walks involving the strands located at j and j' do not entangle. As shown in Table 4.1, this always occurs if $|j' - j| > 3$. If the average is approximated by the value of the bracket for these disjoint links then

$$\kappa_1 = \frac{1}{32}\Big(6\cos(\frac{2\pi}{k+2}) + 4\cos(\frac{4\pi}{k+2}) + 2\cos(\frac{6\pi}{k+2}) + 5\Big)\sec^4(\frac{\pi}{k+2}) + O(1/N) \tag{4.35}$$

$$\kappa_2 = \frac{1}{8}\Big(\cos(\frac{4\pi}{k+2}) - \cos(\frac{2\pi}{k+2}) + 1\Big)\sec^2(\frac{\pi}{k+2})\Big) + O(1/N). \tag{4.36}$$

where the error is of order $1/N$. Thus $\kappa_2 \approx 0$ at the special values $k = 2, 4$ and the normalization operator becomes a scalar multiple of the identity: $\Lambda = \kappa_1^{-1/2}\,\mathbb{I}$. The Kraus generators are now given by

$$\widetilde{E}_{fc} = \kappa_1^{-1/2}\big(\widetilde{a}_{fc}\widehat{h}^2 + \widetilde{d}_{fc}\mathbb{I} + \widetilde{b}_{fc}\widehat{h}^{-2}\big). \tag{4.37}$$

The elementary circulant matrix $\widehat{h}$ can be diagonalized as $F^\dagger \widehat{h} F = \widehat{g} = \sum_{n\in\mathbb{Z}_N} \omega^n \big|n\big\rangle\big\langle n\big|$ where $\omega = e^{2\pi i/N}$. This allows to write the Kraus generators in a diagonal form

$$\begin{aligned} \widetilde{E}_{fc} &= \kappa_1^{-1/2} F\big(\widetilde{a}_{fc}\widehat{g}^2 + \widetilde{d}_{fc}\mathbb{I} + \widetilde{b}_{fc}\widehat{g}^{-2}\big)F^\dagger && (4.38)\\ &\equiv \sum_{k\in\mathbb{Z}_N} \lambda_{fc}(k) P_{f_k} && (4.39) \end{aligned}$$

with $\lambda_{fc}(k) = \kappa_1^{-1/2}\big(\widetilde{a}_{fc}\omega^{2k} + \widetilde{d}_{fc} + \widetilde{b}_{fc}\omega^{-2k}\big)$ and $P_{f_k} = F\big|k\big\rangle\big\langle k\big|F^\dagger$. The action of the superoperator $\widetilde{\mathcal{E}}$ on a spatial density matrix $\rho_{\rm S}$ is then given by

$$\widetilde{\mathcal{E}}(\rho_{\rm S}) = \sum_{f,c} \widetilde{E}_{fc}\,\rho_{\rm S}\,\widetilde{E}_{fc}^\dagger = \sum_{f,c}\sum_{k,l\in\mathbb{Z}_N} \lambda_{fc}(k)\lambda_{fc}^*(l) P_{f_k}\rho_{\rm S} P_{f_l}^\dagger \tag{4.40}$$

and for t time steps

$$\widetilde{\mathcal{E}}^t(\rho_{\rm S}) = \sum_{k,l\in\mathbb{Z}_N}\prod_{i=1}^{t}\sum_{f_i,c_i}\big(\lambda_{f_ic_i}(k)\lambda_{f_ic_i}^*(l)\big)P_{f_k}\rho_{\rm S}P_{f_l}^\dagger. \tag{4.41}$$

This compact form allows to express the diagonal probability distribution $p(s,t)$ at time t: $p(s,t) = \big\langle s\big|\widetilde{\mathcal{E}}^t(\rho_{\rm S}(0))\big|s\big\rangle$. Assuming that the walker is initialized in the position eigenstate $\big|s_0\big\rangle$, that the size of the periodic lattice is N, and that during the 2-step

walk the coin is always reinitialized to state $\big|c=0\big\rangle$, the probability distribution for index $k=2$ is written

$$\begin{aligned} p_{\text{Ising}}(s,t) &= \langle s|\widetilde{\mathcal{E}}^t(|s_0\rangle\langle s_0|)|s\rangle \\ &= \tfrac{1}{2^t N^2}\sum_{r,l\in\mathbb{Z}_N}\omega^{(s-s_0)(r-l)}\big(\omega^{2(r-l)}+\omega^{-2(r-l)}\big)^t \\ &= \tfrac{1}{2^t N^2}\sum_{m=0}^{t}\tbinom{t}{m}\sum_{r,l\in\mathbb{Z}_N}\omega^{(s-s_0)(r-l)}\omega^{2m(r-l)}\omega^{-2(t-m)(r-l)} \\ &= \tfrac{1}{2^t N^2}\sum_{m=0}^{t}\tbinom{t}{m}\sum_{r\in\mathbb{Z}_N}\omega^{r(s-s_0+4m-2t)}\sum_{l\in\mathbb{Z}_N}\omega^{-l(s-s_0+4m-2t)} \\ &= \tfrac{1}{2^t N^2}\sum_{m=0}^{t}\tbinom{t}{m}(N\delta_{s-s_0+4m-2t,0})^2 \\ &= \tfrac{1}{2^t}\tbinom{t}{\frac{2t-(s-s_0)}{4}} \end{aligned} \tag{4.42}$$

This is the binomial distribution where the range of the sites is $s\in[-2t,2t]$ and the probabilities are nonzero only for $s=s_0+4n$, $n\in\mathbb{Z}$, i.e. the U^2 model with $k=2$. $SU(2)_2$ anyon walkers therefore have the same probability distribution as the classical random walk where every step moves two units to the right or left and the variance, scaled so that each two steps move takes place over two time intervals, is $\sigma^2_{SU(2)_2}(t)=t$.

5
Disordered Walks

In the two models studied in the previous chapters, it was assumed that each island is occupied by a single anyon with the same mutual statistics as the mobile anyon. In possible experimental situations, this might be a too stringent condition, as the energies for creating and destroying quasiparticles are small and the exact amount of quasiparticles is hard to control. This motivates the study of anyonic quantum walks with disordered particle configurations. It will be seen that disorder is not necessarily an evil that destroys quantum correlations – the quantum statistical features survive the introduced randomness and Abelian and non-Abelian are observed to behave differently under disorder.

It is a well known result by Anderson that randomised local potentials can suppress diffusion of quantum particles [79], a phenomenon known as Anderson localisation. This mechanism is based on randomisation of phases that correspond to individual particle histories and consequent destructive interference.

The surprising consequences of disorder in quantum systems has motivated the study of disorder in quantum walks. The quantum walk provides a simple testbed for non-trivial quantum effects and allows analytical study of the conditions which cause localization of the walker wave packet. Most studies concentrate on disorder in the parameters of the coin flip operator F, and localization has been observed for many types of spatial disorder in the coin parameter. Linden and Sharam showed that periodically varying coin parameters can lead to both bounded and unbounded walks [80], depending on the period. Konno used path-counting methods to study quantum walks under quenched and annealed disorder, and showed that a coin defect at the origin causes partial localization of the wavepacket [81, 82]. Joye and Merkli [83] and Ahlbrecht *et al* [84] showed that dynamical Anderson localization occurs for spatially inhomogeneous coin, when the coin parameters are chosen randomly from continuous or certain discrete sets. If the coin parameters change in time, the walker spreads ballistically or diffusively, but no localization has been observed. Brun *et al*

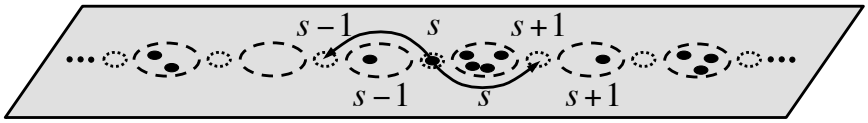

FIGURE 5.1: The disordered anyonic quantum walk. A walker anyon braids counterclockwise around islands filled with a random number of static anyons of the same type. The islands are denoted with dashed circles and the possible positions of the walker are denoted by dotted circles placed in between the islands. The charge configuration is assumed to be fixed during each run of the walk.

[53] studied cyclic coins, and found that the walk is still ballistic unless the period becomes as large as the length of the walk, in which case it is diffusive. Shapira *et al* [85] studied quenched unitary noise numerically and observed that the walk is diffusive in the long term after an initial ballistic period. Similar conclusions were drawn in analytical treatment by Ahlbrecht *et al* [86] and Joye [87].

The transport properties of anyons in random topological environments are studied in this chapter by varying the island occupations of the stationary anyons. The general setup of the disordered anyonic walk is given in Sec. 5.1. The results for Abelian anyons are presented in Sec. 5.2 and the results for non-Abelian Ising anyons are presented in Sec. 5.3. These results are reported in [V. Zatloukal, L. Lehman, S. Singh, J. Pachos and G. Brennen. *Transport Properties of Anyons in Random Topological Environments.*]

5.1 The model

The disordered anyonic quantum walk model consists of N spatial sites and $N-1$ anyonic islands canonically ordered on the surface and labeled by the index s, as shown in Fig. 5.1. The number of anyons on an island s is m_s, and the collection of all occupation numbers is called *a charge configuration*, represented by a vector $\overline{m} = (m_1, \ldots, m_{N-1})$. The charge configuration is assumed to stay fixed during each individual run of the walk, and the average behaviour of the system over all possible configurations is analyzed. Such disorder is called quenched randomness, as opposed to annealed randomness where the random parameters might change in time. Anyons are labeled within an island from left to right by an index $i_s = 1, \ldots, m_s$. The walker anyon hops between neighbouring sites winding counterclockwise around the islands.

The time evolution operator $U = \mathcal{S}\mathcal{F}$ of the disordered walk is only a slight modification of the uniform case. The coin flip and conditional shift operators are

$$\mathcal{F} = \mathbb{I}_{\mathrm{S}} \otimes \mathbb{I}_{\mathrm{F}} \otimes F \tag{5.1}$$

$$\mathcal{S} = \sum_{s=1}^{N-1} (T_{s+1}^{-} \hat{b}_{s,\overline{m}} P_0 + T_s^{+} \check{b}_{s,\overline{m}} P_1) + T_{\mathrm{BC}} \tag{5.2}$$

where the braid generators have been modified to include braiding around all stationary

anyons at island s:

$$\hat{b}_{s,\overline{m}} = b_{s,1} \cdots b_{s,m_s}, \tag{5.3}$$

$$\check{b}_{s,\overline{m}} = b_{s,m_s} \cdots b_{s,1}, \tag{5.4}$$

and $\hat{b}_{s,\overline{m}} = \check{b}_{s,\overline{m}} = 1$ if $m_s = 0$. As before, the Hadamard coin is chosen as the coin flip operator F and the system's initial state is $\big|\Psi(0)\big\rangle = \big|s_0\big\rangle_{\mathrm{S}}\big|\Phi_0\big\rangle_{\mathrm{F}}\big|0\big\rangle_{\mathrm{C}}$, where $s_0 = \lceil N/2 \rceil$ is the initial position of the walker, and $\big|\Phi_0\big\rangle$ is the initial fusion state where the ancillary anyons are braided to the right. The configuration-dependent spatial probability distribution is now given by

$$p_{\overline{m}}(s,t) = \frac{1}{2^t} \sum_{(\overline{a},\overline{a}')\rightsquigarrow s} (-1)^{z(\overline{a})+z(\overline{a}')} \mathrm{Tr}\Big(\mathcal{B}^t_{\overline{a},\overline{m}}\big|\Phi_0\big\rangle\big\langle\Phi_0\big|(\mathcal{B}^t_{\overline{a}',\overline{m}})^\dagger\Big) \tag{5.5}$$

and the configuration-dependent variance is written

$$\sigma^2_{\overline{m}}(t) = \sum_s p_{\overline{m}}(s,t)s^2 - \big(\sum_s p_{\overline{m}}(s,t)s\big)^2. \tag{5.6}$$

The island occupation numbers m_s are assumed to be independent and identically distributed (i.i.d.) random variables with distribution $W(m_s)$. The probability of occurrence of a configuration $\overline{m}$ is then simply $W_{\overline{m}} = \prod_{s=1}^n W(m_s)$, and the configuration average of a quantity $Q_{\overline{m}}$ is denoted $\langle\langle Q \rangle\rangle \equiv \sum_{\overline{m}} W_{\overline{m}} Q_{\overline{m}}$. The average position distribution after a t-step walk is given by

$$\langle\langle p(s,t)\rangle\rangle = \frac{1}{2^t} \sum_{(\overline{a},\overline{a}')\rightsquigarrow s} (-1)^{z(\vec{a})+z(\vec{a}')} \langle\langle \mathrm{Tr}\left(\mathcal{B}^t_{\overline{a},\overline{m}}\big|\Phi_0\big\rangle\big\langle\Phi_0\big|(\mathcal{B}^t_{\overline{a}',\overline{m}})^\dagger\right)\rangle\rangle. \tag{5.7}$$

Note that the coin term does not depend on the charge configuration, and the amplitude for each quantum walk path is thus weighted with the configuration average of the trace over the fusion degrees of freedom. If the stationary anyons are viewed as punctures on the plane, the charge configurations correspond to manifolds with different topology, and one could say that the walker is in a random topological environment.

5.2 Abelian anyons

For Abelian anyons the braid generators $\{b_{s,i_s}\}$ are all equal to $e^{i\varphi}$ where the anyonic exchange angle is $\varphi = \pm\frac{\pi}{n}$, $n \in \mathbb{N}$. The fusion space is one-dimensional, $\mathcal{H}_{\mathrm{F}} \simeq \mathbb{C}$, and the initial fusion state $\big|\Phi_0\big\rangle$ can be chosen arbitrarily. Introducing the linking numbers $\ell_s(\overline{a},\overline{a}') = \big(\#(\hat{b}_s \text{ and } \check{b}_s \text{ in } B_{\overline{a}}) - \#(\hat{b}^\dagger_s \text{ and } \check{b}^\dagger_s \text{ in } B^\dagger_{\overline{a}'})\big)/2$ that count the number of times the walker's trajectory $(\overline{a},\overline{a}')$ winds around an island s, the trace over the fusion space reduces to

$$\mathrm{Tr}\big(\mathcal{B}_{\overline{a},\overline{m}}\big|\Phi_0\big\rangle\big\langle\Phi_0\big|\mathcal{B}_{\overline{a}',\overline{m}}\big) = \prod_{s=1}^N e^{\pm i 2\frac{\pi}{n} m_s \ell_s(\overline{a},\overline{a}')}. \tag{5.8}$$

The probability distribution of the occupation numbers is assumed to be uniform: $W(m) = 1/n$ for $1 \leq m \leq n$. Then the average position distribution of the walker after t steps, $\langle\langle p^{(\pm\frac{\pi}{n})}(s,t)\rangle\rangle$, is given by (5.7) with

$$\langle\langle \mathrm{Tr}\big(\mathcal{B}_{\overline{a},\overline{m}}\big|\Phi_0\big\rangle\big\langle\Phi_0\big|\mathcal{B}_{\overline{a}',\overline{m}}\big)\rangle\rangle = \prod_{s=1}^{N} \delta_{0,\ell_s(\overline{a},\overline{a}') \bmod n}, \tag{5.9}$$

where $\delta_{i,j}$ is the Kronecker symbol.

For Abelian anyons, the probability distribution can be evaluated efficiently for a large number of time steps. The numerical results for the exchange angle $\phi = \pi/8$ are presented in Fig. 5.2. The variance approaches a constant value, which means that the probability mass is confined to some finite region around the initial site. Dynamical localization at point s_0 is defined such that the probability to be at site s vanishes exponentially as a function of the distance from s_0:

$$p(s,t) \propto e^{-\frac{(s-s_0)}{\xi_{\mathrm{loc}}}} \tag{5.10}$$

where ξ_{loc} is defined to be *the localization length*. Thus, the logarithm of the average probability distribution is inversely proportional to the localization length:

$$\ln\Big(\big\langle\big\langle p^{(\pm\frac{\pi}{n})}(s,t\to\infty)\big\rangle\big\rangle\Big) \propto -\frac{s-s_0}{\xi_{\mathrm{loc}}}. \tag{5.11}$$

Figure 5.2 shows that the logarithm of the average probability distribution falls of linearly as a function of $|s-s_0|$, and thus the Abelian anyons exhibit dynamical localization. The results are essentially insensitive to the choice of n (except for the case $n = 1$ which corresponds to fermions, and thus reduces to the Hadamard walk).

The Abelian anyonic quantum walk is equivalent to wave propagation in an array of scatterers that are placed on a line in random locations, as described in the next section. Such a model allows to calculate the probability distribution as a function of distance from the initial location analytically. The localization length can then be estimated analytically as

$$\frac{1}{\ln 2 + \ln(1+2^{n/2})^{2/n}} \leq \xi_{loc} \leq \frac{1}{\ln 2 + \ln(1-2^{n/2})^{2/n}}, \tag{5.12}$$

where the anyonic statistical angle $\varphi = \frac{\pi}{n}$. This theoretical result is in agreement with exact numerical treatment presented in Fig. 5.2.

5.2.1 Multiple scattering model

The propagation of the wave packet of an Abelian anyon in a random background is equivalent to wave propagation on a line with scatterers placed in random locations. The anyonic phase can be translated directly to dynamical phase acquired by the wave as it travels a random distance. The scattering model is described in Fig. 5.3. A monochromatic wave incident from the left scatters on a series of scatterers characterized by "from left / from right" reflection and transmission coefficients $r_j, t_j/r'_j, t'_j$.

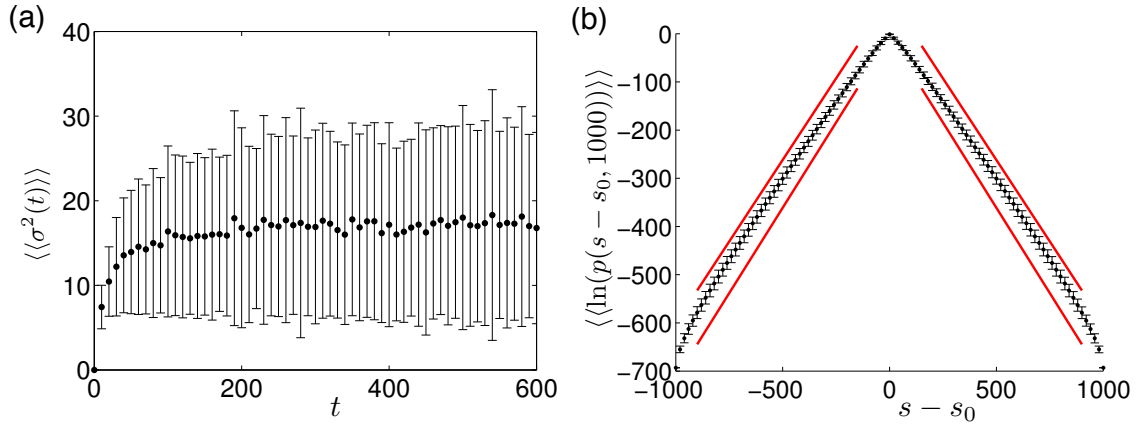

FIGURE 5.2: Numerical results for localisation of Abelian anyons. The exchange statistics is $\varphi = \frac{\pi}{8}$ and the statistics is averaged over a random background of island occupations where the distribution in each is uniform over $m_s \in \{0, \ldots, 7\}$. (a) Average variance as a function of time t for up to 600 time steps. The averages are taken over at least 500 charge configurations. (For clarity, only every 10th step is plotted.) (b) Average of the logarithm of probability distribution at time step $t = 1000$, taken over 10000 charge configurations. Red lines correspond to bounds for the localisation length given in Eq. (5.12). (Only the relevant region $-700 \leq s - s_0 \leq 700$ and every 20th site are plotted.) The localization length can be estimated from the inverse of the slopes: $\xi_{\mathrm{loc}} \approx 1.44$. In both a) and b), the error bars are given by standard deviation.

The distance between two successive scatterers j and $j+1$ is random, such that the phase that the wave acquires when traveling between j and $j+1$ is $e^{i\theta_j}$. This model is simply a discrete version of the continuous model presented in section 2 of Ref. [88].

Denote by $t_{1,N}$ the block amplitude of transmission from the "left of scatterer 1" to the "right of scatterer N"; and by $r'_{1,N}$ the reflection amplitude from the block "1 to N" when approaching from the right. $t_{1,N}$ can be expressed by the series

$$\begin{aligned} t_{1,N} &= t_{1,N-1} e^{i\theta_{N-1}} \sum_{k=0}^{\infty} \left(r_N e^{i\theta_{N-1}} r'_{1,N-1} e^{i\theta_{N-1}} \right)^k t_N \\ &= \frac{t_{1,N-1} e^{i\theta_{N-1}} t_N}{1 - r_N r'_{1,N-1} e^{i2\theta_{N-1}}}. \end{aligned} \tag{5.13}$$

The corresponding transmission probability and its logarithm are given by

$$|t_{1,N}|^2 = \frac{|t_{1,N-1}|^2 |t_N|^2}{|1 - r_N r'_{1,N-1} e^{i2\theta_{N-1}}|^2}, \tag{5.14}$$

$$\ln |t_{1,N}|^2 = \ln |t_{1,N-1}|^2 + \ln |t_N|^2 - \ln |1 - r_N r'_{1,N-1} e^{i2\theta_{N-1}}|^2. \tag{5.15}$$

The reflection and transmission amplitudes $t_{1,N}$, $r'_{1,N}$ are random variables that depend on the configuration of scatterers $1, \ldots, N$, i.e. on the angles $\theta_1, \ldots, \theta_{N-1}$. The θ_j's are assumed to be i.i.d. random variables with a uniform distribution over the discrete

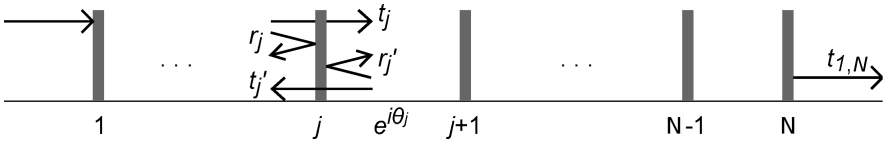

FIGURE 5.3: In the multiple scattering model, the wave approaches (from the left) a series of N scatterers, and is transmitted with the amplitude $t_{1,N}$. The scatterers are arranged in line with random distances between neighbours. Hence, the phases $e^{i\theta_j}$ that the wave acquires during travelling from a scatterer j to $j+1$ are also random. The complex quantities $r_j, t_j/r_j', t_j'$ are the reflection and transmission amplitudes for the wave impinging from the left / right.

set $\{\frac{\pi}{n}m \mid m = 0, \ldots, n-1\}$ ($\frac{\pi}{n}$ is identified with the anyonic exchange angle φ). The statistical average over the angles $\theta_1, \ldots, \theta_{n-1}$ is denoted by $\langle\langle(\ldots)\rangle\rangle$, and

$$\langle\langle(\ldots)\rangle\rangle \equiv \sum_{m_1=0}^{n-1} \frac{1}{n} \ldots \sum_{m_{n-1}=0}^{n-1} \frac{1}{n}(\ldots). \tag{5.16}$$

Averaging of (5.15) leads to

$$\begin{aligned}\left\langle\left\langle \ln|t_{1,N}|^2\right\rangle\right\rangle = \left\langle\left\langle \ln|t_{1,N-1}|^2\right\rangle\right\rangle + \ln|t_N|^2 \\ - \left\langle\left\langle \ln|1 - r_N r'_{1,N-1} e^{i2\theta_{N-1}}|^2\right\rangle\right\rangle .\end{aligned} \tag{5.17}$$

To proceed, take the θ_{N-1}-average in the last term of Eq. (5.17),

$$\begin{aligned}&\sum_{m_{N-1}=0}^{n-1} \frac{1}{n} \ln|1 - r_N r'_{1,N-1} e^{i\frac{2\pi}{n}m_{N-1}}|^2 \\ &= \frac{1}{n} \ln\left| \prod_{m_{N-1}=0}^{n-1} (1 - r_N r'_{1,N-1} e^{i\frac{2\pi}{n}m_{N-1}}) \right|^2 \\ &= \frac{1}{n} \ln|1 - (r_N r'_{1,N-1})^n|^2\end{aligned} \tag{5.18}$$

In the latter the equality

$$\prod_{m=1}^{n} (1 - Ce^{i\frac{2\pi}{n}m}) = 1 - C^n \ , \tag{5.19}$$

was used, which can be proven by using the Newton's identities between elementary symmetric polynomials and power sums [89].

The $\theta_1, \ldots, \theta_{N-2}$-average of (5.18) becomes trivial once when ($|r'_{1,N-1}| \leq 1$) is estimated:

$$\begin{aligned}\ln(1 - (|r_N||r'_{1,N-1}|)^n)^2 &\leq \ln|1 - (r_N r'_{1,N-1})^n|^2 \\ &\leq \ln(1 + (|r_N||r'_{1,N-1}|)^n)^2, \qquad (5.20) \\ \ln(1 - |r_N|^n)^2 &\leq \ln|1 - (r_N r'_{1,N-1})^n|^2 \\ &\leq \ln(1 + |r_N|^n)^2. \qquad (5.21)\end{aligned}$$

The upper and lower bounds of relation (5.17) read

$$\left\langle\left\langle \ln|t_{1,N}|^2\right\rangle\right\rangle \leq \left\langle\left\langle \ln|t_{1,N-1}|^2\right\rangle\right\rangle + \ln|t_N|^2 - \frac{1}{n}\ln(1-|r_N|^n)^2 \tag{5.22}$$

and

$$\left\langle\left\langle \ln|t_{1,N}|^2\right\rangle\right\rangle \geq \left\langle\left\langle \ln|t_{1,N-1}|^2\right\rangle\right\rangle + \ln|t_N|^2 - \frac{1}{n}\ln(1+|r_N|^n)^2 \tag{5.23}$$

respectively. When applied repeatedly, these recurrences yield ($t_{1,1} \equiv t_1$)

$$\begin{aligned}\left\langle\left\langle \ln|t_{1,N}|^2\right\rangle\right\rangle &\leq \sum_{j=1}^{N}\ln|t_j|^2 - \frac{1}{n}\sum_{j=2}^{N}\ln(1-|r_j|^n)^2\ ,\\ \left\langle\left\langle \ln|t_{1,N}|^2\right\rangle\right\rangle &\geq \sum_{j=1}^{N}\ln|t_j|^2 - \frac{1}{n}\sum_{j=2}^{N}\ln(1+|r_j|^n)^2\ ,\end{aligned} \tag{5.24}$$

where the lower index of the averaging brackets $\langle\langle\ldots\rangle\rangle$ has been omitted.

Now assume that $t_j = t, r_j = r$ for all j. On the level of the Abelian anyonic quantum walk, this corresponds to a spatially independent coin. Exponentiating (5.24) results in

$$\begin{aligned}\exp\left\langle\left\langle \ln|t_{1,N}|^2\right\rangle\right\rangle &\leq (1-|r|^n)^{\frac{2}{n}}e^{-N\left[\ln(1-|r|^n)^{\frac{2}{n}}-\ln|t|^2\right]},\\ \exp\left\langle\left\langle \ln|t_{1,N}|^2\right\rangle\right\rangle &\geq (1+|r|^n)^{\frac{2}{n}}e^{-N\left[\ln(1+|r|^n)^{\frac{2}{n}}-\ln|t|^2\right]}.\end{aligned} \tag{5.25}$$

Estimates of the localization length are then obtained as

$$\frac{1}{\ln(1+|r|^n)^{\frac{2}{n}} - \ln|t|^2} \leq \xi_{loc} \leq \frac{1}{\ln(1-|r|^n)^{\frac{2}{n}} - \ln|t|^2}. \tag{5.26}$$

In the asymptotic limit $n \to \infty$ the localization length is $\xi_{loc} \to -\frac{1}{\ln|t|^2}$.

For the upper bound in (5.12) to make sense, $-\ln|t|^2 + \frac{1}{n}\ln(1-|r|^n)^2$ has to be a positive number. This leads to the condition

$$|t|^2 < (1-|r|^n)^{\frac{2}{n}}\ ,\ \text{i.e.}\ \ |t|^n + |r|^n < 1\ . \tag{5.27}$$

Since $|t|^2 + |r|^2 = 1$ (with $|t|, |r| < 1$), the latter is satisfied for $n > 2$.

The case $n = 1$ corresponds to fermions which are known not to localize (their exchange statistics does not induce any interference effects; fermions would still localize if there is randomness in the coin parameter). The marginal case $n = 2$ corresponds to *semions* ($\varphi = \pi/2$), but the present model does not allow any bound for them. However, numerics for an analogous model involving continuous time hopping of semions on a ladder support localisation [90].

To establish a connection between this scattering model and the Abelian anyonic quantum walk with the Hadamard coin, define

$$t = -\frac{1}{\sqrt{2}}\ ,\ t' = \frac{1}{\sqrt{2}}\ ,\ r = \frac{1}{\sqrt{2}}\ ,\ r' = \frac{1}{\sqrt{2}}\ . \tag{5.28}$$

The localization length estimate for $n = 8$ ($\frac{\pi}{8}$-anyons) is now

$$1.412 \leq \xi_{loc} \leq 1.477. \tag{5.29}$$

Note that the results hold for the stationary state of a wave after infinitely many scattering events. This corresponds to the infinite-time asymptotic behavior of the anyonic quantum walk.

5.3 Non-Abelian anyons

The treatment of non-Abelian anyons is more cumbersome than Abelian anyons. The braid representations are not one-dimensional, and the calculation of the configuration average of the trace in Eq. (5.5) becomes difficult to compute. Here the trace over the fusion degrees of freedom for each configuration is once again calculated using the Jones polynomial, and the anyons are assumed to be Ising anyons. This method allows to derive an analytical formula for Ising anyons. This formula is strikingly similar to the equivalent expression for Abelian anyons except for one extra coefficient. Numerical calculations are highly inefficient, but the results suggest that localization does not occur for non-Abelian anyons. It is argued that the decoherence due to the fusion space washes off the quantum interference that leads to localization in disordered systems, and over time the non-Abelian anyonic walker diffuses away in a similar manner to a Brownian particle. The extra coefficient in the non-Abelian expression introduces effective temporal randomness in the system, which is known to cause absence of localization in quantum walks.

5.3.1 Analytical formula for Ising anyons

Using the relation between the fusion trace and the Jones polynomial, the trace for a single configuration can be written

$$\mathrm{Tr}\left(\mathcal{B}^t_{\overline{a},\overline{m}}\big|\Phi_0\big\rangle\big\langle\Phi_0\big|(\mathcal{B}^t_{\overline{a}',\overline{m}})^\dagger\right) = \frac{\left(-q^{3/4}\right)^{w(L(\overline{a},\overline{a}',\overline{m}))}}{d^{|\overline{m}|}} V_{L(\overline{a},\overline{a}',\overline{m})}(q), \tag{5.30}$$

where $L(\overline{a},\overline{a}',\overline{m})$ is the configuration-dependent link and the writhe can be written as $w(L(\overline{a},\overline{a}',\overline{m})) = 2\sum_{s=1}^{N} m_s \ell_s(\overline{a},\overline{a}')$. Note that the walker is never allowed to enter the island and it always braids with the group of stationary anyons as a whole, not with the individual strands within an island. Strictly this formula holds for $SU(2)_2$ anyons, but it has been mentioned above that the braid generators of Ising anyons are equivalent to $SU(2)_2$ generators up to phase and complex conjugation. In the uniform model the phases cancel each other and the probability distribution is invariant under complex conjugation. In the non-uniform model the expression is still invariant under complex conjugation, but the phases from bra- and ket-evolution can be different. It will be shown at the end of this section that these phases contribute trivially to the formula for the probability distribution.

For Ising anyons, the parameter of the Jones polynomial takes the value $q = i$, and the Jones polynomial can be related to the simpler `arf` invariant through [67]

$$V_{L(\overline{a},\overline{a}',\overline{m})}(i) = \sqrt{2}^{|\overline{m}|}(-1)^{\mathtt{arf}(L(\overline{a},\overline{a}',\overline{m}))} \prod_{\substack{s=1\\ m_s>0}}^{N} \widetilde{\ell}_s \ , \tag{5.31}$$

where $\widetilde{\ell}_s \equiv \delta_{0,\ell_s \bmod 2}$. The product in the last expression is equal to 1 only if the link $L(\overline{a},\overline{a}',\overline{m})$ is proper, i.e. the sum of the pairwise linking numbers is even. Furthermore, when the link is totally proper, i.e. all pairs of components have an even linking number, and there is no self-linking, then [69]

$$\mathtt{arf}(L(\overline{a},\overline{a}',\overline{m})) = \sum_{s=1}^{N} m_s c_2(s) + \sum_{1\le s'<s''\le N} m_{s'} m_{s''} \tau(s',s'') \ , \tag{5.32}$$

where $c_2(s)$ is the cubic coefficient in the Conway polynomial of the two-component sublink of $L(\overline{a},\overline{a}',\overline{m})$ consisting of strands corresponding to the walker and island s; $\tau(s',s'')$ is the Milnor triple point invariant of the three-component sublink of $L(\overline{a},\overline{a}',\overline{m})$ consisting of the walker's strand and the strands corresponding to islands s' and s''. In Sec. 3.1 it was shown that for a uniformly filled background, for all the links that contribute to the diagonal elements of the spatial probability distribution, properness implies total properness. For non-uniform filling the same is true for the simple reason that paths that had even linking between the walker and one island anyon will then have multiple pairwise linking when the island has multiple occupancy.

Inserting (5.31) and (5.32) into the expression for the fusion space trace (5.30) yields

$$\begin{aligned}\mathrm{Tr}\left(\mathcal{B}^t_{\overline{a},\overline{m}}\big|\Phi_0\big\rangle\big\langle\Phi_0\big|(\mathcal{B}^t_{\overline{a}',\overline{m}})^\dagger\right) &= (-i^{-\frac{3}{4}})^{w(L(\overline{a},\overline{a}',\overline{m}))}(-1)^{\mathtt{arf}(L(\overline{a},\overline{a}',\overline{m}))} \prod_{\substack{s=1\\ m_s>0}}^{N} \widetilde{\ell}_s \\ &= (-1)^{\sum_{s'<s''} m_{s'} m_{s''} \tau(s',s'')} \prod_{\substack{s=1\\ m_s>0}}^{N} \widetilde{\ell}_s (i)^{\frac{\ell_s}{2} m_s} (-1)^{m_s c_2(s)} \ . \end{aligned} \tag{5.33}$$

For islands s such that $m_s > 0$ and $\widetilde{\ell}_s = 1$, i.e. $\frac{\ell_s}{2} \in \mathbb{Z}$, the coefficient c_2 is given by Eq. (3.7) which simplifies to

$$c_2(s) = \frac{\ell_s}{6}(\ell_s^2 - 1) = \frac{\ell_s}{2}\frac{1}{3}\left[4\left(\frac{\ell_s}{2}\right)^2 - 1\right] \overset{mod\ 2}{=} \frac{\ell_s}{2}, \tag{5.34}$$

and the trace for a single configuration can be written

$$\mathrm{Tr}\left(\mathcal{B}^t_{\overline{a},\overline{m}}\big|\Phi_0\big\rangle\big\langle\Phi_0\big|(\mathcal{B}^t_{\overline{a}',\overline{m}})^\dagger\right) = \prod_{\substack{s=1\\ m_s>0}}^{N} \widetilde{\ell}_s (-i)^{\frac{\ell_s}{2} m_s} \prod_{1\le s'<s''\le n} (-1)^{m_{s'} m_{s''} \tau(s',s'')}. \tag{5.35}$$

where $\widetilde{\ell}_s \equiv \delta_{0,\ell_s \bmod 2}$ and $\tau(s',s'')$ is the Milnor triple invariant of a three-component sublink of $L(\overline{a},\overline{a}',\overline{m})$ formed by strands corresponding to the walker and the islands s'

and s''. Note that for the case of uniform background configuration, $m_s = 1\,\forall s$, this result is equivalent to Eq. (3.8).

The configuration average of the anyonic term can now be calculated using Eq. (5.35). First note that this expression is 4-periodic in m_s for $m_s > 0$. Thus the calculation can be simplified by choosing $W(m) = 1/4$ for $1 \le m \le 4$ and $W(m) = 0$ otherwise. The vacuum charges are therefore not included in this model, but numerical calculations show that the variance is *higher* when the vacuum charges are included. The average trace is now calculated as

$$\begin{aligned}\left\langle\left\langle \mathrm{Tr}\left(\mathcal{B}^t_{\overline{a},\overline{m}}\middle|\Phi_0\right\rangle\left\langle\Phi_0\middle|(\mathcal{B}^t_{\overline{a}',\overline{m}})^\dagger\right)\right\rangle\right\rangle &= \sum_{\overline{m}\in\{1,\ldots,4\}^N} \frac{1}{4^N}\prod_{s=1}^{N}\widetilde{\ell}_s(-i)^{\frac{\ell_s}{2}m_s} \\ &\quad\times\prod_{1\le s'<s''\le n}(-1)^{m_{s'}m_{s''}\tau(s',s'')} \qquad (5.36)\\ &= \left[\prod_{s=1}^{N}\widetilde{\ell}_s\right]\frac{1}{4^{N-1}}\sum_{\overline{m}\in\{1,\ldots,4\}^{N-1}}\prod_{s=1}^{N-1}(-i)^{\frac{\ell_s}{2}m_s} \\ &\quad\prod_{1\le s'<s''\le N-1}(-1)^{m_{s'}m_{s''}\tau(s',s'')} \\ &\quad\times\frac{1}{4}\sum_{m_N=1}^{4}\left[(-i)^{\frac{\ell_N}{2}}\right]^{m_N}\left[\prod_{s'=1}^{N-1}(-1)^{m_{s'}\tau(s',N)}\right]^{m_N} \\ &= \ldots\times\begin{cases}1 & \text{if } (-i)^{\frac{\ell_N}{2}}(-1)^{\sum_{s'=1}^{N-1}m_{s'}\tau(s',N)}=1\\ 0 & \text{otherwise}\end{cases} \qquad (5.37)\end{aligned}$$

Hence, $\left\langle\left\langle \mathrm{Tr}\left(\mathcal{B}^t_{\overline{a},\overline{m}}\middle|\Phi_0\right\rangle\left\langle\Phi_0\middle|(\mathcal{B}^t_{\overline{a}',\overline{m}})^\dagger\right)\right\rangle\right\rangle = 0$ whenever $\ell_N \neq 0 \bmod 4$ (i.e. when $(-i)^{\frac{\ell_N}{2}}$ is not a real number). Furthermore, if $\ell_N = 4 \bmod 8$, then $\tau(s', N) = 0$ for all $r = 1, \ldots, N-1$ (recall that $\tau(s', s'')$ can be nonzero only if $\ell_{s'}, \ell_{s''} = 0$), and therefore $(-1)^{\frac{\ell_N}{4}}(-1)^{\sum_{s'=1}^{N-1}m_{s'}\tau(s',N)} = -1$. Hence, $\left\langle\left\langle \mathrm{Tr}\left(\mathcal{B}^t_{\overline{a},\overline{m}}\middle|\Phi_0\right\rangle\left\langle\Phi_0\middle|(\mathcal{B}^t_{\overline{a}',\overline{m}})^\dagger\right)\right\rangle\right\rangle = 0$ whenever $\ell_N \neq 0 \bmod 8$. By the same reasoning, analogous holds for any island $s = 1, \ldots, N$. By defining $\widetilde{\widetilde{\ell}}_s \equiv \delta_{0,\ell_s \bmod 8}$ the trace becomes

$$\left\langle\left\langle \mathrm{Tr}\left(\mathcal{B}^t_{\overline{a},\overline{m}}\middle|\Phi_0\right\rangle\left\langle\Phi_0\middle|(\mathcal{B}^t_{\overline{a}',\overline{m}})^\dagger\right)\right\rangle\right\rangle = \prod_{s=1}^{N}\widetilde{\widetilde{\ell}}_s\sum_{\vec{m}\in\{1,\ldots 4\}^N}4^{-N}(-1)^{\sum_{1\le s'<s''\le n}m_{s'}m_{s''}\tau(s',s'')}. \qquad (5.38)$$

The expression $(-1)^{m_{s'}m_{s''}\tau(s',s'')}$ is invariant under shifting $m_{s'} \to m_{s'} + 2$ or $m_{s''} \to m_{s''} + 2$. Therefore, the sum over $\overline{m} \in \{1, \ldots, 4\}^N$ contains 2^N classes of 2^N equivalent configurations. Also, $m_j = 0$ is equivalent with $m_j = 2$. Now the average of the trace

can finally be written as

$$\left\langle\left\langle \mathrm{Tr}\left(\mathcal{B}^t_{\overline{a},\overline{m}}|\Phi_0\rangle\langle\Phi_0|(\mathcal{B}^t_{\overline{a}',\overline{m}})^\dagger\right)\right\rangle\right\rangle = \left[\prod_{s=1}^{N}\widetilde{\widetilde{\ell}}_s\right]\frac{1}{2^N}\sum_{\vec{m}\in\{0,1\}^N}\prod_{1\le s'<s''\le n}(-1)^{m_{s'}m_{s''}\tau(s',s'')} \tag{5.39}$$

$$= \mathcal{T}_{\overline{a}\overline{a}'}\prod_{s=1}^{N}\delta_{0,\ell_s(\overline{a},\overline{a}')\ \mathrm{mod}\ 8} \tag{5.40}$$

where $\mathcal{T}_{\overline{a}\overline{a}'} = \frac{1}{2^N}\sum_{\overline{m}\in\{0,1\}^N}\prod_{1\le s'<s''\le N}(-1)^{m_r m_s\tau(s',s'')}$ can be interpreted as an arithmetic mean of the quantity $(-1)^{\mathtt{arf}(L^*(\overline{a},\overline{a}',\overline{m}))}$ taken over all sublinks $L^*(\overline{a},\overline{a}',\overline{m})$ of a link $L(\overline{a},\overline{a}',\overline{m})$. On comparing (5.40) to the Abelian expression (5.9) for $N=8$, they are identical except for the prefactor $\mathcal{T}_{\vec{a}\vec{a}'}$. Considering Eq. (5.9) as the coherent expression where the quantum interference of probability amplitudes causes localisation, the $\mathcal{T}_{\vec{a}\vec{a}'}$ coefficient can be viewed as a noise term which might or might not destroy the interference. In Sec. 5.3.3 it is argued that at short time scales, this term does not preserve memory and introduces temporal randomness. By results of Ref. [91], localisation does not occur in the presence of both spatial and temporal randomness, therefore it is conjectured that non-Abelian anyons do not localise in the asymptotic limit $t\to\infty$.

Note that Eq. (5.40) implies that the formula for the average probability distribution is the same for Ising and $SU(2)_2$ anyons. As discussed in Sec. 2.2, the braid generators for these models are equivalent up to a phase i and complex conjugation. In disordered walks, the distribution of stationary anyons is non-uniform and the walker may thus pick up non-trivial phases from bra- and ket-evolution. The difference between these phases is given by the writhe w, which is the difference between positive and negative crossings in the link diagram. The total phase difference is then $i^w = i^{2\sum_{s=1}^N m_s\ell_s}$. But Eq. (5.40) says that the average of the trace is zero unless ℓ_s is a multiple of 8. Therefore for any integer h, $i^w = i^{2\sum_{s=1}^N m_s 8h} = (i^4)^{4h\sum_{s=1}^N m_s} = 1$, and the results hold similarly for Ising and $SU(2)_2$ anyons.

5.3.2 Numerical results

Numerical calculations were performed for non-Abelian anyons using two methods. First, the probability distribution for the discrete-time model was calculated analytically using Eqs. (5.5) and (5.35) up to 23 time steps (46 anyons in the lattice). The average variance $\left\langle\left\langle\sigma^{2(\mathrm{Ising})}(t)\right\rangle\right\rangle$ over configurations $m_s\in\{0,\ldots,4\}$ with at least 100 charge configurations is plotted in Fig. 5.4 a). The error bars were obtained by the standard deviation of the variance of the spatial probability distribution. The average variance is approximately a straight line with slope 0.456 from 10 to 23 time steps, but the error bars of the variance overlap with the errorbars of the Abelian case, so Abelian and non-Abelian anyons can not be distinguished on this short time scale. Considering only occupations $m_s\in\{1,\ldots,4\}$ (no vacuum charges), the variance is smaller, ie. the wave packet is diffusing slower (not shown).

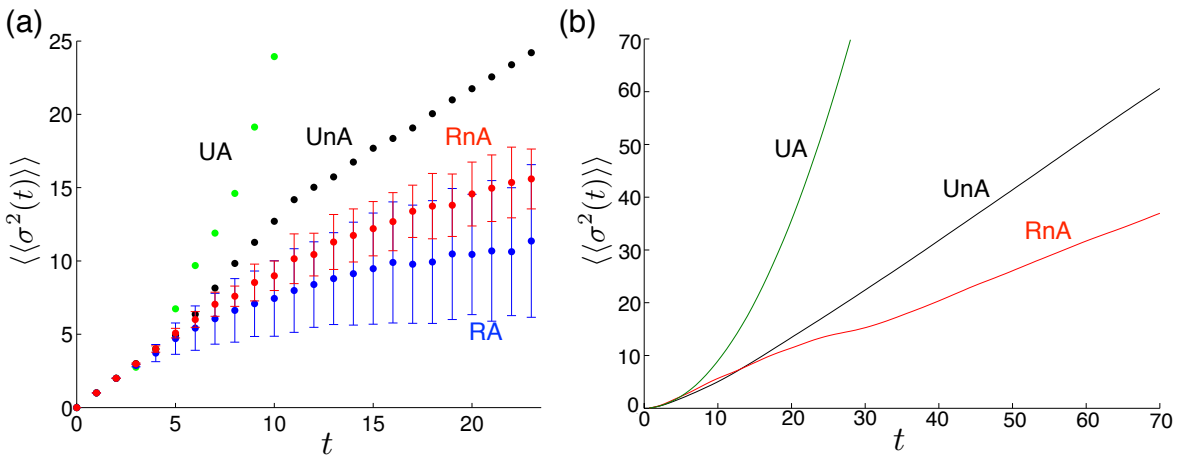

FIGURE 5.4: Numerical results for transport of Abelian and non-Abelian anyons. a) Exact results for the variance of the discrete time quantum walk with anyons over an $n = 46$ sized lattice. The results are shown for uniform background of Abelian anyons with $\frac{\pi}{8}$ statistics (Uniform Abelian=UA), uniform background of Ising anyons (Uniform non-Abelian=UnA), random background of Ising anyons averaged over 100 background configurations (Random non-Abelian=RnA), and random background of Abelian anyons averaged over 500 background configurations (Random Abelian=RA). b) Variance of anyons in a Hubbard model on a ladder realising a continuous time anyonic quantum walk over an $N = 100$ sized lattice. The slope for the case RnA averaged over 50 configurations is 0.5426 and the slope remains positive and less than one within one sigma variance (error bars suppressed for clarity). Numerics are obtained using an approximate method employing real time evolution of an anyonic MPS with bond dimension equal to 100.

To obtain results for longer time scales, an anyonic Hubbard model [92] was used. In this model, time evolves continuously and the evolution is governed by a Hamiltonian H. The spatial and coin modes are represented in a redundant manner in Fock space such that each site is assigned a three-level quantum system simultaneously describing the occupation of the site and coin mode: states $\left|0\right\rangle_s, \left|1\right\rangle_s, \left|2\right\rangle_s$ corresponding to having an empty site, a walker with coin state 0 on the site and walker with coin state 1 at site s, respectively. The quantum walk state space is thus $\mathcal{H}_{\text{space,coin}} = (\mathbb{C}^3)^{\otimes N_{\text{sites}}}$. The total Hamiltonian is given by the sum of the shift and coin flip terms $H = H_{\text{shift}} + H_{\text{flip}}$, where

$$H_{\text{shift}} = J \sum_s (T^-_{s+1} \hat{b}_s P_1 + T^+_s \hat{b}_s P_2) + \text{h.c.}$$

$$H_{\text{flip}} = \sum_s (\kappa \left|2\right\rangle_s \left\langle 1\right| + \kappa^* \left|1\right\rangle_s \left\langle 2\right|)$$

with $J \in \mathbb{R}, \kappa \in \mathbb{C}$. The operators $T^\pm_s = (\left|1\right\rangle_{s\pm1}\ {}_s\langle 1| + \left|2\right\rangle_{s\pm1}\ {}_s\langle 2|) \otimes \mathbb{I}_{\text{fusion}}$ are translation operators between sites s and $s \pm 1$, $\hat{b}_s$ are braid generators defined similarly as in the discrete model and $P_c = \sum_s \left|c\right\rangle_s \left\langle c\right| \otimes \mathbb{I}_{\text{fusion}}$ are projectors to the coin states. Here $\left|c\right\rangle_s$ corresponds to occupation of state c at site s, i.e. $\left|c = 0\right\rangle_s$ corresponds to no

mobile anyon at site s, $\big|c=1\big\rangle_s(\big|c=2\big\rangle_s)$ is a mobile anyon with coin state $\big|0\big\rangle(\big|1\big\rangle)$ at site s.

The above Hamiltonian is the generator of continuous-time evolution for total time T. Running the continuous-time walk for time T simulates the discrete-time quantum walk in a stroboscopic manner, such that the walker makes $T/\delta t$ steps of infinitesimal length δt: $e^{-iHT} = (e^{-iH\delta t})^{T/\delta t}$. The numerical calculations were done using the "Time-Evolving Block Decimation" (TEBD) algorithm [93] based on matrix product states. The TEBD algorithm was used to perform real time evolution of an initial state with the mobile anyon placed at the middle of the lattice and with couplings $\kappa = J = 1$. The implementation of the TEBD algorithm explicitly preserves anyonic charge [94, 95] and also particle number [96] corresponding to the presence of a single walker. This model realises a continuous-time anyonic quantum walk with reflecting boundaries. Fig. 5.4 b) shows that for non-Abelian anyons the variance grows linearly as a function of time, indicating no signature of localisation.

5.3.3 Correlations in time

To analyse the long-term behaviour of the non-Abelian case, an analogy is drawn to decoherent quantum walks by interpreting the anyonic quantum walk as a quantum walk with an environment. The fusion space is a very special kind of environment, since it is non-local and evolves unitarily, and such environments are not well studied in the literature. Thus, anyonic environments open a new line of study on effects of environment and decoherence in quantum systems.

As shown in Ref. [91], the quantum walk is diffusive also in the presence of both temporal and spatial disorder, in other words localization does not occur in a spatially disordered system if temporal randomness is also present. The quantum coherent terms that are needed for localization in the spatially disordered case are thus destroyed by decoherence from temporal randomness. When a coin changes completely randomly, the identity of the next coin is not dependent on the previous coins at all, and the environment which induces the change has no memory. In the following, it is argued that the anyonic environment is effectively memoryless and the the randomness of the environment in time causes the walker to spread diffusively.

Equation (5.40) shows that the average trace of Ising anyons is almost identical to that of Abelian anyons, except for the term involving the Milnor triple invariant τ. The Milnor triple invariant gives the number of Borromean rings in a three-component link. The $\mathcal{T}_{\vec{a}\vec{a}'}$-term potentially induces temporal randomness in the walk, such that the environment acts effectively in a Markovian way. The effect of this term is that it multiplies the contribution from each path by the configuration average over $(-1)^{\sum_{1\leq s'<s''\leq n} m_{s'}m_{s''}\tau(s',s'')}$. While this term preserves memory of the whole history of the particle's trajectory, at short time scales it could fluctuate in a disordered manner. The value of τ changes when a new Borromean ring is formed, which requires at least 4 time steps. Also, the formation of a Borromean ring requires a very specific pattern in the particle's trajectory which is in no way periodic. In addition, because of the condition on the last coin outcomes $a_t = a'_t$, there are new path patterns up to $t-1$ time steps introduced on every time step which were not allowed for the previous time

step, so these paths are not correlated to previous evolution at all.

The time correlations of the τ invariant can be tracked by defining the correlator

$$C(t,t') = \frac{\left\langle (-1)^{\tau_t}(-1)^{\tau_{t-t'}}\right\rangle - \left\langle (-1)^{\tau_t}\right\rangle\left\langle (-1)^{\tau_{t-t'}}\right\rangle}{1-\left\langle (-1)^{\tau_t}\right\rangle^2}$$

where $\tau_t = \sum_{1\le s'<s''\le n}\tau(s',s'')$ is the sum of three-component invariants for all sublinks for a path up to t time steps and $\left\langle\ \cdot\ \right\rangle_{(\vec{a},\vec{a}')\rightsquigarrow s_0}$ is the expectation value over all paths leading to the initial site s_0 (the subindex has been suppressed above for clarity). The term in the denominator is a normalization factor, which is defined to be the value of the term in the numerator in the perfectly correlated case $t'=0$. For simplicity, the correlator is calculated only for the uniform filling ($m_s = 1 \quad \forall s$) using the same method as described in Sec. 3.1. The time correlations can be analysed by keeping the final time t fixed and calculating the correlator for increasing values of t'. The intermediate time value $\tau_{t-t'}$ is calculated by erasing the t' last braid generators from the total braid word, such that braiding is switched off after $t-t'$ time steps. For some braid words, the quantity $\tau(s',s'')$ is not well defined in this method, in which case set $\tau(s',s'')=0$. The correlator for $t=18$ is plotted in Fig. 5.5, which shows that the correlations fall off exponentially after one step, indicating that effectively the τ invariant maintains memory only for a short period of time, and the environment is Markovian at long time scales. Note that because of the condition $a_t = a'_t$, the braiding at the last time step can always be trivially undone, therefore the last two time steps are perfectly correlated. The correlator can also be calculated for other sites $s \neq s_0$. In these cases, the rapid falloff is observed for the central region $s_0 - t/\sqrt{2} \le s \le s_0 + t/\sqrt{2}$, and outside this region the falloff becomes linear at the furthest edge sites. The edge behaviour is however irrelevant, as the behaviour of the quantum walk is determined by the central region only.

The fundamental reason for the classical-like behaviour of the walker is the strong entanglement between the quantum walk states and the fusion states, and the highly mixing nature of the fusion space environment. The walker states stay entangled with the fusion states for long time periods, and recurrences where these states become uncoupled happen very rarely. Additionally, it was observed in the simulations that increasing the number of possible configurations of anyons (ie. increasing randomness) decreases the variance for Abelian anyons, but increases the variance for non-Abelian anyons. One could interpret that there are two competing effects in the non-Abelian walk, localization due to spatial randomness, and decoherence due to the fusion space environment. Since increasing the amount of random configurations makes the walker less localized, it could be argued that decoherence wins this competition and the behaviour is diffusive at long time scales.

Finally, the effect of temporally random phases in the spatially random Abelian walk was also investigated. In this model the wave function is multiplied by a random -1 phase with some probability p_{-1} if the walker crosses a site belonging to the temporally fluctuating region of sites. The calculations with different values of p_{-1} and different sizes of the region up to 500 time steps showed that the behaviour becomes diffusive in all these cases.

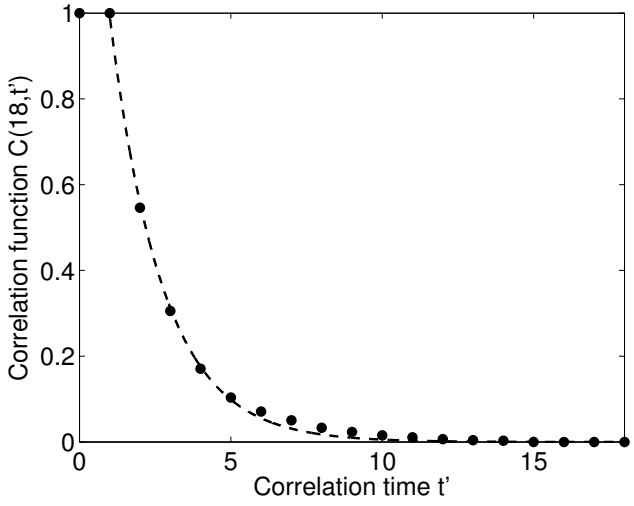

Figure 5.5: Correlator $C(t, t')$ as a function of t' with total number of time steps $t = 18$. The line shows the best exponential fit $C(18, t') = 1.7679\, e^{-0.57699\, t'}$.

6

Conclusion

The propagation of an initially localized anyon wave packet in a chain of stationary anyons has been studied for various anyon models, using a quasi-one-dimensional discrete-time anyonic quantum walk model. The spatial probability distribution at each time step can be computed by evaluating quantum link invariants, specifically the Jones polynomial and the Kauffman bracket polynomial. The evaluation of the probability distribution is exponentially hard in the number of time steps. Three distinct behaviours of the time evolution of the probability distribution are identified: localizing, diffusing and ballistic. These are defined in terms of time dependence of the variance of the distribution. The results are both numerical and analytical.

It has been demonstrated that Abelian and non-Abelian anyons behave in a qualitatively different manner. Abelian anyons exhibit properties which are analogous to non-anyonic quantum walks: ballistic transport in case of translationally invariant systems, and localization under spatial disorder. Non-Abelian anyons behave in a way similar to classical Brownian particles, diffusing slowly across the space. It is an intriguing observation that although the total evolution of the system is unitary and highly non-Markovian, the effective system dynamics is similar to a classical random walk, which is Markovian and non-deterministic. This effect can be explained by decoherence. The quantum speedup in the non-anyonic quantum walk seems to originate from the quantum correlations between the position space and coin space. The non-Abelian anyons possess a collective Hilbert space, the fusion space. Thus the evolution of the spatial and coin degrees of freedom is not unitary, and decoherence degrades the quantum correlations.

This chapter presents a detailed summary of results and discussion, and an outlook for further studies.

6.1 Summary of results and discussion

Finite systems with periodic boundary conditions were briefly studied in Secs. 2.4.2 and 2.4.3 for Ising anyons. For a small lattice size, the von Neumann entropy of the position+coin space fluctuates randomly around some average value, as does the entropy of only the position space. The mixing is very similar for time-averaged probability distribution of the classical random walk, quantum walk and anyonic walk. For a large lattice size, the von Neumann entropy increases in time and approaches the maximum value. The mixing time of the anyons is slightly slower than that of the quantum walk, but the converge is smoother.

Chapter 3 considers the uniform charge configuration on an infinite lattice. If the anyons were Abelian, the anyonic phase $e^{i\varphi}$ cancels out and the dynamics is equivalent to a non-anyonic quantum walk, which is ballistic. The probability distribution can be computed by evaluating the Jones polynomial, and the evaluation of Jones polynomial is polynomially hard in the number of crossings in the case of Ising anyons. However, evaluation of the whole probability distribution is exponentially hard in the number of crossings. The variance of the probability distribution was calculated numerically up to 25 time steps, and it was observed to approach the variance of the classical random walk which is linearly proportional to number of time steps t. By using the assumption that the properness of a link is uncorrelated from the coin terms and the sum over the Milnor triple point invariants, the variance can be approximated as $\sigma^2_{\text{Ising}}(t) = \tilde{\sigma}^2(t) + E(t)$, where $E(t)$ is an analytical error term. It was also shown that the density of proper paths is bounded from above by $p_P(t) < \frac{C}{t^2}$, which is enough to show that the non-Abelian anyonic walk is diffusive:

$$\tilde{\sigma}^2(t) = \sigma^2_{\text{RW}}(t) + O(1).$$

The slowdown of the walker particle is explained by decoherence. The fusion Hilbert space of non-Abelian anyons grows exponentially in the number of anyons, and as the walker propagates further it becomes entangled with an ever growing portion of this Hilbert space. It was observed in Sec. 2.4.2 that when the Hilbert space of the anyons is large, the von Neumann entropy of space+coin degrees of freedom approaches the maximum value, ie. the quantum walk becomes maximally entangled with the fusion degrees of freedom. In other words, the quantum walk system approaches the completely mixed state and becomes effectively classical. Similarly, the mere position degrees of freedom approach the maximally mixed state such that the entanglement between position and other degrees of freedom is washed out.

The study was extended to spin-1/2 irreps of $SU(2)_k$ for arbitrary levels of k in Chapter 4. The model was changed by relaxing the unitarity condition for the total evolution of the system, and tracing out the coin and fusion degrees of freedom on every second time step. The complexity of the numerical calculations was thus reduced and the walk could be simulated efficiently for any level k. For Abelian anyons, the phases cancel out similarly as in the fully coherent walk. The behaviour in this case is ballistic [72]. Numerical calculations were carried out for various levels of k up to 100 iterations of the superoperator and the variance of non-Abelian anyons was found to be linearly dependent on the number of time steps for all k, with only slight deviation in the slope

for various k. The lowest coefficient of the variance (≈ 0.9877) was found for $k = 3$, the highest (≈ 1.0655) for $k \to \infty$, and the coefficient of $k = 2$ (Ising anyons) is ≈ 1.0. The probability distribution for $k = 2$ can be approximated as

$$p_{SU(2)_2}(s,t) = \frac{1}{2^t}\binom{t}{\frac{2t-(s-s_0)}{4}}$$

which is equal to the classical random walk distribution. Case $k = 1$ corresponds to Abelian anyons and the walk was found to be ballistic in this case.

There are two kinds of decoherence mechanisms at work in the U^2 model, one due to the fusion space of the anyons and the other because the entanglement between the spatial modes and the coin is lost in the tracing. Since the walk is diffusive for $k = 2$ even when no tracing is done, it is not surprising that it is diffusive in the U^2 model as well. For higher values of k, it is known that when the walk is unitary the probability distribution approaches the quantum distribution at small time scales when k increases [55]. The additional decoherence introduced by the tracing is therefore enough to render the walk diffusive for all values of k.

The anyonic walk in disordered backgrounds was studied in Chapter 5. In this model, the behaviour of Abelian anyons is non-trivial. Numerical calculations show that the probability distribution is peaked around the initial site, with exponentially vanishing probability as a function of distance from the initial site. This is the signature of dynamical localization. By using a scattering model, it was shown that the localization length is bounded by

$$\frac{1}{\ln(1+|r|^n)^{\frac{2}{n}} - \ln|t|^2} \leq \xi_{loc} \leq \frac{1}{\ln(1-|r|^n)^{\frac{2}{n}} - \ln|t|^2}$$

with the anyonic braiding phase $e^{i\varphi}$, $\varphi = \frac{\pi}{n}$. These results present a new kind localization phenomenon for Abelian anyons, where localization is caused by quenched topological disorder. Random fluctuations of anyonic occupations between runs, but not during runs, cause the walker to stay at its initial location with very high probability. These results are analogous to non-anyonic quantum walks with spatial fluctuations in the coin parameters.

For non-Abelian Ising anyons, the probability distribution was evaluated analytically up to 23 time steps by averaging over 100 charge configurations. The variance is higher than that of Abelian anyons, but these results are not conclusive enough to determine whether the walk localizes or not. Further numerical calculations were performed using a continuous-time anyonic TEBD algorithm and these results show diffusive behaviour for Ising anyons. It was argued that in the long time limit, the non-Abelian term in the formula for the probability distribution introduces temporal fluctuations in the walk. These fluctuations arise when the worldlines of the anyons form structures called Borromean rings. As the formation of such structures should not be very strongly correlated with other features of the walk, by results of Ref. [91] the walk is diffusive in the presence of both spatial and temporal randomness. This argument was further supported by considering the time correlator of the non-Abelian term. The correlator falls off exponentially as a function of time steps, which indicates that the non-Abelian term does not exhibit strong correlations in time.

6.2 Outlook

The results in Chapter 3 hold equivalently for Ising anyons and spin-1/2 irreps of $SU(2)_2$. It is an open problem whether the spin-1/2 irreps of $SU(2)_k$ behave diffusively for arbitrary levels of k when the charge configuration is uniform and the walk is fully coherent. One would expect so given that braiding interactions cause strong entanglement between the walker and the fusion degrees of freedom also for $k > 2$. Furthermore, some intuition may be drawn from the U^2 model. Since the non-anyonic U^2 walk is ballistic but the anyonic walk is diffusive for all levels of k, it seems plausible that the unitary anyonic walk is diffusive also for higher values of k.

It is interesting to note that the slowdown of the non-Abelian anyon could be exploited in topological quantum computing. There the errors appear as unwanted pairs of anyons which are created from vacuum. If these erroneous particles braid non-trivially with the primary particles and fuse back to the vacuum, the logical state of the system can change. Thus, the propagation of unwanted anyons could be slowed down by placing ancillary background anyons in the system, and the logical operations could be done by dragging the anyons along certain paths which implement the correct transformations.

The U^2 model could be easily generalized to U^n models where the walk evolves coherently for n time steps instead of two. Evaluation of higher number of time steps becomes increasingly hard, because the number of different Kauffman brackets that need to be computed increases as the walker is allowed to do more steps between the tracing operations. One might expect that for large n, the walker propagates diffusively for n steps for small k and ballistically for large k, before the tracing is carried out. However, as the variance of the anyonic U^2 walk is linear even when $k \gg 2$, it is expected that in the long time limit the variance is linear for all U^n models, although the walker might spread ballistically in the initial stage of the walk.

One interesting application of the results of Chapter 5 could be in distinguishing Abelian and non-Abelian anyonic statistics experimentally. As discussed in Sec. 2.5, the anyonic quantum walk could possibly be simulated in a ladder of point contacts in Fractional Quantum Hall samples. In principle, the conductivity between two points is proportional to the probability for a quasiparticle to propagate from one point to the other. If the quasiparticle is initially localized at the initial point, the conductivity at the final point should then be proportional to the quantum walk probability to reach the corresponding site.

The results in Chapter 3 show that if each island is occupied by a single Ising anyon, the transport of the mobile Ising anyon is diffusive. This could be interpreted that the system is a normal conductor. If the anyons are Abelian, the transport is ballistic and the system could be viewed as a superconductor. In practice however, the island occupations are difficult to control. But by the results of the disordered model, the fluctuations of the occupation numbers could be exploited to highlight the statistical signatures of the quasiparticles. If the occupation numbers stay fixed during the propagation of individual quasiparticles, the average pattern under quenched randomness is diffusing for non-Abelian anyons and localizing for Abelian anyons. That is, if the quasiparticles are Abelian and the distance between the points is larger than

the localization length, the system is an insulator. The non-Abelian anyons behave diffusively and the system is a normal conductor.

The properties of the continuous-time Hamiltonian model introduced in Sec. 5.3.2 are largely unknown. This non-chiral Hubbard-type model seems to reproduce the quantum walk dynamics faithfully, although an exact mapping between the continuous-time and discrete-time models, analogously to that for non-anyonic quantum walks [97], is not yet available. Of particular interest are the properties of the ground state of this model. The interactions are purely topological, and such phases of matter are currently under theoretical interest. The phenomena in such systems can be considered as second-order emergent phenomena, as the existence of quasiparticles in the ground states of some parent systems is a mysterious emergent phenomenon itself. Some work in this direction has recently been done in chains of anyons which interact via fusion of quasiparticles [5].

Another research direction could be extending the study to topological interactions between mobile quasiparticles. In real systems, there exist necessarily simultaneous mobile quasiparticles which also interact with each other. Studies of multiparticle quantum walks have recently been conducted for fermionic and other types of interactions [98, 99], and certain types of interactions have been shown to support stable molecular states [100]. Dynamical braiding interactions between mobile anyons have not been studied before, and our intuition about the properties of these kinds of phases of matter is weak.

Anyons are inherently two-dimensional particles, and the models studied here were only quasi-one-dimensional. The physics of two-dimensional lattices has recently proven to be very rich, and particles interacting in two dimensions support an overwhelming variety of phases, which may be of interest in quantum computing applications. A natural extension of the anyonic quantum walk would thus be walks on two-dimensional graphs. The analytical treatment of large number of anyons is complex, but the mathematics of these systems is developing. There are many examples in physics where extending or decreasing spatial dimensions brings forward a host of new phenomena. Perhaps something is waiting for us in two dimensions.

References

[1] T. Kitagawa, M. S. Rudner, E. Berg, and E. Demler. *Exploring topological phases with quantum walks.* Phys. Rev. A **82**(3), 033429 (2010).

[2] T. Kitagawa, M. A. Broome, A. Fedrizzi, M. S. Rudner, E. Berg, I. Kassal, A. Aspuru-Guzik, E. Demler, and A. G. White. *Observation of topologically protected bound states in a one dimensional photonic system.* Nature Communications **3**, 882 (2012).

[3] T. Kitagawa. *Topological phenomena in quantum walks; elementary introduction to the physics of topological phases.* Quant. Inf. Proc. (2012). Preprint arXiv:1112.1882.

[4] H. Obuse and N. Kawakami. *Topological phases and delocalization of quantum walks in random environments.* Phys. Rev. B **84**(19), 195139 (2011).

[5] A. Feiguin, S. Trebst, A. W. W. Ludwig, M. Troyer, A. Kitaev, Z. Wang, and M. H. Freedman. *Interacting anyons in topological quantum liquids: The golden chain.* Phys. Rev. Lett. **98**(16), 160409 (2007).

[6] C. Cohen-Tannoudji, B. Diu, and F. Lalo. *Quantum Mechanics*, vol. 2 (John Wiley & Sons, 1977).

[7] J. Leinaas and J. Myrheim. *On the theory of identical particles.* Il Nuovo Cimento B **37**(1), 1 (1977).

[8] F. Wilczek. *Magnetic flux, angular momentum, and statistics.* Phys. Rev. Lett. **48**(17), 1144 (1982).

[9] F. Wilczek. *Quantum mechanics of fractional-spin particles.* Phys. Rev. Lett. **49**(14), 957 (1982).

[10] E. Witten. *Quantum field theory and the Jones polynomial.* Comm. Math. Phys. **121**(3), 351 (1989).

[11] V. G. Drinfel'd. *Quantum groups.* In *Proceedings of the International Congress of Mathematicians*, pp. 798–820 (Amer. Math. Soc., Providence, 1987).

[12] M. de Wild Propitius and F. A. Bais. *Discrete gauge theories* (1996). Lecture notes. arXiv:hep-th/9511201.

[13] G. Moore and N. Seiberg. *Classical and quantum conformal field theory.* Comm. Math. Phys. **123**(2), 177 (1989).

[14] C. Nayak, S. H. Simon, A. Stern, M. H. Freedman, and S. D. Sarma. *Non-abelian anyons and topological quantum computation.* Rev. Mod. Phys. **80**(3), 1083 (2008).

[15] V. Mourik, K. Zuo, S. M. Frolov, S. R. Plissard, E. P. A. M. Bakkers, and L. P. Kouwenhoven. *Signatures of majorana fermions in hybrid superconductor-semiconductor nanowire devices.* Science **336**(6084), 1003 (2012).

[16] R. P. Feynman. *Space-time approach to non-relativistic quantum mechanics.* Rev. Mod. Phys. **20**(2), 367 (1948).

[17] R. P. Feynman and A. R. Hibbs. *Quantum Mechanics and Path Integrals* (McGraw-Hill, 1965).

[18] M. G. G. Laidlaw and C. M. DeWitt. *Feynman functional integrals for systems of indistinguishable particles.* Phys. Rev. D **3**(6), 1375 (1971).

[19] Y.-S. Wu. *General theory for quantum statistics in two dimensions.* Phys. Rev. Lett. **52**(24), 2103 (1984).

[20] E. Artin. *Theory of braids.* The Annals of Mathematics **48**(1), pp. 101 (1947).

[21] K. Reidemeister. *Knotentheorie* (Chelsea Publishing Co., New York, 1948).

[22] L. H. Kauffman. *Knots and Physics* (World Scientific, 1991).

[23] J. C. Baez and J. P. Muniain. *Gauge fields, knots, and gravity* (World Scientific, 1994).

[24] J. W. Alexander. *A lemma on systems of knotted curves.* Proc. Nat. Acad. **9**, 93 (1948).

[25] V. F. R. Jones. *A polynomial invariant for knots via von Neumann algebras.* Bull. Amer. Math. Soc. **12**(1), 103 (1985).

[26] L. H. Kauffman. *State models and the Jones polynomial.* Topology **26**(3), 395 (1987).

[27] J. Preskill. *Lecture notes on quantum computation.* California University of Technology.

[28] J. K. Pachos. *Introduction to Topological Quantum Computation* (Cambridge University Press, 2012).

[29] P. Bonderson. *Non-abelian anyons and interferometry* (2007). PhD Thesis, California University of Technology.

[30] D. Aharonov, V. Jones, and Z. Landau. *A polynomial quantum algorithm for approximating the Jones polynomial*. In *Proc. 38th ACM symposium on Theory of computing (STOC '06)*, pp. 427–436 (ACM, New York, NY, USA, 2006).

[31] D. Aharonov, V. Jones, and Z. Landau. *A polynomial quantum algorithm for approximating the Jones polynomial*. Algorithmica **55**(3), 395 (2009).

[32] J. L. S. J. and L. H. Kauffman. *Topological quantum computing and the Jones polynomial*. vol. 6244, p. 62440Z (SPIE, 2006). ArXiv:quant-ph/0605004.

[33] F. Jaeger, D. L. Vertigan, and D. J. A. Welsh. *On the computational complexity of the Jones and Tutte polynomials*. Math. Proc. Cambridge Phil. Soc. **108**(01), 35 (1990).

[34] D. Aharonov, I. Arad, E. Eban, and Z. Landau. *Polynomial quantum algorithms for additive approximations of the Potts model and other points of the Tutte plane* (2007). ArXiv:quant-ph/0702008.

[35] M. H. Freedman. *P/NP, and the quantum fieldcomputer*. Proc. Nat. Acad. Sci. **95**(1), 98 (1998).

[36] M. H. Freedman, M. Larsen, and Z. Wang. *A modular functor which is universal for quantum computation*. Comm. Math. Phys. **227**(3), 605 (2002).

[37] M. H. Freedman, A. Kitaev, and Z. Wang. *Simulation of topological field theories by quantum computers*. Comm. Math. Phys. **227**(3), 587 (2002).

[38] M. H. Freedman, A. Y. Kitaev, M. J. Larsen, and W. Zhenghan. *Topological quantum computation*. Bull. Amer. Math. Soc. **40**(1), 31 (2003).

[39] W. Feller. *An Introduction to Probability Theory and Its Applications*, vol. 1 (John Wiley & Sons, 1950), 3 ed.

[40] Y. Aharonov, L. Davidovich, and N. Zagury. *Quantum random walks*. Phys. Rev. A **48**(2), 1687 (1993).

[41] E. Farhi and S. Gutmann. *Quantum computation and decision trees*. Phys. Rev. A **58**(2), 915 (1998).

[42] A. M. Childs, E. Farhi, and S. Gutmann. *An example of the difference between quantum and classical random walks*. Quant. Inf. Proc. **1**(1-2), 35 (2002).

[43] D. Meyer. *From quantum cellular automata to quantum lattice gases*. J. Stat. Phys. **85**(5), 551 (1996).

[44] A. Ambainis, E. Bach, A. Nayak, A. Vishwanath, and J. Watrous. *One-dimensional quantum walks*. In *Proc. 33th ACM symposium on Theory of computing (STOC '01)*, pp. 37–49 (ACM, Hersonissos, Greece, 2001).

[45] D. Aharonov, A. Ambainis, J. Kempe, and U. Vazirani. *Quantum walks on graphs*. In *Proc. 33th ACM symposium on Theory of computing (STOC '01)*, pp. 50–59 (ACM, New York, NY, USA, 2001).

[46] J. Kempe. *Quantum random walks: an introductory overview*. Contemporary Physics **44**(4), 307 (2003).

[47] N. Konno. *Quantum Walks*, vol. 1954 of *Quantum Potential Theory*, pp. 309–452 (Springer, 2008).

[48] S. E. Venegas-Andraca. *Quantum walks: a comprehensive review*. Quant. Inf. Proc. (2012). Preprint arXiv:1201.4780.

[49] V. Kendon. *Decoherence in quantum walks - a review*. Math. Struct. Comp. Sci. **17**(6), 1169 (2007).

[50] T. D. Mackay, S. D. Bartlett, L. T. Stephenson, and B. C. Sanders. *Quantum walks in higher dimensions*. J. Phys. A **35**(12), 2745 (2002).

[51] T. A. Brun, H. A. Carteret, and A. Ambainis. *Quantum random walks with decoherent coins*. Phys. Rev. A **67**(3), 032304 (2003).

[52] T. A. Brun, H. A. Carteret, and A. Ambainis. *Quantum to classical transition for random walks*. Phys. Rev. Lett. **91**(13), 130602 (2003).

[53] T. A. Brun, H. A. Carteret, and A. Ambainis. *Quantum walks driven by many coins*. Phys. Rev. A **67**(5), 052317 (2003).

[54] V. Kendon and B. Tregenna. *Decoherence can be useful in quantum walks*. Phys. Rev. A **67**(4), 042315 (2003).

[55] G. K. Brennen, D. Ellinas, V. Kendon, J. K. Pachos, I. Tsohantjis, and Z. Wang. *Anyonic quantum walks*. Ann. Phys. **325**(3), 664 (2010).

[56] M. A. Nielsen and I. L. Chuang. *Quantum Computation and Quantum Information* (Cambridge University Press, 2000), 1 ed.

[57] M. Dolev, M. Heiblum, V. Umansky, A. Stern, and D. Mahalu. *Observation of a quarter of an electron charge at the $\nu = 5/2$ quantum hall state*. Nature **452**(7189), 829 (2008).

[58] I. P. Radu, J. B. Miller, C. M. Marcus, M. A. Kastner, L. N. Pfeiffer, and K. W. West. *Quasi-particle properties from tunneling in the $\nu = 5/2$ fractional quantum hall state*. Science **320**(5878), 899 (2008).

[59] de C. Chamon, D. E. Freed, S. A. Kivelson, S. L. Sondhi, and X. G. Wen. *Two point-contact interferometer for quantum hall systems*. Phys. Rev. B **55**(4), 2331 (1997).

[60] E. Fradkin, C. Nayak, A. Tsvelik, and F. Wilczek. *A Chern-Simons effective field theory for the Pfaffian quantum Hall state*. Nucl. Phys. B **516**(3), 704 (1998).

[61] A. Stern and B. I. Halperin. *Proposed experiments to probe the non-abelian nu=5/2 quantum hall state*. Phys. Rev. Lett. **96**(1), 016802 (2006).

[62] P. Bonderson, A. Kitaev, and K. Shtengel. *Detecting non-abelian statistics in the nu=5/2 fractional quantum hall state*. Phys. Rev. Lett. **96**(1), 016803 (2006).

[63] R. L. Willett, L. N. Pfeiffer, and K. W. West. *Measurement of filling factor 5/2 quasiparticle interference with observation of charge e/4 and e/2 period oscillations*. Proc. Nat. Acad. Sci. **106**(22), 8853 (2009).

[64] R. L. Willett, L. N. Pfeiffer, and K. W. West. *Alternation and interchange of e/4 and e/2 period interference oscillations consistent with filling factor 5/2 non-abelian quasiparticles*. Phys. Rev. B **82**(20), 205301 (2010).

[65] B. I. Halperin, A. Stern, I. Neder, and B. Rosenow. *Theory of the Fabry-Perot quantum Hall interferometer*. Phys. Rev. B **83**(15), 155440 (2011).

[66] S. D. Sarma, M. Freedman, and C. Nayak. *Topologically protected qubits from a possible non-abelian fractional quantum hall state*. Phys. Rev. Lett. **94**(16), 166802 (2005).

[67] H. Murakami. *The arf invariant and the conway polynomial of a link*. Mathematics Seminar Notes, Kobe University **11**(2, part 2), 335 (1983).

[68] J. W. Alexander. *Topological invariants of knots and links*. Trans. Am. Math. Soc. **30**(2), 275 (1928).

[69] R. Kirby and P. Melvin. *Local surgery formulas for quantum invariants and the Arf invariant*, vol. 7 of *Proceedings of the Casson Fest (Arkansas and Texas 2003)*, pp. 213–233 (University of Warwick, 2004). ArXiv:math/0410358.

[70] G. Mohanty. *Lattice Path Counting and Applications* (Academic Press, 1980).

[71] A. J. Bracken, D. Ellinas, and I. Tsohantjis. *Pseudo memory effects, majorization and entropy in quantum random walks*. J. Phys. A **37**(8), L91 (2004).

[72] D. Ellinas and I. Smyrnakis. *Quantization and asymptotic behaviour of quantum random walk on integers*. Physica A **365**(1), 222 (2006).

[73] D. Ellinas and I. Smyrnakis. *Asymptotics of a quantum random walk driven by an optical cavity*. J. Optics B **7**(7), S152 (2005).

[74] D. Ellinas and I. Smyrnakis. *Quantum optical random walk: Quantization rules and quantum simulation of asymptotics*. Phys. Rev. A **76**(2), 022333 (2007).

[75] P. J. Davis. *Circulant Matrices* (AMS Chelsea, New York, 1994), 2nd ed.

[76] L. Berg. *Solution of large linear systems with help of circulant matrices.* ZAMM - Journal of Applied Mathematics and Mechanics **55**(7-8), 439 (1975).

[77] G. Strang. *A proposal for Toeplitz matrix calculations.* Studies in Applied Mathematics **74**, 171 (1986).

[78] T. Chan. *An optimal circulant preconditioner for Toeplitz systems.* SIAM Journal on Scientific and Statistical Computing **9**(4), 766 (1988).

[79] P. W. Anderson. *Absence of diffusion in certain random lattices.* Phys. Rev. **109**(5), 1492 (1958).

[80] N. Linden and J. Sharam. *Inhomogeneous quantum walks.* Phys. Rev. A **80**(5), 052327 (2009).

[81] N. Konno. *One-dimensional discrete-time quantum walks on random environments.* Quant. Inf. Proc. **8**(5), 387 (2009).

[82] N. Konno. *Localization of an inhomogeneous discrete-time quantum walk on the line.* Quant. Inf. Proc. **9**(3), 405 (2010).

[83] A. Joye and M. Merkli. *Dynamical localization of quantum walks in random environments.* J. Stat. Phys. **140**(6), 1 (2010).

[84] A. Ahlbrecht, V. B. Scholz, and A. H. Werner. *Disordered quantum walks in one lattice dimension.* J. Math. Phys. **52**(10), 102201 (2011).

[85] D. Shapira, O. Biham, A. J. Bracken, and M. Hackett. *One-dimensional quantum walk with unitary noise.* Phys. Rev. A **68**(6), 062315 (2003).

[86] A. Ahlbrecht, H. Vogts, A. H. Werner, and R. F. Werner. *Asymptotic evolution of quantum walks with random coin.* J. Math. Phys. **52**(4), 042201 (2011).

[87] A. Joye. *Random time-dependent quantum walks.* Comm. Math. Phys. **307**(1), 65 (2011).

[88] C. A. Mller and D. Delande. *Disorder and interference: localization phenomena* (2010). Lecture notes. arXiv:1005.0915.

[89] I. G. MacDonald. *Symmetric Functions and Hall Polynomials* (Oxford: Clarendon Press, 1995), 2nd ed.

[90] V. Zatloukal. *Anyons and their significance in quantum mechanics and statistical physics* (2011). Masters thesis, Czech Technical University in Prague.

[91] A. Ahlbrecht, C. Cedzich, R. Matjeschk, V. B. Scholz, A. H. Werner, and R. F. Werner. *Asymptotic behaviour of quantum walks with spatio-temporal coin fluctuations.* Quant. Inf. Proc. **11**(5), 1219 (2012).

[92] S. Singh, R. N. C. Pfeifer, G. Vidal, and G. K. Brennen. In preparation.

[93] G. Vidal. *Efficient simulation of one-dimensional quantum many-body systems.* Phys. Rev. Lett. **93**(4), 040502 (2004).

[94] R. N. C. Pfeifer, P. Corboz, O. Buerschaper, M. Aguado, M. Troyer, and G. Vidal. *Simulation of anyons with tensor network algorithms.* Phys. Rev. B **82**(11), 115126 (2010).

[95] R. Knig and E. Bilgin. *Anyonic entanglement renormalization.* Phys. Rev. B **82**(12), 125118 (2010).

[96] S. Singh, R. N. C. Pfeifer, and G. Vidal. *Tensor network states and algorithms in the presence of a global U(1) symmetry.* Phys. Rev. B **83**(11), 115125 (2011).

[97] F. W. Strauch. *Connecting the discrete- and continuous-time quantum walks.* Phys. Rev. A **74**, 030301 (2006).

[98] P. P. Rohde, A. Schreiber, M. Stefanak, I. Jex, and C. Silberhorn. *Multi-walker discrete time quantum walks on arbitrary graphs, their properties and their photonic implementation.* New J. Phys. **13**(1), 013001 (2011).

[99] S. D. Berry and J. B. Wang. *Two-particle quantum walks: Entanglement and graph isomorphism testing.* Phys. Rev. A **83**(4), 042317 (2011).

[100] A. Ahlbrecht, A. Alberti, D. Meschede, V. B. Scholz, A. H. Werner, and R. F. Werner. *Molecular binding in interacting quantum walks.* New J. Phys. **14**(7), 073050 (2012).